KUNGL TEKNISKA HÖGSKOLAN

acreo

Poled fiber devices

Niklas Myrén

Doctoral Thesis

Department of Physics and Quantum Optics
Royal Institute of Technology
Stockholm 2005

Royal Institute of Technology
Department of Physics and Quantum Optics
Stockholm Center for Physics, Astronomy and Biotechnology
Roslagstullsbacken 21
SE-106 91 Stockholm, Sweden

Acreo AB
Electrum 236
SE-164 40 Kista, Sweden

Akademisk avhandling som med tillstånd av Kungliga Tekniska Högskolan framlägges till offentlig granskning för avläggande av teknisk doktorsexamen i fysik, fredagen den 10 juni 2005, kl 10 Sal FD5, Alba Nova, Roslagstullsbacken 21. Avhandlingen kommer att försvaras på engelska.

TRITA-FYS 2005:22
ISSN 0280-316X
ISRN KTH/FYS/--05:22--SE

ISBN 91-7178-053-x

Cover: All-fiber optical modulator based on thermally poled fiber with internal electrodes

Poled fiber devices

Abstract

The topic of this thesis is the development of devices for telecom applications based on poled optical fibers. The focus is on a specific function, optical switching/modulation.

Some of the most important results are summarized below. Optical switching at telecom wavelengths (1.55 μm) is demonstrated in an all-fiber switch based on a fiber with internal electrodes. The fiber is made electro-optically active with a thermal poling process in which a strong electric field is recorded in the glass at a temperature of 255 ^{o}C. After poling, the fiber is put in one arm of a Mach-Zehnder interferometer and by applying a voltage across the two electrodes the refractive index is modulated and the optical signal switched from one output port to the other. A switching voltage of 190 V at 1550 nm was achieved, which to the best of our knowledge is the lowest value reported. By carefully matching the lengths of the fibers in the two arms of the interferometer the optical bandwidth could be made as large as 20 nm. The extinction ratio, determined by the power ratio in the two arms, was 30 dB and the highest modulation frequency was 30 MHz. Poled fibers were packaged to increase the thermal and mechanical stability and to make handling easier. 40 Gb/s transmission test through the device showed no bit-error-rate performance degradation. Protection switching of a 10 Gb/s signal is also demonstrated.

The depletion region in a poled fiber was found to be wedge-shaped and very wide, 13 μm and completely overlapped with the core. In a time-resolved poling experiment the recorded electric field was measured. The sign of the field changed after ~20 min, when the depletion region passed through the core, which led to the conclusion that an electric field is present also outside of the depletion region.

A ring laser was constructed with an erbium doped fiber as the gain medium. A fiber modulator was placed inside the cavity and when a small RF signal, with a frequency matched to the cavity ground frequency, was applied to the modulator the laser was mode-locked. The output pulse train contained pulses of sub ns duration and is the first demonstration of mode-locking using poled fibers.

A sampled grating with 16 channels spaced by 50 GHz was inserted into the cavity. The fiber modulator had optical bandwidth of 7 nm with center wavelength that depends on the applied voltage. By applying of 10 – 210 V to the modulator it was possible to tune the laser to 11 of the 16 channels for a total tuning range of over 4 nm.

A scheme to deposit 1 μm thin silver electrodes inside the holes of an optical fiber is demonstrated together with a new method of creating periodic electrodes by periodically ablating the silver film electrodes. The periodic electrodes are used to create a quasi-phase matched (QPM) nonlinearity in a fibers which is showed in a proof of principle experiment.

Keywords: Poling, twin-hole fiber, fiber electrodes, silver film electrodes, silver diffusion, quasi-phase matching, optical switching, frequency conversion, optical modulation

Preface

The work described in this thesis was performed at Acreo AB in Kista and has been partially founded by the European Commission IST project GLAMOROUS (2000-28366).

Finishing of this thesis was made possible with financial support from prof. Fredrik Laurell's Laser physics group at KTH.

The thesis consists of an introduction to give a background to the work performed, which is followed by a description of the experiments carried out and the reprints of the publications listed below.

List of publications

Paper I

M. Fokine, L. Kjellberg, P. Helander, N. Myrén, L. Norin, H. Olsson, N. Sjödin and W. Margulis
A Fibre-Based Kerr Switch and Modulator
30th European Conference on Optical Communications (ECOC´2004), Tu4.3.3, Stockholm, Sweden, Sept (2004)

Paper II

C. S. Franco, G. A. Quintero, N. Myrén, A. Kudlinski, H. Zeghlache,H. R. Carvalho, A. L. C. Triques, D. M. González, P. M. P. Gouvêa, G. Martinelli, Y. Quiquempois, B. Lesche, I. C. S. Carvalho, W. Margulis
Measurement of Depletion Region Width in Poled Silica
Accepted for publication in Applied Optics (April 2005)

Paper III

N. Myrén, M. Fokine, O. Tarasenko, L-E Nilsson, H. Olsson, W. Margulis
In-fiber electrode lithography
Journal of the Optical Society of America B, 21, 2085-2088 (2004)

Paper IV

N. Myrén, H. Olsson, L. Norin, N. Sjödin, P. Helander, J. Svennebrink and W. Margulis,
Wide wedge-shaped depletion region in thermally poled fiber with alloy electrodes
Optics Express 13, 6093–6099 (2005)

Paper V

N. Myrén and W. Margulis
Time evolution of frozen-in field during poling of fiber with alloy electrodes
Optics Express 13**,** 3438-3444 (2005),

Paper VI

N. Myrén and W. Margulis
All-fiber electrooptical mode-locking and tuning
Submitted for publication in Photonics Technology Letters (April 2005)

Paper VII

J. Li, N. Myrén, W. Margulis, B. Ortega,G. Puerto, D. Pastor, J. Capmany, M. Belmonte and V. Pruneri
Systems measurements of 2x2 poled fiber switch
Submitted for publication in Photonics Technology Letters (May 2005)

Other publications and conference contributions by the author not included in this thesis:

A. N. Myrén, W. Margulis, M. Fokine, L. Kjellberg, O. Tarasenko, ″Periodic electrodes fabricated by laser ablation,″ Conference on Bragg grating, poling and photosensitivity (BGPP), Monterey, California, September (2003)

B. N. Myrén, W. Margulis, G. Karlsson and F. Laurell, S. Taccheo ″Tuning of an Er-Yb:glass mini-laser using external feedback from fiber Bragg grating,″ Conference on Lasers and Electro-Optics (CLEO) Los Angeles, California, May (2002)

C. N. Myrén, M Fokine, Å. Claesson, O. Tarasenko, L-E. Nilsson, L. Kjellberg, H. Olsson, L. Norin, P. Helander and W. Margulis ″Fibre components with internal electrodes (Invited),″ Dops Nyt, 18(4), 20-23 (2004)

D. N. Myrén and W. Margulis, ″Mach-Zehnder modulator based on thermally poled optical fiber,″ Optik i Sverige - Conference of the Swedish Optical Society, Linköping, Sweden, Nov (2004)

E. W. Margulis and N. Myrén, ″Progress on poled glass and devices (Invited),″ Proceedings of OFC 2005 - Optical Fiber Communication Conference., Anaheim, CA, USA, March (2005)

F. N. Myrén, H. Olsson, L. Norin, N. Sjödin, P. Helander and W. Margulis, ″A thermally poled twin-hole fused silica fiber with alloy electrodes,″ Glamorous workshop, POWAG, Bath, UK, July (2004)

G. G. Karlsson, N. Myrén, W. Margulis, S. Tacheo, F. Laurell, ″Widely tunable fiber-coupled single-frequency Er-Yb:glass laser,″ Applied Optics, 42, 4327, July (2003)

H. B. Ortega, J. Li, N. Myrén, G. Puerto, W. Margulis, V. Pruneri, M. Belmonte, D. Pastor, J. Capmany, ″Electrooptic poled fibre switch/modulator,″ WFOPC workshop on fibers and optical passive components Sicily, June (2005)

I. N. Myrén and Walter Margulis, ″All-fibre electro-optic tuning of fibre laser,″ Submitted to ECOC (2005)

Applied patents:

J. ″In-fiber lithography″ W. Margulis, N. Myrén and M. Fokine

K. ″Poling of optical fibers and the like″ N. Myrén and W. Margulis

Acknowledgements

Many thanks goes to my supervisor and inspiring mentor **Walter Margulis**. No matter how busy, he always took time to answer my numerous questions. I thank him also for listening to my ideas and for feeding me with new ones. I also thank my main supervisor **Fredrik Laurell** for having me in his group and saving me when the times got tough at Acreo.

I wish to thank **Leif Kjellberg** for giving me support building gadgets and gizmos used in this work and **Oleksandr Tarasenko** for helping me preparing fibers.

I thank all the people at our fiberlab in Hudiksvall for supplying me with fibers, especially **Håkan Olsson**, **Niclas Sjödin**, **Per Helander** and **Lars Norin**.

Thank you also **Ola Gunnarsson, Åsa Claesson** and **Michael Fokine** for taking the time to answer all questions. I thank **Ingemar Petermann** for the interesting discussions on real life matters and **Fredrik Carlsson** for producing the special gratings needed in some experiments. I would like to thank **Mikhail Popov** for theoretical discussions on different aspects of fiber optics and **Gunnar Karlsson** for fruitful collaborations. I appreciate the assistance given from **Erik Petrini** during AFM measurements and from **Olof Öberg** during SEM characterization. I thank all the people at PUC, Rio, for having me in your lab and for being such inspiring people. I really appreciate all the support from the colleagues at the photonics department and the people working within the Glamorous project. Finally I wish to say how much I appreciate my wonderful family and friends.

Thank you all!

Table of contents

1 Introduction

The ever-increasing need for higher capacity in the telecom networks calls for cheaper and more robust optical components. The cost of optical components is not only determined by the fabrication but also by the cost of installing and maintaining them. Protection switching in today´s WDM systems is mainly done by Micro Electronic Mechanical Systems (MEMS) switches. Another function that is important as more wavelength channels are added to the systems is to optically change the wavelength of a single channel or a range of channels from one wavelength to another. The devices needed to perform the above-mentioned tasks are costly and because of their non-fiber configuration, they introduce relatively high loss that must be compensated for by adding optical amplifiers.

Inexpensive and low loss silica fibers are used in almost all transport links of optical networks. The most attractive property silica is that it affects the guided radiation extremely little and therefore one would guess that it is a poor material for active devices. Furthermore, silica glass is a centrosymmetric material, and therefore does not possess second-order susceptibility in the electric dipole approximation. By thermally poling silica however, e.g. by heating up the material and applying high voltage, the centro-symmetry is broken and the material becomes electro-optically active. This poling process can be applied both to bulk silica glass and to silica fibers. By manufacturing fibers with one hole on each side of the core and inserting electrodes into these holes the fibers can be poled so that they respond to externally applied electric fields.

Most of the work done in this thesis was performed in the frame of the Glamorous (GLass-based MOdulators, ROUters and Switches) project. The three and a half year project was funded by the European Union, started September 1st 2001, and finished in the beginning of 2005. The project had nine participants, ranging from universities and research institutes to companies. The scientific and technological objective of Glamorous was to demonstrate development of groundbreaking technology that allows fabrication of active glass-based components that are industrially viable. This was to be accomplished by increasing the nonlinearity in the glass material through poling. The value of the permanently induced electro-optic coefficient should be sufficiently high to allow poled fibers and waveguides to perform advanced optoelectronics functions by responding to electrical fields with high speed. Since fibers have low cost and low loss, are light, small, easily spliced and modular, such devices could then be used as building blocks in a number of environments where logical decisions are to be taken.

The more specific original goals of the project were mainly to:
1) optimize the thermal poling conditions (in terms of time, temperature and voltage) and to increase the stability of poled samples (to >10 years at room temperature).
2) construct a 2x2 electro-optical switch with a time response <100 μs and driving voltage x poled length <50 Vm.
3) A wavelength converter with conversion efficiency > -10 dB, number of simultaneously switched channels ≥8 at <2W pump power.

The work performed by the author was mainly focused on tasks 1 and 2 as described above. Before starting the project it was known that an all-fiber modulator would have uses outside of the telecom market, but this was purposely left out of the project goals. At the end of the Glamorous project, the technical specifications were met in most ways, but the telecom market was very weak. From the response we got at various conferences, it was

discovered that the a fiber device with the performance achieved has greater market potential in areas outside of telecom, e.g. active Q-switching and mode-locking of fiber lasers, modulation for laser displays and for chopping. At present, we are looking for industrial partners to invest in the technology to enable a product ready for the market.

2 Nonlinear Optics

2.1 Background

In the optical phenomena that we encounter everyday the interaction between light and matter is a linear process in the sense that there is no mixing between light waves in the material and in that processes are independent of the intensity of illumination. An optical material can be thought of as a collection of positively charged ions surrounded by electron clouds. An optical wave entering the material creates a propagating perturbation in the position of the positive and negative charges. In a dielectric material, there are no free charges and the displacement of the dipoles give rise to a polarization of the medium. In the case of linear optics, the polarization of each dipole is a linear function of the electric field it is subjected to. When applying intense radiation the material response moves away from the linear regime and the polarization becomes a nonlinear function of the electric fields. One can make a mechanical analogy with two particles connected with a spring. If the particles are pulled apart only slightly the restoring force of the spring is a linear function of the displacement but for larger forces, the displacement depends on higher order terms of the displacement (Figure 2.1).

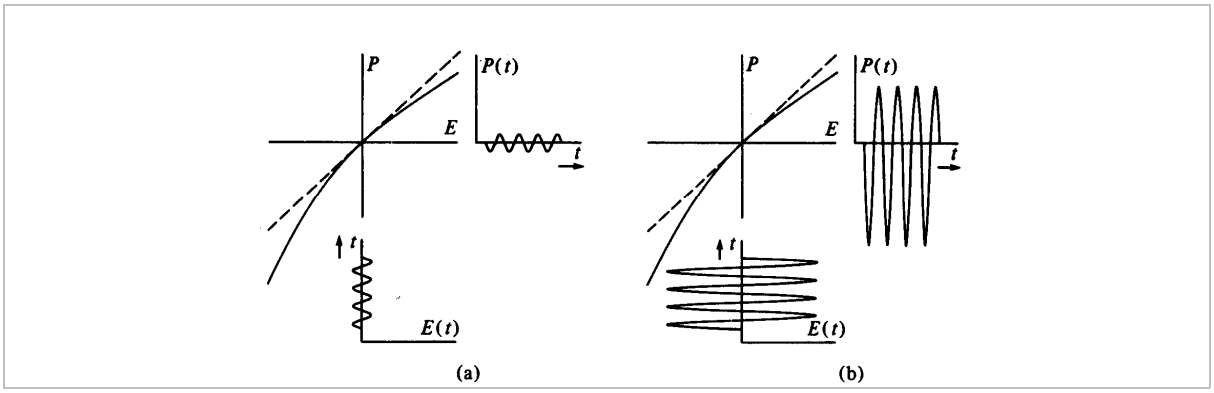

Figure 2.1 Figure (a) shows the linear regime. The incident intensity is low and the induced polarization is to a good approximation a linear function of the electric field. Figure (b) shows the nonlinear regime where the polarization of the material depends on higher order terms of the electric field [1].

In the dipole approximation the polarization can be expressed as a power series in E on the form [1]:

$$P = P_L + P_{NL} = \varepsilon_0 \chi^{(1)} E + \varepsilon_0 (\chi^{(2)} E^2 + \chi^{(3)} E^3 + ...) \qquad \textit{(eq. 2.1.1)}$$

where P_L is the linear contribution and P_{NL} is the nonlinear contribution and $\chi^{(N)}$ is a susceptibility tensor of order N and rank $(N+1)$ e.g. $\chi^{(2)}_{ijk}$.

In order to observe nonlinear phenomena the incident optical field in the material must be comparable to the internal field that binds the electrons and ions together, ~3×10^{10} V/m [1]. Incident intensity of ~10^{14} W/cm^2 gives a comparable field and this type of radiation is easily achieved with a focused laser beam, e.g. a q-switched and mode-locked Nd:YAG. In

some cases, the radiation from the individual dipole oscillations add-up constructively along the medium and give a much higher intensity. This is known as phase matching and makes it possible to compensate for weak nonlinear coefficients by increasing the interaction length. In waveguides such as optical fibers, this is particularly advantageous since a laser beam can propagate long distances without significant loss of energy or spreading.

2.2 Wave equation

The electromagnetic field in an optical fiber can be described by Maxwell's equations. The derivation below follows closely that in ref [2]:

$$\begin{aligned} \nabla \times \mathbf{E} &= -\frac{\partial \mathbf{B}}{\partial t} \\ \nabla \times \mathbf{H} &= \mathbf{J}_f + \frac{\partial \mathbf{D}}{\partial t} \\ \nabla \bullet \mathbf{D} &= \rho_f \\ \nabla \bullet \mathbf{B} &= 0 \end{aligned} \qquad \textit{(eq. 2.2.1)}$$

In the absence of free charges and free currents, as in a silica fiber, we have $\mathbf{J}_f = 0$ and $\rho_f = 0$ which simplify the Maxwell equations to:

$$\begin{aligned} \nabla \times \mathbf{E} &= -\frac{\partial \mathbf{B}}{\partial t} \\ \nabla \times \mathbf{H} &= \frac{\partial \mathbf{D}}{\partial t} \\ \nabla \bullet \mathbf{D} &= 0 \\ \nabla \bullet \mathbf{B} &= 0 \end{aligned} \qquad \textit{(eq. 2.2.3)}$$

D and **B** are the total flux densities in the medium under the applied fields **E** and **H.** They are related through the consecutive relations given by:

$$\mathbf{D} = \varepsilon_o \mathbf{E} + \mathbf{P} \qquad \textit{(eq. 2.2.4)}$$

$$\mathbf{B} = \mu_o \mathbf{H} + \mathbf{M} \qquad \textit{(eq. 2.2.5)}$$

where **P** and **M** are the induced polarization and magnetization of the material. In nonmagnetic materials, such as silica, **M**=0.

Maxwell's equations can be used to find a wave equation that describes light propagating in the fiber. Taking the rotation of each side of eq. 2.2.3 gives:

$$\nabla \times \nabla \times \mathbf{E} = -\left(\nabla \times \frac{\partial \mathbf{B}}{\partial t} \right) \qquad \textit{(eq. 2.2.6)}$$

Now, from eq. 2.2.5 we know that:

$$\mathbf{B} = \mu_o \mathbf{H} \qquad \textit{(eq. 2.2.7)}$$

which gives:

$$\frac{\partial \mathbf{B}}{\partial t} = \mu_o \frac{\partial \mathbf{H}}{\partial t} \qquad \textit{(eq. 2.2.8)}$$

inserting (2.2.8) in (2.2.6) gives:

$$\nabla \times \nabla \times \mathbf{E} = -\mu_o \frac{\partial}{\partial t}\left(\nabla \times \mathbf{H}\right) = -\mu_o \frac{\partial^2 \mathbf{D}}{\partial t^2} \qquad \textit{(eq. 2.2.9)}$$

from eq. 2.2.4:

$$-\mu_o \frac{\partial^2 \mathbf{D}}{\partial t^2} = -\mu_o \varepsilon_o \frac{\partial^2 \mathbf{E}}{\partial t^2} - \mu_o \frac{\partial^2 \mathbf{P}}{\partial t^2} \qquad \textit{(eq. 2.2.10)}$$

finally, with

$$\mu_o \varepsilon_o = 1/c^2 \qquad \text{(eq. 2.2.11)}$$

we get:

$$\nabla \times \nabla \times \mathbf{E} = -\frac{1}{c^2}\frac{\partial^2 \mathbf{E}}{\partial t^2} - \mu_o \frac{\partial^2 \mathbf{P}}{\partial t^2} \qquad \textit{(eq. 2.2.12)}$$

P in this case contains both a linear and nonlinear contributions.

The linear terms in **P** can be directly expressed in **E** using the relation $n^2 \equiv 1+\chi^{(1)}$ under the assumption that the loss is very small giving a negligible imaginary part.

Since in a step-index fiber the refractive index $n(\omega)$ is independent of the spatial coordinates [3] we can use the vector identity:

$$\nabla \times \nabla \times \mathbf{E} = \nabla(\nabla \bullet \mathbf{E}) - \nabla^2 \mathbf{E} \qquad \textit{(eq. 2.2.13)}$$

from (2.2.3) we have

$$\nabla \bullet \mathbf{E} = \mathbf{0}$$

and finally we get:

$$\nabla^2 \mathbf{E} = \frac{n^2}{c^2}\frac{\partial^2 \mathbf{E}}{\partial t^2} + \mu_o \frac{\partial^2 \mathbf{P}_{\mathbf{NL}}}{\partial t^2} \qquad \textit{(eq. 2.2.14)}$$

When dealing with nonlinear effects it is convenient to separate out the spatial dependence and only look at the field propagating along the fiber. If these are assumed to be monochromatic infinite plane waves and the x-axis points along the fiber, the electric field is given by:

$$\mathbf{E}(x,t) = \frac{1}{2}\left[E_o(\omega,t)e^{i(kx-\omega t)} + E_o^*(\omega,t)e^{-i(kx-\omega t)}\right] \qquad \textit{(eq. 2.2.15)}$$

where E_o is the envelope of the electric field. We can further simplify the expression by assuming than the envelope, E_o, only slowly varies in amplitude and phase along the fiber. This is called the slowly varying envelope approximation (SVEA) [1]. It is expressed as:

$$\left|\frac{\partial^2 E_o}{\partial x^2}\right| << \left|k\frac{\partial E_o}{\partial x}\right| \qquad \textit{(eq. 2.2.16)}$$

k is the wave-vector defined as $k = n\omega / c$. Using SVEA we can reduce the second-order differential equation into an ordinary one.

$$\frac{\partial \mathbf{E}}{\partial x} = \frac{i\mu_o c\omega}{2n}\mathbf{P}^{\mathbf{NL}} \qquad \textit{(eq. 2.2.17)}$$

2.3 Second Harmonic Generation in silica

Second harmonic generation (SHG) is the creation of radiation with a frequency ω_2 two times that of the input radiation ω_1.

$$\omega_2 = 2\omega_1 \qquad \textit{(eq. 2.3.1)}$$

SHG is a second-order nonlinear process that couples the input fields to the generated radiation through the second-order nonlinear tensor $\chi^{(2)}$. Any material that is invariant under inversion (centrosymmetric) has $\chi^{(2)} = 0$ and therefore cannot exhibit second-order nonlinear processes in the electric dipole approximation. Silica glass used in optical fibers is much like a frozen liquid and therefore does posses some short-range order, but at long range the material is randomly oriented. If the silica glass matrix is inverted around any point in space, then on a macroscopic scale, the material appears unchanged. This implies that it is impossible to generate second harmonic (SH) radiation in optical fibers. This is true in practice, but there are other, weak, effects in the glass that do generate SH, as dealt with in ref [4]. Furthermore, the symmetry can be broken by applying a strong electric DC field to the material. The electric field induces a static polarization, which breaks the symmetry and allows SH processes. The method to induce SHG with the application of a non-permanent DC field is usually referred to as electric field induced second harmonic generation (EFISH) [5]. The arising nonlinear polarization terms are of the type [6]:

$$\frac{3}{4}\chi^{(3)}(0,\omega,\omega)E_{ext}E_{OPT}^2\exp\left[i(2k_\omega x - 2\omega t)\right] + c.c. \qquad \textit{(eq. 2.3.2)}$$

where E_{ext} is the applied electric field, and E_{OPT} is the propagating optical field. The 0 in the frequency arguments corresponds to the DC field.

The applied external field can be permanently recorded in a so-called thermal poling process i.e. the application of an electric field while the silica sample is hot (280 ^{o}C) [7]. This is described in more detail in chapter 6. If the external electric field is kept constant while the sample is cooled down to room temperature, a permanent field is stored and the material can be used for SHG without applying an external field. Second-order processes in silica are often described by the effective second-order nonlinear coefficient $\chi_{eff}^{(2)}$, coupled through the third-order nonlinear susceptibility, which is expressed as [8]:

$$\chi_{eff}^{(2)} \equiv 3\chi_{xxxx}^{(3)}\,\mathbf{E_{rec}} \qquad \textit{(eq. 2.3.3)}$$

where $\mathbf{E_{rec}}$ is the recorded electric field.

2.4 Phase-matching

Most optical materials have dispersion and thus the refractive index is different for the pump and the generated wavelengths. In a frequency doubling experiment this means that there will be a phase mismatch between the fundamental and the second harmonic, here expressed as a mismatch in *k*-vectors [1].

$$\Delta k = k_{2\omega} - 2k_{\omega} = \frac{2\omega n_{2\omega}}{c_o} - \frac{2(\omega n_{\omega})}{c_o} = \frac{2\omega(n_{2\omega} - n_{\omega})}{c_o} \neq 0 \qquad \textit{(eq. 2.4.1)}$$

The SH generated at a certain point in the fiber interferes with the SH already present and because of the difference in phase arising from refractive index difference the net effect is an oscillating energy flow back and forth between the fundamental and the SH. The spatial length over which the radiation changes from completely in phase to out of phase by π/2 is defined as the coherence length (beat length) of the process, L_c.

$$L_c = \left| \frac{\pi}{\Delta k} \right| \qquad \textit{(eq. 2.4.2)}$$

The fundamental of a Nd:YAG laser (λ=1064 nm) propagating in a fused silica glass sample experiences a refractive index n_{ω} = 1.45 while the generated SH at 532 nm will experience a refractive index $n_{2\omega}$ = 1.461188. The data for the refractive indices was interpolated from ref [9]. The difference in refractive indices leads to a mismatch in *k*-vectors between fundamental and SH (eq. 2.4.1). The calculated coherence length using the above values for the refractive index is found from (eq. 2.4.2) L_c = 23.8 μm (for bulk sample). Margulis et al. made an experiment were a Ge-doped fiber was poled optically with the high intensity pulses of a Q-switched and mode-locked Nd:YAG laser. The optical poling process recorded a grating that phase matched the SH process. When this fiber was etched in HF a structure with a period ($2L_c$) of 39.2 μm was revealed [10]. The difference between the value calculated for a bulk sample and the value measured for a fiber arises since the effective refractive index in a waveguide depends also on the Ge doping and the geometrical shape of the structure.

In order for frequency conversion to be efficient, the difference in refractive indices between pump and SH must be compensated for. Phase-matching can be achieved in many different schemes, which include taking advantage of existing birefringence and using different optical axis for fundamental and harmonics, using different modes and waveguide design. In this project, the design of the fiber had to be compatible with standard telecom fibers in order to take full advantage of the low splicing loss etc. and therefore quasi phase matching (QPM) [11] as described in Figure 2.2 was the most natural choice.

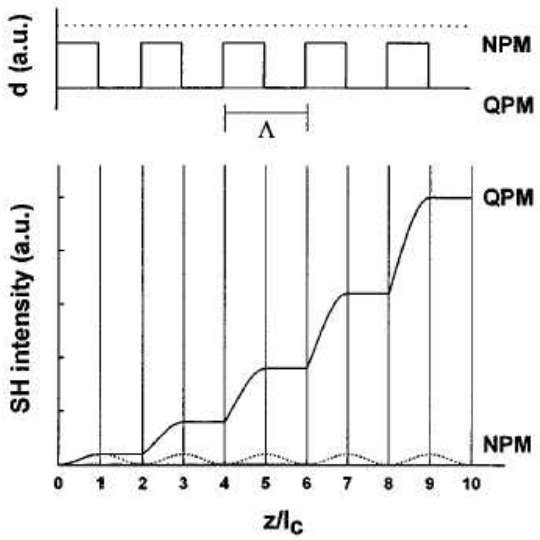

Figure 2.2. Principle of QPM, 50% duty cycle. The non phase-matched (NPM) case shows how the energy oscillates between the SH and the fundamental. In the QPM case the SH intensity increases in a step-like manner [12].

The QPM technique is very useful in optical fibers since other means of phase-matching are less flexible and more complicated to implement. QPM is not really phase-matching in the sense that it completely removes the phase difference between the propagating waves. The principle of the technique is to make the SH process less efficient or introduce a sign reversal, in the areas where the SH and pump are out of phase. QPM in silica fibers has been shown to give conversion efficiency of over 20% for nanosecond pulses at 1532 nm [13]. In this case the primary coating was removed and the fiber was polished to a D-shape after which a periodic electrode was deposited on the flat surface by means of lithography. After poling, the fiber had a periodic structure with nonlinear and inactive areas. A disadvantage of this method is that polishing makes the fiber fragile and thereby difficult to handle. As described in section 11.2 a new method was invented to create periodic structures in the electrodes inside a fiber without having to remove the coating or polish the fiber. In the Glamorous project a new technique was demonstrated, that of periodically erasing the recorded field by illuminating the fiber with a UV laser [14].

2.5 Electro-Optic effect

The main goal in the Glamorous project was to make a wavelength converter and a switch/modulator. Since it is difficult to directly modulate the intensity of the radiation inside a fiber, it is common to introduce phase modulation which is transformed into an amplitude modulation with a polarizer or a Mach-Zehnder interferometer (MZI). For switching purposes, a MZI is the most natural choice since changing the phase in one arm of the Mach-Zehnder switches the radiation from one output port to the other. A MZI with two input ports and two output ports is denoted a 2x2 switch throughout this thesis (Figure 2.3). Any configuration of input ports and output ports can be constructed by adding more interferometers e.g. a 2x4 switch can be built by connecting one Mach-Zehnder to each of the output ports.

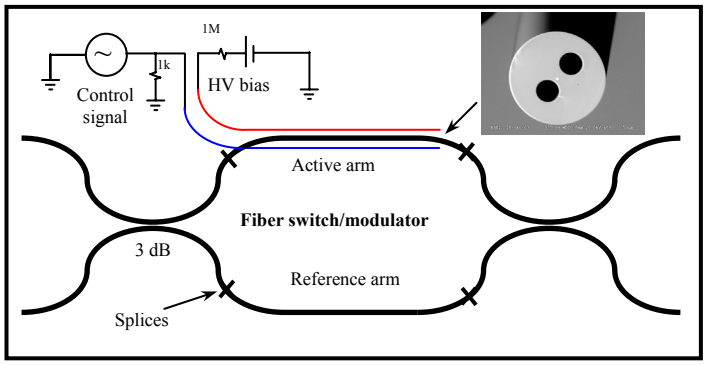

Figure 2.3. A Mach-Zehnder interferometer. The output can be shifted from one output port to the other by applying a voltage to one of the arms in the interferometer. The voltage changes the refractive index of the glass with Δn, which in turn changes the phase of the electromagnetic wave with $\Delta\varphi$.

The response of the Mach-Zehnder arises from a change in refractive index when an electric field is applied to the material. The magnitude of the voltage needed for switching is calculated below.

From eq. 2.2.4:

$$D = \varepsilon_o E + P \qquad \textit{(eq. 2.5.1)}$$

As motivated before the polarization of the material expressed as a power series in E in the dipole approximation:

$$P = P_L + P_{NL} = \varepsilon_0 \chi^{(1)} E + \varepsilon_0 (\chi^{(2)} E^2 + \chi^{(3)} E^3 + \ldots) \qquad \textit{(eq. 2.5.2)}$$

The linear permittivity, defined as [15]:

$$\varepsilon_r = 1 + \chi^{(1)}$$

(2.5.2) can be rewritten as

$$\frac{D}{\varepsilon_o E} = \varepsilon_r + (\chi^{(2)} E \ + \chi^{(3)} E^2 + \ldots) = \varepsilon_r + \Delta\varepsilon \ = \varepsilon \qquad \textit{(eq. 2.5.3)}$$

With

$$\varepsilon = n^2 = (n_o+\Delta n)^2 \approx (\text{for small } \Delta n) \approx n_o^2 + 2\, n_o\, \Delta n \qquad \textit{(eq. 2.5.4)}$$

from which it follows that (ignoring terms of higher order than cubic and with $\chi^{(2)} = 0$):

$$\Delta n = \frac{\varepsilon - n_o^2}{2n_o} = \frac{\varepsilon - \varepsilon_r}{2n_o} = \frac{\Delta\varepsilon}{2n_o} = \frac{1}{2n_o}(\chi^{(3)}E^2) \qquad \textit{(eq. 2.5.5)}$$

With $E = E_{rec} + E_{ext}$ and expressing in terms of $\chi^{(3)}_{xxxx}$ and with eq. 2.5.5

$$\Delta n = \frac{1}{2n_o}(3\chi^{(3)}_{xxxx}E_{rec}^2 + 6\chi^{(3)}_{xxxx}E_{rec}E_{ext} + 3\chi^{(3)}_{xxxx}E_{ext}^2) \qquad \textit{(eq. 2.5.6)}$$

With [8]

$$\chi^{(2)}_{eff} = 3\chi^{(3)}_{xxxx}E_{rec}$$

where the cross term ($E_{rec}E_{ext}$) gives rise to the linear part of the refractive index modulation. In a Mach-Zehnder, the optical path length of one arm (L) must be changed by $\lambda/2$ in order to switch the optical power from one output arm to the other. The change in refractive index for switching is thus given by:

$$\Delta n = \frac{\lambda}{2L}$$

With a second-order nonlinear susceptibility $\chi^{(2)}_{eff}$ = 1 pm/V (a common value reported for bulk samples) [7] and assuming that $E_{ext} << E_{rec}$, a typical telecom wavelength, λ = 1550 nm, the unperturbed refractive index n_o = 1.5 and a length of the device L = 30 cm, the applied electric field needed for switching is given by:

$$E_{ext} = \frac{\lambda n_o}{2L\chi^{(2)}_{eff}} = \frac{(1550\times10^{-9})1.5}{2\times0.3(1\times10^{-12})} = 3.9\times10^6\,\frac{V}{m} \qquad \textit{(eq. 2.5.7)}$$

With a distance between the electrodes d = 15 μm the voltage V required for switching is estimated to $V = E_{ext}d = 3.9\times10^{6} \times 15\ 10^{-6} = 59$ V. In this example, a induced nonlinearity of 1 pm/V was used since it is often seen in the poling literature. Unfortunately, there are many different definitions of the second-order nonlinearity, which makes it difficult to compare the results in various papers. In the present thesis, with the above used definition, the highest value of $\chi_{eff}^{(2)}$ obtained was 0.26 pm/V, thus giving approximately 4 times higher switching voltage than that calculated above.

3 Fiber based Mach-Zehnder interferometer

3.1 Introduction

Characterization of thermally poled fibers can be performed in many different ways. Two common methods are through SH generation or by evaluating the performance of the fiber in some interferometric structure to determine the resulting phase shift from an applied voltage. Intuitively, the SH method is the simplest and most efficient method. It is done by illuminating the fiber with e.g. 1064 nm radiation from a Nd:YAG laser and detecting the SH harmonic generation at 532 nm [16-19] and thereby determining the effective second-order nonlinearity. In principle this experiment is simple to perform, but serious limitations arise when it is executed. The high power Nd:YAG laser present in our lab is inconvenient to use and require continuous alignment. Furthermore, since a photomultiplier is used experiments are preferably performed with no ambient lightning. The fibers used throughout this thesis have cores highly doped with germanium to tightly confine the optical mode and are not single-mode at 1064 nm. When illuminating these fibers it turned out that even before thermal poling the fibers generated high levels of SH radiation due to optical poling, which is a process in which a phase-matching grating can be recorded under intense IR radiation [20-25]. The level of SH varied from fiber to fiber, but it was often higher than the contribution arising from thermal poling. Fibers with amounts of germanium comparable to that of standard telecom fibers are also optically poled when increasing the input power and therefore the method to use SH generation to characterize the fibers was abandoned.

A Mach-Zehnder interferometer can be constructed as shown in Figure 2.3. The structure consists of one active arm (the poled fiber) and one reference arm, spliced between two 3 dB couplers. The optical output power is changed by applying an electric field to the electrodes in the active arm. Many important parameters of the field recorded during poling can be obtained with this set-up [26-28].

3.2 Bandwidth

The total length of the two fibers between the 3 dB couplers in Figure 2.3 are denoted L_1 and L_2, respectively. The difference in length between the two arms is thus $L_1 - L_2 = \Delta L$. When inserting light in one of the input ports of the Mach-Zehnder interferometer the output varies periodically with the wavelength if the arms are not perfectly matched in length as shown in Figure 3.1. The periodicity is determined by ΔL and is independent of the total length of the arms [29]. A maximum in transmission, e.g. at λ_1, corresponds to wavelength were the light in the two arms recombine constructively in the second coupler. The number, p, of whole wavelengths that fit in ΔL is given by: $\Delta L = (p\lambda_1) / n$, were n is the effective refractive index of the fiber. As the wavelength is increased to λ_2 a new maximum is found, this time given by the expression: $\Delta L = ((p - 1)\ \lambda_2) / n$. By combining the above equations, the expression for the Mach-Zehnder bandwidth is determined:

$$\Delta\lambda = (\lambda_1\lambda_2) / (\Delta L\ n) \approx (\lambda_1)^2 / (\Delta L\ n) \qquad \textit{(eq. 3.1)}$$

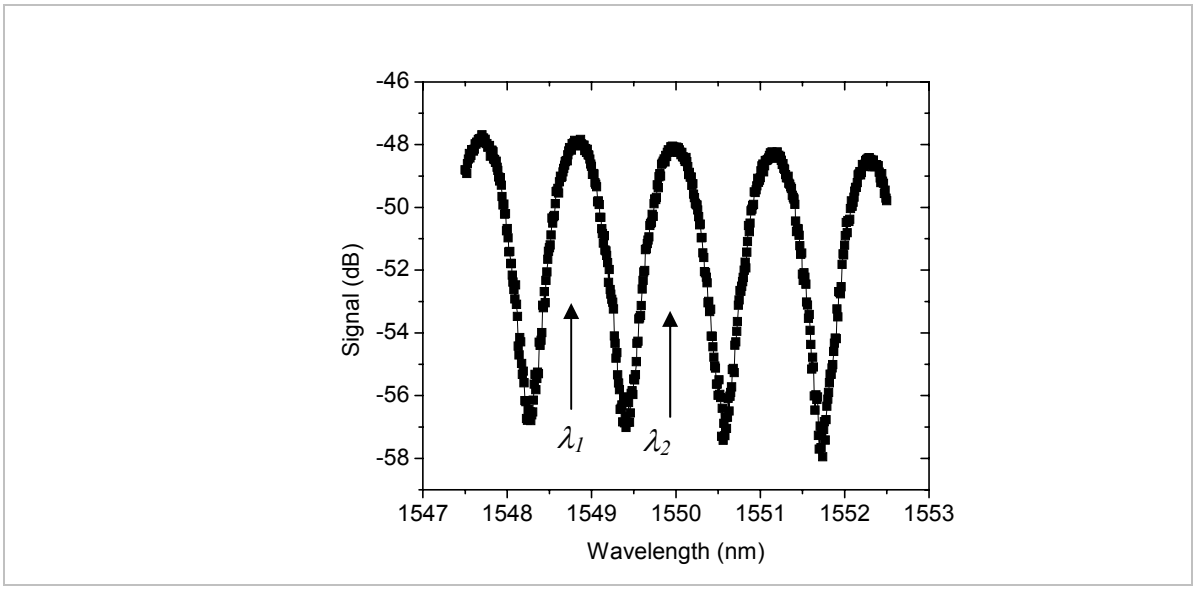

Figure 3.1. Intensity vs. wavelength in Mach-Zehnder interferometer with difference in arm length resulting in a bandwidth of ~1 nm.

The theoretical bandwidth of a MZI is plotted in Figure 3.2 to give an idea of how large a bandwidth it is possible to achieve in a fiber interferometer. By inspecting Figure 3.1, $\Delta\lambda$ is estimated to ~1 nm, which gives ΔL = 1.6 mm, a small value considering that the overall length of the interferometer is ~1 m. However, a 1 nm bandwidth is not sufficient for a switch targeted to meet the specifications of the telecom market, where a bandwidth of >30 nm is desired.

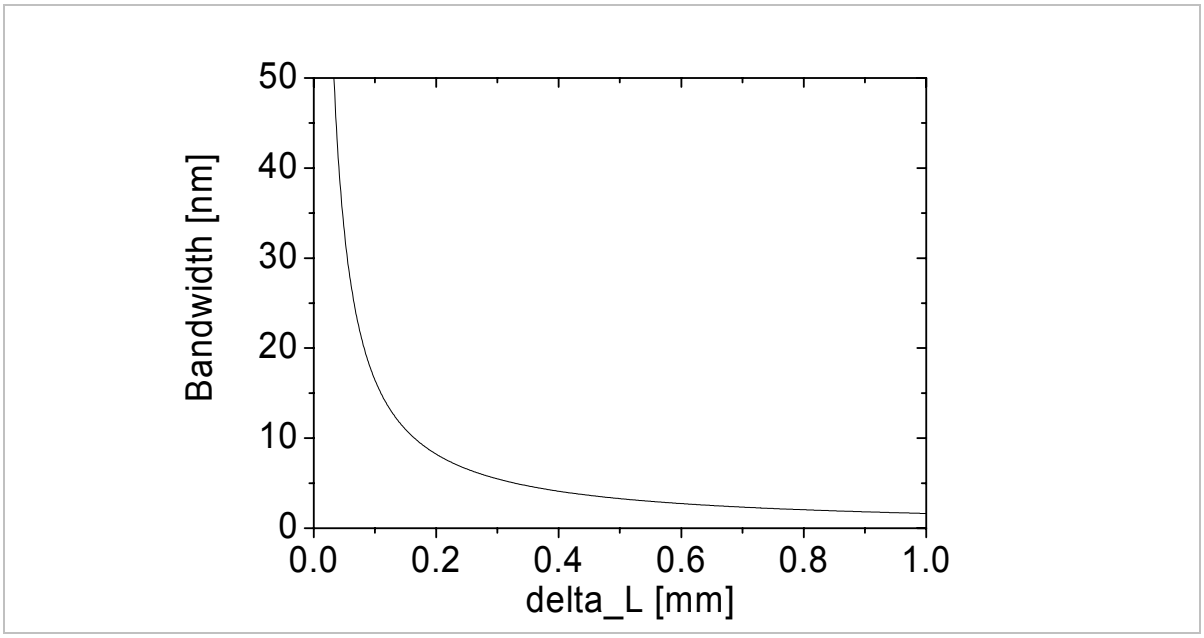

Figure 3.2. Theoretical bandwidth of MZI vs. arm length mismatch.

By carefully measuring the length of the fibers and matching them during cleaving it is possible achieve ΔL small as 1 mm. Making the mismatch smaller than that is difficult without a method where ΔL is actively monitored and adjusted. After splicing the active

and the passive fibers between couplers to obtain a functioning interferometer, a tunable laser was coupled into one input port of the MZI. An optical spectrum analyzer (OSA) was used to detect the signal at one of the output ports. Scanning the wavelength over a suitable interval gave a graph similar to the one in Figure 3.1 where a short periodicity corresponds to a poor match in arm lengths, while a long periodicity corresponds to a good match. By carefully stretching one of the fibers and at the same time observing how the spectrum changes, it is possible to determine which of the two arms is the shortest. By carefully stretching and bending the fiber it is possible to obtain a bandwidth of ~10 nm, corresponding to a mismatch of slightly more than 100 μm. This matching is not straightforward to perform since the interferometer is based on loose fibers and therefore very unstable. If the fibers are bent, even just a little, the optical path length changes and so does the output of the MZI. This makes it difficult to match the arm lengths more accurately than 100 μm unless the fibers are mounted to a substrate. The Figure 3.3 (dashed) shows an example of an interferometer with a bandwidth of ~10 nm. By bending and stretching the fibers after mounting them it was possible to slightly change the optical path length to further enhance the bandwidth so that it approached the full span of the tunable laser, 100 nm**.** In future devices it is will be favorable to use ribbon fibers so that two fibers can be cut to the same length without an active procedure.

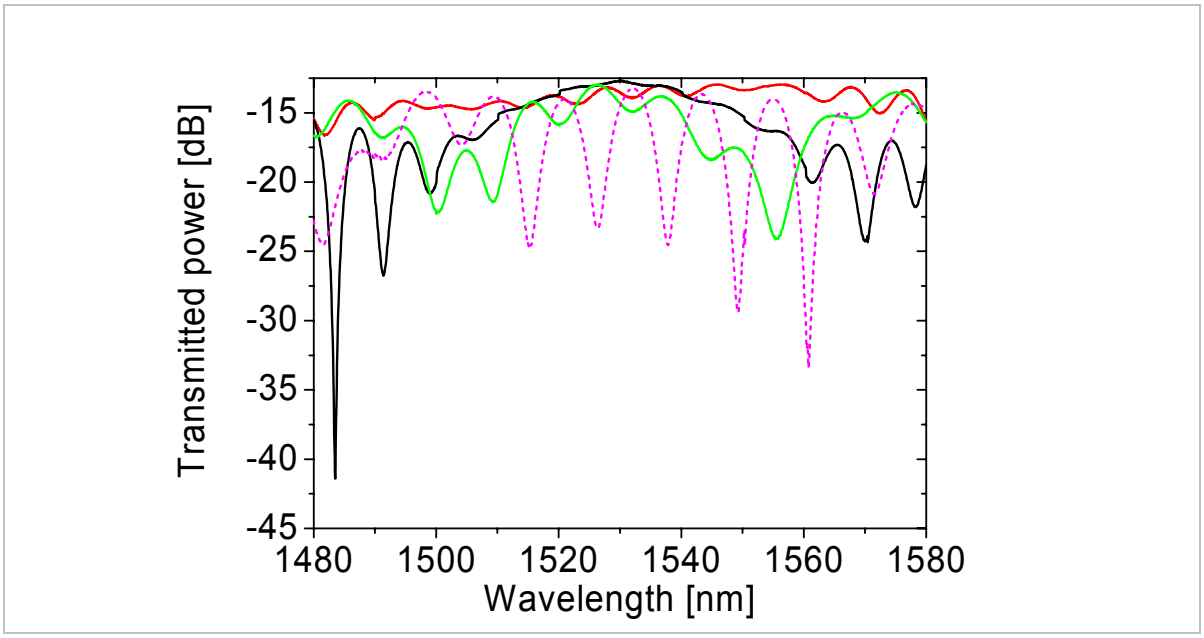

Figure 3.3. Intensity vs. wavelength in a Mach-Zehnder interferometer where the lengths of the arms have been actively adjusted to increase the bandwidth. Each curve was obtained by slightly twisting and stretching the fibers.

3.3 Extinction ratio

The contrast between maximum and minimum power in one of the two output ports is defined as the extinction ratio (ER). If the polarization is identical in the two arms at the second coupler, the ER is determined by how well the power in the two arms is balanced. In order to obtain high ER, two identical fibers were used in the passive and in the active arm. This type of approach may well be used in the future, if it is considered advantageous to use a push-pull configuration where the interferometer has two active arms. The voltage response of one device is shown in Figure 3.4 where the extinction ratio is 24 dB.

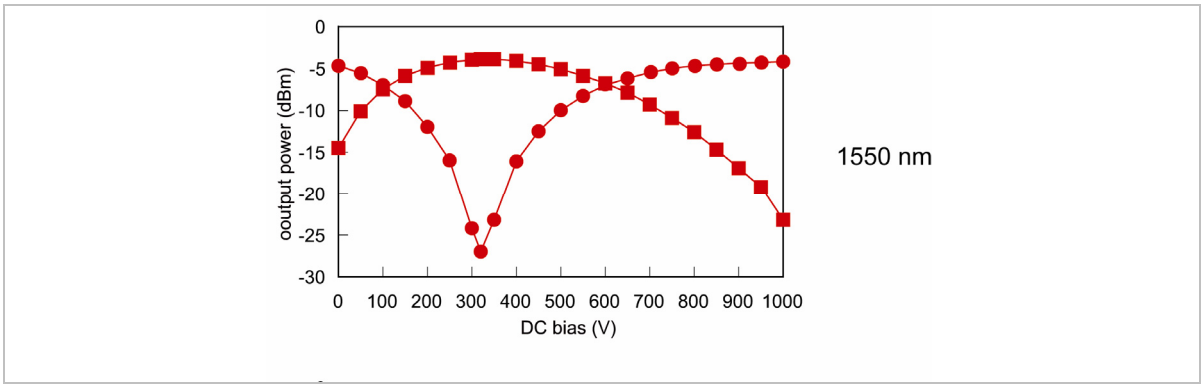

Figure 3.4. Absolute power in the two output ports of a Mach-Zehnder interferometer. A DC bias was applied to the electrodes and ramped up to 1000 V, which changed the output power in the two ports. The ER is 24 dB in this device.

The ER is related to the minimum and maximum optical power through:

$$ER(dB) = 10\log\frac{I_{\max}}{I_{\min}} \qquad \textit{(eq. 3.2)}$$

where I_{max} and I_{min} are the minimum and maximum optical powers at one port, respectively. From eq. 3.2 the relative power in the two arms can be determined. The optical intensities in the two arms are denoted $I_1 \propto (E_1)^2$ and $I_2 \propto (E_2)^2$ where E_1 and E_2 are the electric field intensities of arm 1 and 2, respectively. Since the maximum intensity is found when the electrical fields in the two arms add up constructively, $I_{max} \propto (E_1 + E_2)^2$. In the same way $I_{min} \propto (E_1 - E_2)^2$. If we express $E_2 = x\,E_1$, eq. 3.2 can be rewritten as:

$$ER(dB) = 10\log\frac{(E_1 + xE_1)^2}{(E_1 - xE_1)^2} \qquad \textit{(eq. 3.3)}$$

By putting ER = 24 dB into eq. 3.3, one obtains x = 0.88, and therefore the intensities are related as $I_2 / I_1 = 0.88^2 / 1^2 = 0.77$. This example illustrates that even if the optical powers in the two arms differ by ~25% it is still possible to obtain an extinction ratio better than 99.5%.

4 Silica Glass fibers

Silica glasses have very low optical loss over a wide range of wavelengths, from the ultraviolet to the near infrared (Figure 4.1). This in combination with the ease of manufacturing has made it the material of choice in nearly all optical fibers used in the telecom networks [30].

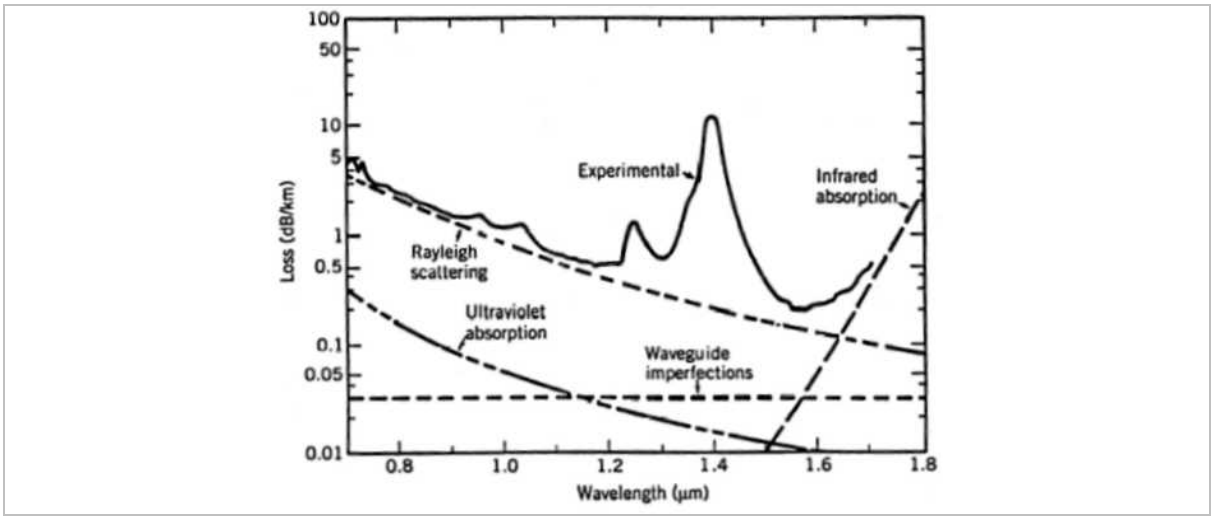

Figure 4.1. Transmission loss in optical fiber. Long haul networks often operate in the 1.5 μm area because of the low absorption (~0.2 dB/km). OH ions have a strong absorption peak at 2.73 μm [3] and the overtone at 1.37 μm is seen in the figure [31].

In optical fibers the radiation is trapped in the core because of the refractive index step between the core and the cladding that is realized either by adding dopants to the core that increases the refractive index such as GeO_2 and P_2O_5, or by adding dopants to the cladding, that decrease the refractive index, such as Boron and Fluorine [3,32]. The core can be co-doped with other ions in order to increase the functionality, such as rare earth ions [33] to make fiber amplifiers. Typically, the index-step (Δn) between the core and the cladding is $5x10^{-3}$ in a single-mode fiber, which is to be compared to the index of the latest fibers used in this thesis with Δn ~$3\ x10^{-2}$.

Fabrication of fibers is made in two stages, first a cylindrical preform (diameter ~2 cm) is manufactured with the desired geometrical dimensions and the wanted refractive index profile and then the preform is drawn to a fiber. Several methods are used to manufacture preforms, of which the most common is modified chemical vapor deposition (MCVD) [34-37]. In this process, a fused silica tube is used as a base and layers of SiO_2 are deposited on the inside of the tube by flowing $SiCl_4$ and O_2 at a temperature of about 1800 ^oC. The preform is heated by a sweeping H_2/O_2 burner to make uniform layers of deposition. When the cladding is thick enough $GeCl_4$ or $POCl_3$ is added to the mixture and the core is deposited as a thin layer on the inside of the tube, which is then collapsed before it is drawn to a fiber in a drawing tower. During fiber drawing the temperature and drawing speed needs to be precisely controlled to ensure good uniformity of core and cladding. During fiber manufacturing the OH impurities in the fiber need to be kept at a minimum to achieve acceptable loss (Figure 4.1) with typical values of the OH content being less than 10 ppb for transport fibers. Besides absorption from impurities, there are always small fluctuations

in refractive index causing Rayleigh scattering, which dominates the loss at shorter wavelengths ($R \propto 1/\lambda^4$).

The fibers used in this thesis have one hole placed on each side of the core. Metal put into the holes is used as electrodes to apply an electric field to control the light in the fiber. The holes are manufactured by drilling the collapsed preform and are typically ~8 mm in diameter. Since the final fiber preferably has the same diameter as a standard telecom fiber (=125 μm) the reduction factor for a 30 mm preform is ~250 times. The fibers used in this thesis were manufactured at Acreo's fiberlab in Hudiksvall.

5 Fibers with internal electrodes

5.1 Insertion of electrodes

The electrodes in the fibers have two purposes. First, they serve as the electrodes during poling and second, they serve as the electrodes for applying an electric signal after poling, to modulate the refractive index. If the electrodes are located on the outside of the glass for example when using d-fibers [21,26,38] care must be taken to avoid electric breakdown. Fortunately, the dielectric strength of silica is very high, 8×10^8 V/m in 6 μm thick silica samples [39] and by placing the electrodes inside the fiber, high electric fields can be applied with minimized risk of breakdown.

Almost any electrically conducting material can be used to create the electrodes, the two most frequently reported being thin (~20 μm diameter) wires inserted from side-polished openings in the fiber or alloy electrodes pumped into the holes from the end of the fiber, see Figure 5.1. Wires need to be significantly thinner than the hole diameter in order to make insertion feasible. Even so, the procedure is very time-consuming since the wire easily bends it is difficult to produce electrodes longer than 20 cm. The wires do not fill up the entire cross section of the holes and therefore the location therein is random, with the result that the electric field varies along the fiber. Furthermore, the applied voltage is not fully exploited since part of the voltage drops in the air gap between the wire and the glass. However, there is one advantage of using wire electrodes. The air gap between the glass and the wire creates a large refractive index step, so that the guided radiation is mainly confined in the glass. In the case of alloy electrodes that are in contact with the glass, the guided mode easily penetrates into the metal which results in losses.

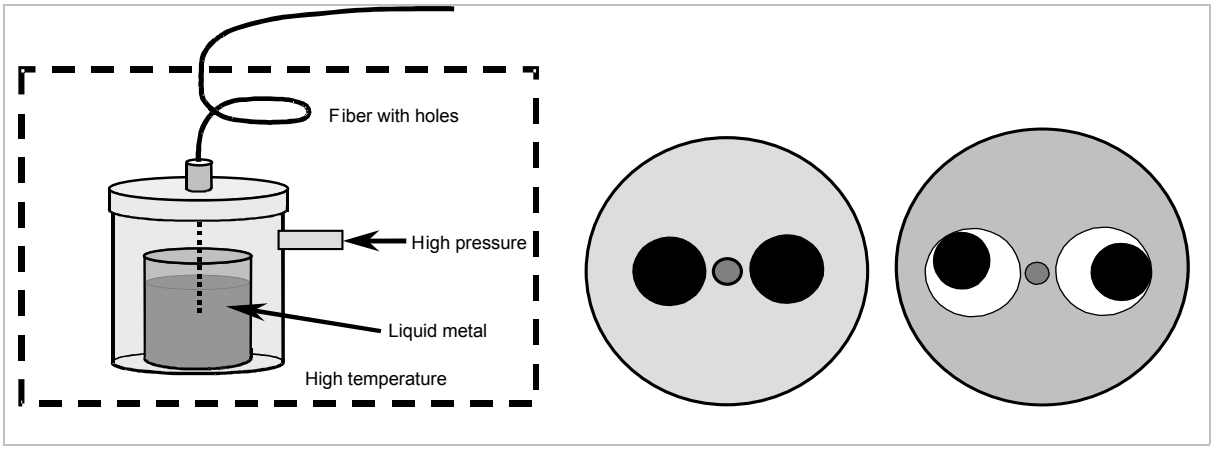

Figure 5.1. The procedure used for filling twin-hole fibers with molten alloy is illustrated in the left figure. The metal is pumped into the holes at a pressure of 6 bars with the temperature kept ~25 ^oC above the melting temperature. The middle figure shows a fiber with alloy electrodes filling the entire holes. The right drawing shows wire electrodes that are randomly located within the cross-section [40].

The alloy electrodes are inserted into the fiber using a small pressure cell as shown in Figure 5.1. The cell constitutes of a small container in which the electrode material is placed and a lid with a teflon seal through which the fibers enter the container and come into contact the liquid metal. Prior to filling, the device is placed inside an oven and heated

to a temperature a few tens of degrees above the melting temperature, T_m, of the metal to be used. AuSn alloy (Au 80%, Sn 20%) with T_m = 280 ^{o}C is inserted by heating the oven to 300 ^{o}C. After keeping the pressure cell in the oven for ~1 h the metal melts and the compressed air of 6 bars is turned on. The pressure pushes the metal into the holes of the fiber and electrodes are created in the part of the fiber placed inside of the oven. After this step, the oven is switched off and the system allowed to cool down. When the temperature is well below T_m of the metal, the pressure cell is removed from the oven and the fibers inspected. At this point, the fiber has electrodes starting at the end of the fiber placed in the cell, reaching all the way to the point where the fiber left the oven and therefore was cold.

If a fiber with metal in its ends is spliced to another fiber, the high temperature in the fusion arc evaporates the metal, which destroys the splice. For this reason, the column of metal inside the fiber is moved to make sure that the ends of the fiber are free from electrodes. The alloy is removed from the pressure cell and the system is once again heated to slightly above the melting temperature. The compressed air is turned on, and by adjusting the length of the fiber protruding from the oven, the metal column is moved the desired length. Most metals contract during solidification and therefore it is undesirable that several parts of the electrode solidify at the same time since when this happens the liquid metal between the solid parts is not able to fill the entire volume during solidification, which results in gaps in the electrode. Therefore, after the metal is moved, the fiber is slowly (~1 mm/s) pulled out of the oven to make sure that the solidification starts from a point near one end of the fiber which minimizes the risk of creating discontinuities. Note that with this method it is possible to create electrodes in several tens of fibers simultaneously. After insertion of the metal the fiber is inspected to determine the quality of the electrodes.

5.2 Electrode material

BiSn alloy (Bi 58%, Sn 42%) with melting temperature T_m = 138 ^{o}C was used as electrode material in the first poling experiments. This alloy is liquid at the poling temperature and all tests carried out to confirm a recorded electric field in fibers poled with BiSn electrode failed. The fibers always had Kerr effect, indicating that an electric field could be applied to the glass at room temperature, but it was not possible to record a field during thermal poling. The failure to pole was attributed to the fact that the interface between the liquid electrode and the glass walls of the holes is supplied with Na^{+} and other cations from the molten, impure alloy. For this reason, it is impossible to establish a space charge layer, because new ions are constantly supplied by the liquid electrode and replace the ones displaced by the poling field.

It is, of course, interesting to pole fibers with liquid electrodes. In a component intended for SHG, the fiber can be poled with a low melting point alloy that can be removed at low temperature after poling (without erasing the nonlinearity) so that the loss is reduced. To this end, high purity gallium (7N) with T_m = 30 °C was purchased, and a 3 m long piece of fiber was poled with this liquid metal. The verification of the recorded field was done by etching and indicated that the fiber was poled. To the best of our knowledge, there are no previous reports in the literature of poling with liquid electrodes. The fiber was tested in a SHG experiment where an attempt was made to periodically erase the nonlinearity to achieve QPM, but no second-order nonlinearity was found. The reasons for this are not known at present and are being investigated.

In order to determine how molten electrodes affects the poling process, attempts were made to poles several bulk samples of fused silica with a variety of alloy electrodes, that were molten when the poling field was applied. All attempts to pole with BiSn failed and with AgSn (3.5 % Ag, 96.5% Sn), T_m = 221 ^{o}C, weak poling was obtained. Relatively good poling was obtained with electrodes of AuSn even in liquid form. More importantly, AuSn melts at 280 °C. It is therefore possible to insert the metal at 300 °C, and pole the fiber at 260 °C, while keeping the poling electrodes in solid form. The alloy was therefore used in all fiber poling experiments. The specific (eutectic) composition consisted of 80% wt Au and 20% wt Sn, with a melting point of 280 °C and resistivity 1.6×10^{-5} Ωcm.

Other, exotic electrode materials were considered. Preferably, the electrodes should be highly conductive, easily inserted into the fiber, durable, have a refractive index lower than that of silica (n = 1.46) and be transparent in order to minimize the loss. For example, NaCl dissolved in water was tried in a Kerr experiment with a non-poled fiber. The liquid behaves like an electrode, but after ~1 h of testing it broke, most likely because of a discontinuity in one of the electrodes.

5.3 Loss in the fiber caused by the electrodes

A fiber ideal for poling needs to have a number of characteristics fulfilled. It should be compatible with a standard telecom fiber in terms of ease of splicing with resulting low splice loss and should have a strong electro-optic response. The fiber should also have low propagation loss. As is described later in section 6.3, the recorded field in poled fibers extend outside of the depletion region. This knowledge is very recent and therefore all the fibers used throughout this thesis had the core placed close to the anode, since when designing the fibers it was believed that the nonlinearity was only present in the ~10 μm thick depletion region. However, placing the core too close to the electrode dramatically increases the loss caused by the metal. Hopefully, in the future it is possible to design a fiber which utilizes the electric field outside of the depletion region and thereby further reduce the loss.

The energy guided by the core has an approximately Gaussian distribution which extents outside of the physical core radius, r_{core}. The mode field diameter, defined as the radial distance at which the electric field strength has decrease by a factor 1/e can be decreased by increasing the Ge concentration of the core i.e. by increasing the refractive index step, Δn. A comparison between the field distribution in a standard single-mode fiber (SMF 28) and fiber F030625-1E, one of the first Acreo fibers designed for poling, is shown in Figure 5.2. The simulated mode field diameter is 3.2 μm with the highly doped core as compared to 10.4 μm in an SMF 28 and thus the loss caused by the electrodes is reduced.

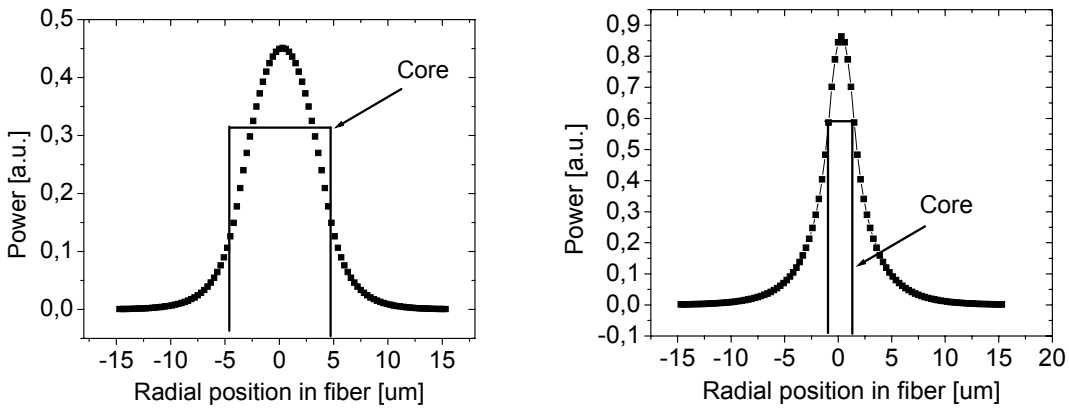

Figure 5.2. The left picture shows a simulation of the mode field in a fiber with the same index step and core diameter as that in a standard telecom fiber (SMF 28). λ = 1.55 μm, r_{core} = 4.15 μm, Δn = 0.0052. The right picture shows the simulated mode field in a fiber with a highly Ge doped core, r_{core} = 1.15 μm, Δn = 0.023. The simulated cores are illustrated with solid lines for comparison.

In a commercial device, depending on the application, an acceptable loss is roughly 3 dB for the total device. Subtracting splice losses of 0.5 dB/splice the propagation loss can be no greater than 2 dB. Given a device length of ~30 cm, the acceptable propagation loss level is 6 dB/m. The fiber simulated in Figure 5.2 (right) with alloy electrodes in the holes has a loss of 2.4 dB/cm @ 1.5 μm and a measurement of a similar fiber is shown in Figure 5.3. This loss is unacceptable and in order to decrease the loss a new fiber was designed which is described later in this section.

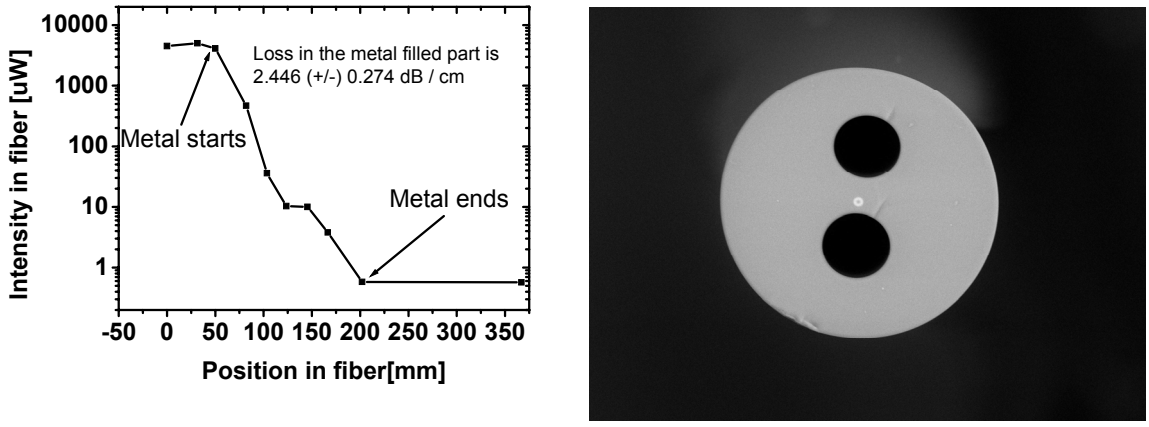

Figure 5.3. Cutback measurement to determine the loss in metal filled fiber (F030402-1F). This fiber has a loss of 2.5 dB/cm in the metal filled section and 0.4 dB/m without metal in the holes. The index step between the core and the cladding Δn = 0.015, diameter of the core D_{core} = 4.3 μm and the core-hole distance was 4 μm (edge-to-edge).

The loss in fibers with electrodes was also simulated by a colleague of the author, Mikhail Popov. A commercial Beam Propagation Method software (BeamProp) was employed. The metal filling the holes was simulated with data available for pure bismuth at 0.59 μm, not at 1.55 μm. Data were not found for the AuSn alloy used in our experiments. The refractive index of the electrode was represented by a complex number: $n_{Bi} = 1.78 + j\ 2.8$. The simulations were very sensitive to the distance between the core and the electrodes and showed that as soon as a small part the tail of the propagating mode reached the electrodes the loss increased dramatically. Moving the core 2 μm closer to the electrodes gave a ~50 times increase in loss for a simulated SMF 28 like fiber. This confirmed the importance of increasing the refractive index step to get a well confined mode with small mode-diameter. The simulation also confirmed that the loss is higher for TE polarization, with electric field orthogonal to an axis going through the holes, than for TM.

The wavelength at which a fiber can support higher order modes is approximately described by (eq. 5.1). Increasing the core diameter increases the cut-off and gives a smaller mode field diameter. If the cut-off is increased beyond 1550 nm the fiber is not single-mode at telecom wavelengths.

For a step-index fiber, the cut-off wavelength, λ_{cutoff}, is given by the following formula [3]:

$$\lambda_{cutoff} = \frac{2\pi}{2.4048} R_{core} \sqrt{n_{core}^{\ 2} - n_{clad}^{\ 2}} \qquad \textit{(eq. 5.1)}$$

where R_{core} is the radius of the core, n_{core} is the refractive index of the core, and n_{clad} is the refractive index of the cladding. Ideally the cut-off should be close to the operating wavelength to ensure the smallest possible mode field diameter.

In the first fibers produced, the loss introduced by the electrodes was a few dB/cm for the polarization with the lowest loss and almost no light was transmitted for the polarization with the highest loss. The polarization with the electric field aligned vertically (TM) in Figure 5.3 (right) is much less affected by the alloy electrodes, since it does not introduce as much surface currents in the metal. The latest fiber produced, F040407-1b2 has a loss of 1.1 dB/m for the best polarization and 2.8 dB/m for the worst polarization. The improvement was achieved by increasing Δn to 0.03 and by increasing the core-hole distance to 7 μm (edge-to-edge). A device based on this fiber can have almost 1 m long electrodes and still produce an acceptable loss at 1.5 μm.

5.4 Contacting the electrodes

A technique was implemented where the fiber is side-polished [8,41] to gain access to the electrodes without preventing splicing, see Figure 5.4 left. A polishing machine consisting of a revolving cylinder coated with fine sand paper was used. The contact to an external wire was accomplished by attaching 20 μm thick gold coated tungsten wires to the alloy using conductive epoxy. In other cases, the wire was inserted directly into the alloy that was melted locally with the tip of a soldering iron (Figure 5.4 right). The contact established with epoxy was sufficiently good for our purposes, but the long-term stability of silver epoxy is questionable, and proper bonding should be advantageous.

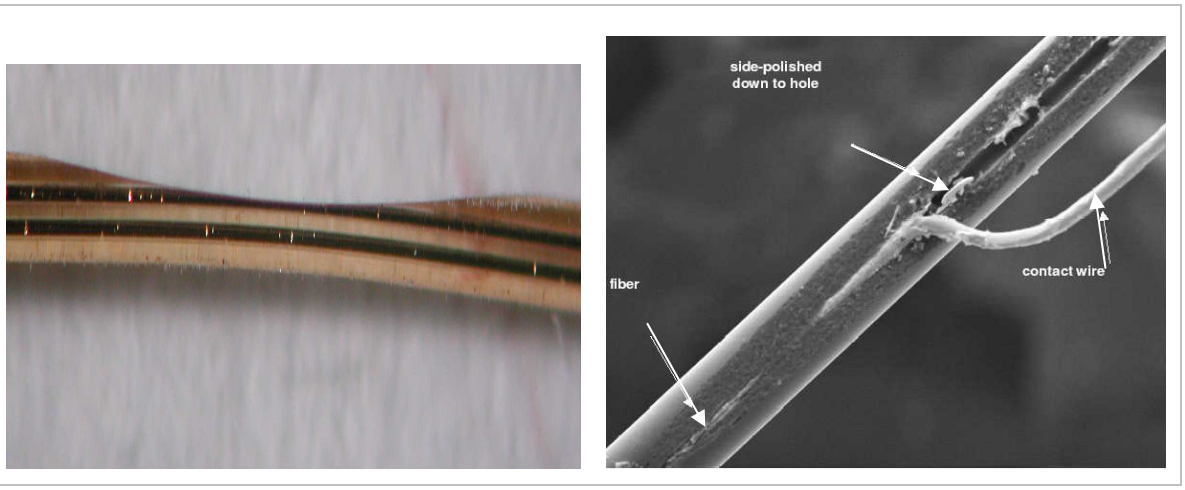

Figure 5.4. Left: Photo of side-polished fiber where one metal electrode is exposed; Right: SEM of bonded wire inserted into a polished opening of the fiber by heating the alloy electrode.

6 Thermal Poling

6.1 Introduction

All centro-symmetric materials, such as fused silica glass, lack second-order nonlinear susceptibility, $\chi^{(2)}$. The symmetry is broken and an effective second-order nonlinearity can be present by applying an electric field to a silica sample. Thermal poling is a process to record an electric field in the glass, and thereby create a permanent change of the symmetry. The procedure consists of heating the sample to an optimum poling temperature (~250 - 290 ^{o}C) [7,42] and simultaneously applying a strong electric field for a sufficiently long time. In this temperature range, alkali ions such as K^+, Li^+ and especially Na^+, are very mobile and easily migrate through the glass matrix [43,44]. The ionic current through the glass is large (~μA) when the voltage is applied and then decreases to a steady state value [7] that is usually reached in 15-90 minutes. At this point, the sample is cooled down to room temperature while the electric field is still applied. At room temperature, the mobility of the Na^+ ions is very low and the positions determined at the poling temperature are frozen. The applied field is now removed, and the result is a nonlinear layer about 10 μm thick located just below the positive electrode (anode) [7,45]. This layer is depleted of impurity ions and is often referred to as "the depletion region". There exist theories that the electric field arises in part from polarization of bonds or defects [46,47] in the glass to give higher values of $\chi^{(2)}$ than predicted by a model considering only charge migration. This effect has not been observed in the present thesis. Since the first the first reports on thermal poling, nonlinearities in silica have been achieved in a variety of ways which include corona poling [48], electron implantation [49] and UV poling [50-52]. UV poling seems promising with reports of for example in silica thin films of 12.5 pm/V [53].

The highest possible value of the second-order nonlinearity can be estimated by multiplying the recorded field with the intrinsic third-order nonlinearity as described in eq. 2.3.3. The intrinsic third-order nonlinearity in silica has been found to be $\chi^{(3)}_{xxxx} = 2\times10^{-22}$ m^2/V^2 [54-58]. The maximum field possible to record in the glass is limited by the dielectric strength, reported to be equal to 8×10^8 V/m in 6 μm thick silica samples [39] and similar values were found in ref [59,60]. This value varies strongly with sample thickness and temperature. In order to create a strong nonlinearity the two factors to optimize are thus the recorded electric field and $\chi^{(3)}_{xxxx}$. An experiment was designed so that the maximum achievable second-order susceptibility could be estimated. Twin-hole fibers with a distance d = 15 μm between the holes were provided with electrodes. A voltage was applied to the electrodes and slowly ramped up at room temperature, showing that it was possible to apply V = 6.5 kV before dielectric breakdown occurred. This gives a dielectric strength, $E_{break} = V / d = 4.3\times10^8$ V/m, about half of that obtained in [39]. The discrepancy is most likely explained by differences in geometries of the electrodes used in the experiments. The estimated maximum second-order nonlinear coefficient is then (from eq. 2.3.3) $\chi^{(2)}_{eff} = 3\times2\times10^{-22}$ [m^2/V^2] × 4.3×10^8 [V/m] = 0.26 pm/V. Thermally poled bulk samples have a reported nonlinear coefficient of up to ~1 pm/V [7], a value that has remained more or less constant since the first reports on thermal poling. For fibers the nonlinear coefficient is usually a few times lower than for bulk samples most likely since the core did not completely overlap with the recorded electric field [61-63]. The lower nonlinear coefficient is also in part explained by the electric field distribution in thin samples where the field is present also outside of the depletion region as shown in Figure 6.2.

Investigations into $\chi^{(3)}$ were performed by other groups within the Glamorous consortium. Some progress was made, but no glass with high $\chi^{(3)}$ and compatibility with regular silica glass was found. One of the main targets of the project was to use a material with similar properties as silica, e.g. in terms of manufacturing, stability and splicing. Therefore, all exotic materials, e.g. polymers were ruled out from start. Various soft glasses were investigated, but also ruled out since it was not considered likely that a new material could be developed, drawn to a fiber and poled in the short time span of the project.

6.2 Creation of the depletion region

The mobility of Na^+ increases to $\mu = 1\times10^{-13}$ $m^2s^{-1}V^{-1}$ when silica glass is heated to 280 ^oC according to [64]. This value vary greatly in different reports. For example, the authors of [65] interpolated the value in [66] to find that $\mu = \sim5\times10^{-12}$ $m^2s^{-1}V^{-1}$ with 1 ppm carrier concentration at 270 °C. When poling fibers and other thin samples it is possible to apply very high electric fields. With the breakdown field, E_{break}, applied to the glass, the diffusion length of the sodium ions, h, is given as $h = \mu E_{break} t$ = 100 μm in one second, much larger than width of the depletion layer, ~10 μm, found after ~10 minutes [paper II]. This high mobility means that there must be other mechanisms slowing down the evolution of the recorded field. Furthermore, if the formation of the depletion layer was only dependent on one type of charge carrier the depletion layer would reach a steady state after a certain time and then the ion transport would stop which is incompatible with experimental results [65]. At this point in time the applied electric field would be concentrated in the depletion region and the alkali ions would be more or less static. This contradicts experimental results in which there exist an optimum poling time, e.g. 20 min for 0.5 mm thick fused silica samples at 280 ^oC [67]. The existence of an optimum poling time cannot be explained in a model where only one charge-carrier is taken into account. It has been proposed in literature that hydrogenated species (such as H^+ or H_3O^+) are injected into the glass assisted by the strong electric field at the surface of the sample [41,65,68]. This was later confirmed using Secondary Ion Mass Spectroscopy (SIMS) [43]. Explanation of experimental results requires the mobility of the hydrogenated species to be ~10^3-10^4 times lower than that of sodium [65]. Near the surface (~0.5 μm) of the sample there is a H^+ or H_3O^+ or reservoir before poling, originating from the surrounding atmosphere [43]. The hydrogen is though to origin from a diffusion process where molecular water diffuse into the glass and then react with the SiO_2 network to make OH groups [65]. If the sample is poled in air this reservoir gives an almost unlimited supply of H^+ ions and the main factor determining the amount of charge injection is the surface conditions e.g. the type of electrodes used. If hydrogen blocking electrodes are deposited on the glass then hydrogen already present near the surface prior to electrode deposition can be migrate deeper into the glass. If the electrodes are of contact/pressed-on type, hydrogen can pass between the electrode and the glass surface and there will be a large supply of hydrogen available [65], unless the sample is poled in vacuum. During poling the electric field drives positive alkali ions towards the cathode to form a layer under the anode depleted of positive ions (Figure 6.1). This layer forms on a time-scale of minutes [65,69]. At the cathode side, the alkali ions are neutralized [47] and as the positive alkali ions are driven away from the anode side of the glass a negatively charged volume is created close to the surface[47,70]. In Figure 6.1, 2, the sample has been heated to the poling temperature and when the voltage is applied the highly mobile alkali ions, mainly Na^+, drift towards the cathode where some ions are ejected out of the sample and neutralized. The depletion region now has a net negative

charge. In Figure 6.1, 3, the high electric field between the anode and the negatively charged region of the sample injects positive hydrogenated ions (generally H_3O^+) into the glass that replace the migrated sodium ions. The positive charges injected neutralize most the depletion region, with only a thin negatively charged layer, buried some ~10 µm below the anode surface remaining (Figure 6.1, 4). After the sample is cooled down and the voltage switched off, positive charges are attracted by the net negative charge of the sample and deposited on the surfaces to give a zero net charge. The resulting electric field points from both the anode and cathode surface towards the thin negative layer. In a bulk sample, e.g. 500 µm thick, the negative layer is closest to the anode surface (~10 µm), and therefore most charges deposit on that surface. The resulting electric field is therefore much larger within the depletion region than outside it while as in thin samples, e.g. fibers, the field outside of the depletion region can be intense. This is explained in more detail in the following section.

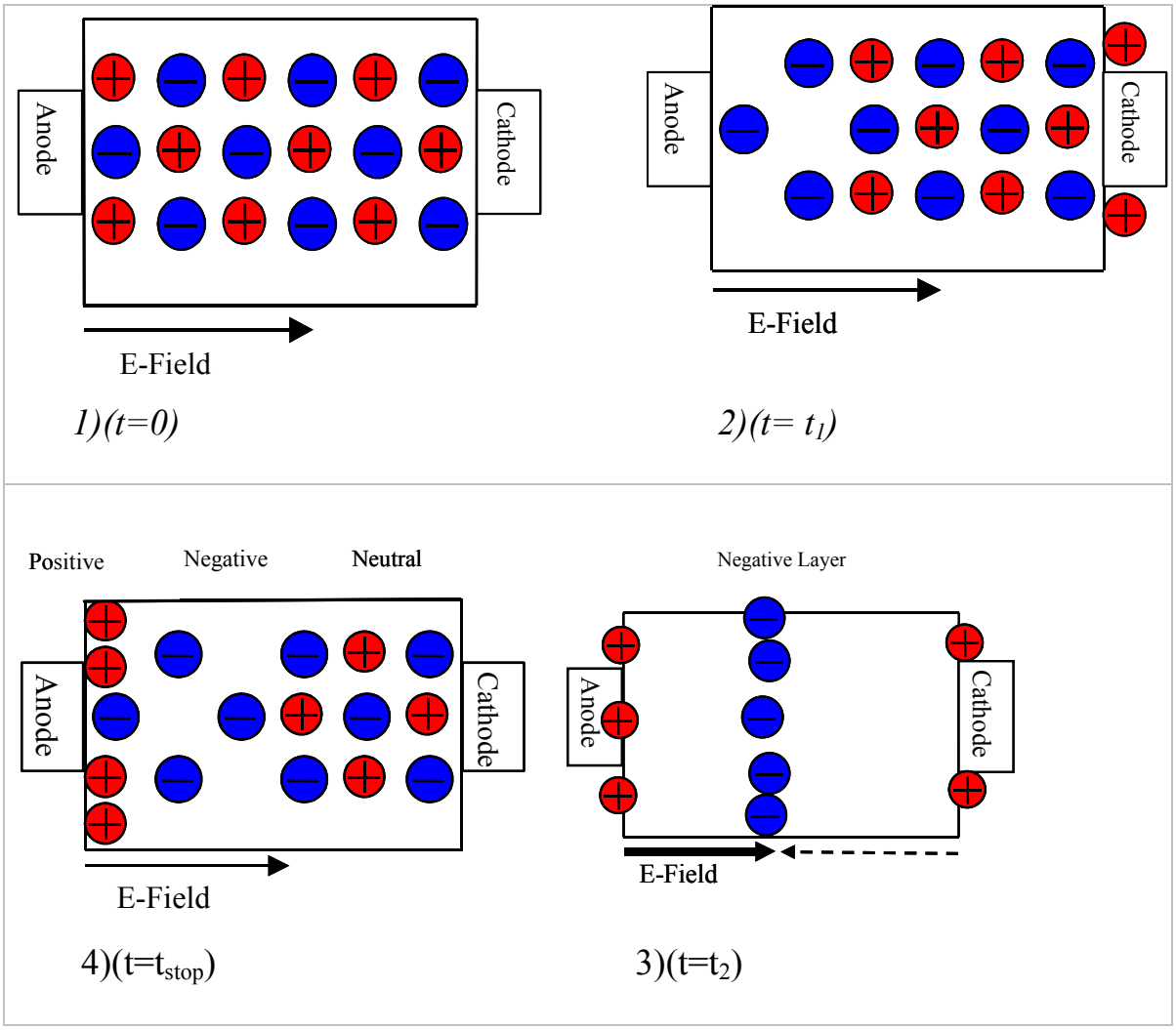

Figure 6.1. Creation of a depletion layer. 1) (time, t = 0) The sample is heated to the poling temperature 2)(t = t_1) The voltage is applied and the highly mobile alkali ions, mainly Na^+, drift towards the cathode. 3)(t= t_2) The high electric field between the anode and the negatively charged region of the sample injects positive hydrogen ions into the glass. 4) Positive charges (H^+) injected neutralize most the depletion region and only a thin negatively charged region close to the sample surface remains.

6.3 Creation of the depletion region in thin samples

The mechanism when poling fibers is much the same as when poling bulk samples. The field distribution between the two electrodes (d = 18 μm) obeys the condition $\int E\, dl = 0$, from the fact that the net charge of the sample after poling is zero, as first demonstrated experimentally in a bulk sample [71]. As shown there, the electric field recorded during poling extends between the anode and the end of the depletion region, where there is a layer of negative charge. When the poling bias is switched off, the potential difference between anode and cathode drops to zero, implying that $\int E\, dl = 0$. The recorded field is established by the presence of the negative charges buried at the end of the depletion region. These attract positive charges to the surface of the anode electrode, but particularly in thin samples, also attract positive charges to the surface of the cathode electrode. This result is illustrated in Figure 6.2 below.

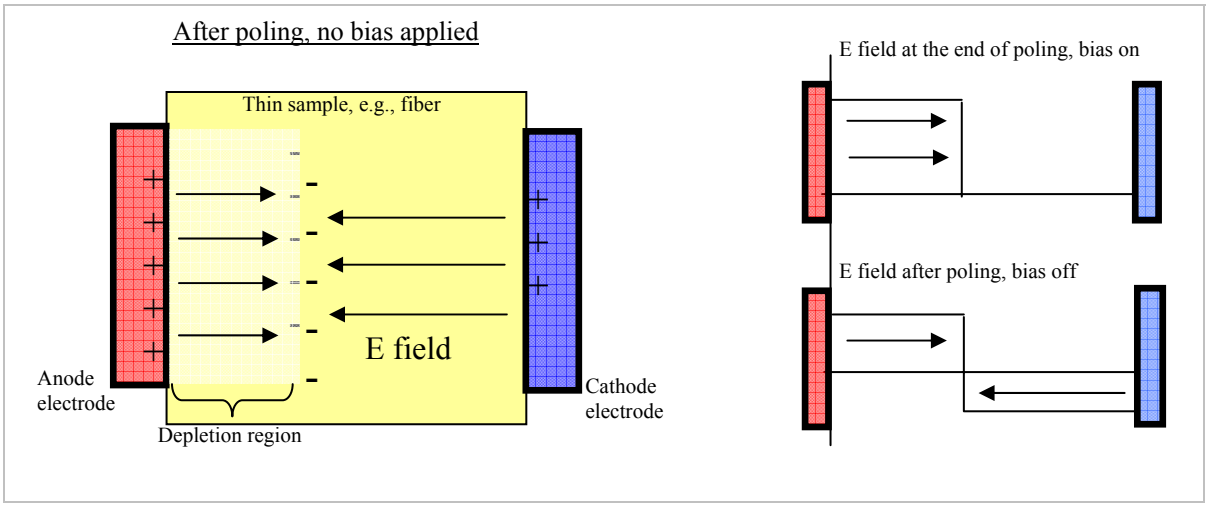

Figure 6.2. After poling, when the voltage bias is switched off, positive charges are attracted from the metal surfaces of both anode and cathode to shield the field in the metal. If the negative charges recorded in the poled sample are closer to the cathode side, the field outside the depletion region is larger than inside it.

After poling an electric field is established between the anode electrode and the end of the depletion layer, and also between the cathode electrode and the end of the depletion layer. These fields point in opposite directions, and the sum of their modulus is approximately equal to the field present in the depletion region when the external poling bias was present as shown in Figure 6.2, right. The upper figure shows the field with applied DC bias, when there is a potential difference between the two surfaces of the sample equal to the poling bias. When the poling voltage is switched off the potential difference between electrodes is zero, and it is recognized that the amplitude of the field established between each electrode and the negative charge layer is inversely proportional to the distance between the electrode and the charges. From the picture of a poled fiber shown in Figure 7.11, the width between the anode electrode and the negative charges is estimated to approximately 13 μm, while the distance between the cathode and the charges is only 5 μm. In the present case, the measured recorded voltage V_{rec} = 1.1 kV gives $E_{rec} = V_{rec} / d = 0.61\times10^8$ V/m in the 13 μm depletion region. In the 5 μm thick region between the charges and the cathode, from the condition $\int E\, dl = 0$, one infers $E = -(13 / 5)\, E_{rec} = -1.59\times10^8$ V/m. This implies that the charges displaced by poling the fiber, buried at the end of the depletion region are sufficient

to create a field equal to the difference, 2.2×10^8 V/m, comparable to the values reported for bulk samples. We have been able to improve considerably this value with a new poling technique (patent applied for), and have recorded an equivalent voltage V_{rec} ~8 kV (defined as the voltage needed to cancel the electric field recorded in the fiber), to the best of our knowledge the highest value yet obtained in fibers.

7 Poling of fibers

7.1 Introduction

There are reports on several different electrode configurations used in fiber poling experiments. In the two first experiments done in 1994 d-fibers were used. Long et al. thermally poled a fiber to induce a linear electro-optic coefficient of 0.05 pm/V [72]. Kazansky et al poled fibers both thermally and with e-beam and found $\chi^{(2)} = 0.2$ pm/V [41]. In another early attempts to pole a fiber, a commercial polarization maintaining fiber was used. The fiber was etched to decrease the anode-core distance and then placed between two electrodes [26]. To prevent dielectric breakdown through the surrounding air, both the fiber and the electrodes were covered with polyimide. The total distance between the electrodes was ~45 μm and the poling voltage would have been limited to ~100 V, had it not been for the polyimide. Usually the depletion region is wider for a large poling voltage and with the polyimide 2.7 kV could be applied [26] to give a electro-optic coefficient of 0.3 pm/V. The technological advancement of preform- and fiber production has made it possible to produce micro-structured fibers with complicated cross sections. Most fiber poling experiment reported recently use fibers with electrodes embedded in holes that run along the fiber on each side of the core, Figure 7.1. One big advantage in doing so is that very high electrical fields can be applied with little risk of dielectric breakdown.

One main difference between poling of bulk glass and fibers is the distance between the electrodes, ~20 μm for fibers as compared to the distance in bulk, usually 500 μm or more. The small distance between the electrodes limits the highest voltage that can be used during poling. At poling temperature (280 ^{o}C) the breakdown field is reported to be ~5×10^{8} V/m for silica glass [73,74]. If this value is true for the fiber shown in Figure 7.1, it limits the maximum poling voltage, V_{break} to ~7.5 kV, given that $V_{break} = E_{break}\, d$, where d is the distance between the holes. Most of our fibers did not withstand such a high voltage and broke when applying approximately 5 kV. This could be so because the field intensity between two metallic cylinders is larger than between two metallic plates put apart the same distance. If the hole-to-hole spacing is increased the poling voltage can be increased which makes it possible to increase thickness of the depletion layer since the width scales approximately linearly with the applied voltage. The drawback of increasing the hole-to-hole distance is that once the fiber is poled, a given applied voltage produces a smaller electric field and hence the device is less sensitive to the modulation voltage.

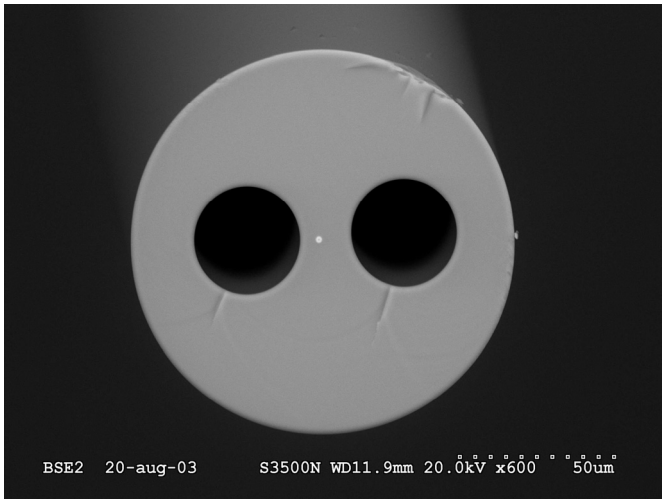

Figure 7.1 SEM image of twin-hole fiber (F030625-1E). The diameter of the fiber is 125 μm and the holes are 35 μm wide. The core is seen as a bright dot placed a little closer to the left hole. Index step of core Δn = 0.023, 4-5 times that of a SMF 28, diameter of core 2.3 μm, core-hole distance = 5.5 μm (anode). The hole-hole distance is 18 μm.

7.2 Fibers used for poling

All fibers in this thesis that were designed for poling had fused silica inner cladding, ensuring a ~1 ppm degree of alkali impurities to guarantee the creation of a space charge region. Usually synthetic silica is too pure and lacks mobile ions needed for efficient thermal poling. The fibers were all designed with the anode hole closer to the core than the cathode, to ensure good overlap between the core and the poled region. Observe that when designing the fibers we did not expect a recorded electric field outside the depletion region in poled fibers, as explained in section 6.3 and also in [paper V]. This information gives much freedom when designing the fibers and makes it possible to limit the loss caused by the electrodes by increasing the core-hole distance.

In the present section, we describe results obtained with a fiber named F031023-1c. It has a refractive index step $\Delta n = 0.025$ and N.A. = 0.27 which confines the optical mode mainly to the core. The diameter of the core is 3.6 μm and the fiber is single-mode at 1550 nm. The edge-to-edge distance between the core and the nearest hole is 4.6 μm and furthest hole 10.1 μm. The two holes are 29.5 μm in diameter and have a separation $d = 18.3$ μm, Figure 7.2.

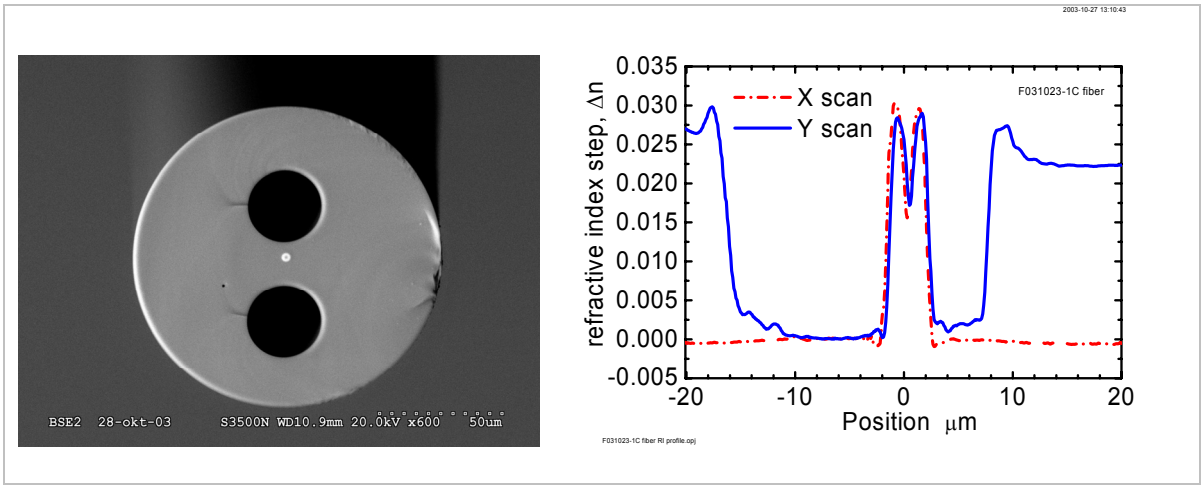

Figure 7.2. Left image shows SEM of fiber F031023-1c. Notice the small dark dot in the middle of the core that is caused by a dip in the germanium concentration. The anode electrode is inserted into the top hole before poling. Right figure: Refractive index scan of the fiber cross-section. The holes can be seen in the solid line (Y direction). Notice the refractive index dip in the middle of the core arising from uneven Ge concentration during preform manufacturing. The refractive index step, Δn = 0.025, about 6 times higher than in a SMF 28.

7.3 Growth of electro-optical response

According to Faccio et al. [67] the optimum poling time is shorter for thin than for thick samples since the initial electric field that drives the movement of ions is larger. This result, together with simulations reported [64], indicate that the optimum poling time for fibers is <1 minute. This is much shorter than the time it takes to fully develop a depletion region in bulk samples ~30 min. In all poling experiments the process is very dependent on the composition of the glass, the electrodes used and the geometry of the sample. For this reason it is very useful to measure the evolution of the electro-optical coefficient. A set-up based on a 2x2 interferometer was designed so that the poling procedure can be characterized in real time. The is described in more detail below.

The length of the electrodes in the present study was 20 cm, a compromise between maximizing the phase shift and keeping the loss caused by the electrodes reasonably small. A hotplate was used to heat the contacted fiber to 255 °C, which was poled by applying + 4.3 kV to the anode electrode and grounding the cathode. In order to characterize the growth of the electro-optical response, the fiber component was kept in an unstabilized 2x2 Mach-Zehnder interferometer (as described in chapter 3) [26,27,75,76]. A tunable laser amplified by an EDFA was used as a light source, since it had narrow linewidth and long coherence length, ensuring good contrast even if the two arms of the interferometer were not perfectly balanced in length and optical power. The MZI was very unstable because part of the interferometer was heated during poling and the fibers were not mounted together. The amplitude of the output signal varied between minimum and maximum transmission approximately once every second when the temperature of the hotplate had stabilized at the poling temperature.

The growth of the linear electro-optical effect was studied by examining the evolution of the maximum contrast obtained for a small sinusoidal electrical signal. Before poling, only

a weak Kerr response was measured in the interferometer. Therefore, a sinusoidal probe signal of a few hundred volts and frequency of 1 kHz led to a weak amplitude modulation of the light transmitted by the MZI. A HV pulse lasting for 1-2 minutes was applied to the anode electrode of the heated fiber, which weakly poled it. The HV pulse was switched off momentarily, and the sinusoidal probe showed a slightly enhanced modulation. This process was repeated many times, the high voltage pulses poled the fiber, and the small sinusoidal electrical signal probed the interferometer in the absence of the poling voltage. The thermal fluctuations changed the amplitude of the optical modulation, which has a maximum when the interferometer is in quadrature. The reading was always taken at maximum amplitude. After a total time interval that could exceed half an hour, the poling process was saturated, and the amplitude of the modulation induced by the sinusoidal signal did not grow anymore. A plot in time of the evolution of the electro-optical response is illustrated in Figure 7.3 where the last two points were measured at room temperature where. The higher amplitude in these two points indicate that the fiber was poled after the hotplate was switched off.

The characterization was carried out at 1550 nm, where the fiber used was single-mode. Incidentally, except for an estimate of the nonlinearity induced in a Photonic Crystal Fiber by the ORC (Southampton) in 2002, the studies in this report are the first of poled fibers carried out at 1.55 μm in the literature.

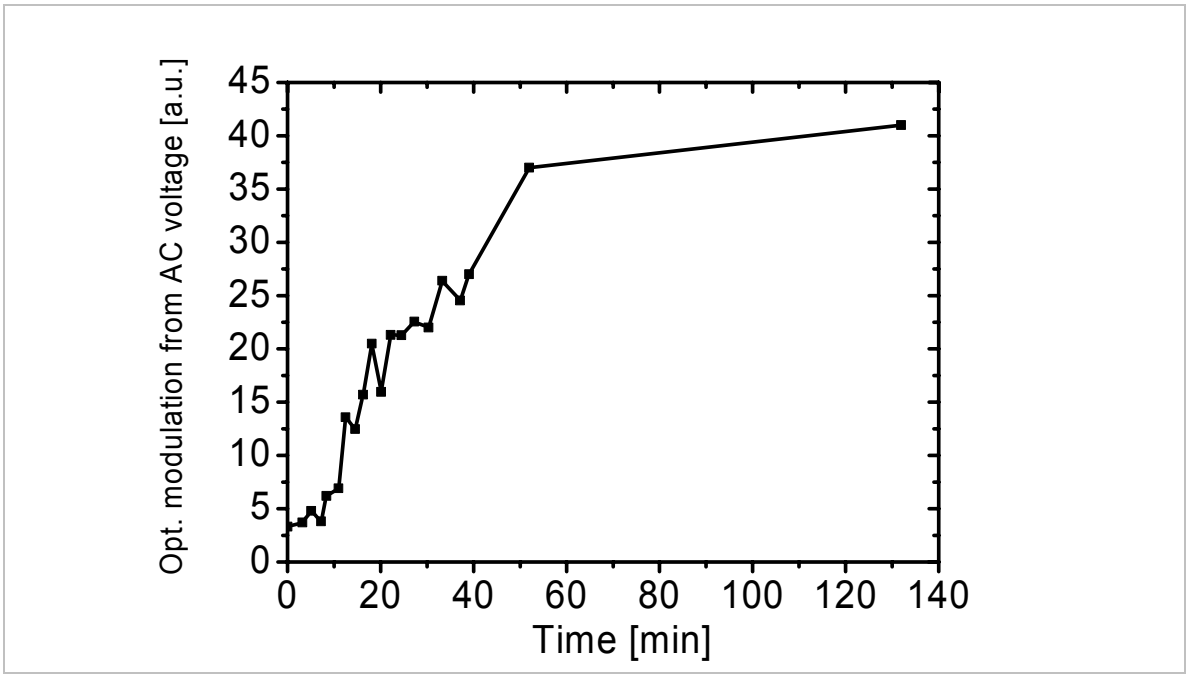

Figure 7.3. Example of poling evolution at 255 ℃. The optical response of a 2x2 fiber switch to a 400 V sinusoidal signal is plotted. The poling voltage is switched off periodically for a short time interval during which the measurements were made. The two last points were measured at room temperature.

In the measurement shown in Figure 7.3 the poling voltage was applied in pulses. The characterization of the poling efficiency by switching off the poling bias for a short time while the sample is at high temperature has the disadvantage that partial erasure of the recorded field cannot be excluded. Therefore a new method was developed where the small sinusoidal signal was coupled to the cathode of the fiber, while at the same time applying

high voltage to the anode. This enabled measuring of the evolution of the electro-optic effect, while at the same time poling the fiber. By repeating the same measurement for several different poling temperatures, it could be determined how the speed of the evolution varied with temperature as shown in Figure 7.4. At 235 °C there is an optimum poling time of ~350 minutes, after which the electro-optic response starts to decay. By further increasing the temperature to 255 °C the optimum was reached after only 20 minutes. The sharp increase in the evolution is attributed to the mobility of sodium which dramatically increases in the given temperature interval. Notice also that the behavior at 255 °C and 265 °C is very similar, indicating that the evolution cannot be significantly speeded up by increasing the temperature. Notice that the electro-optic coefficient is a direct consequence of the electric field in the glass and that in this measurement the DC electric field is including the externally applied poling voltage. Therefore, care has to be taken when interpreting the data to correctly distinguish between the recorded- and the applied poling field. The maximum in Figure 7.4 indicates when the depletion region has the most efficient overlap with the core. Furthermore, the electric field distribution changes after cooling the down the sample since the resistivity of the glass is increased many orders of magnitude. This means that an applied field after poling is going to be evenly distributed between the electrodes much like in a capacitor and therefore give smaller intensity modulation.

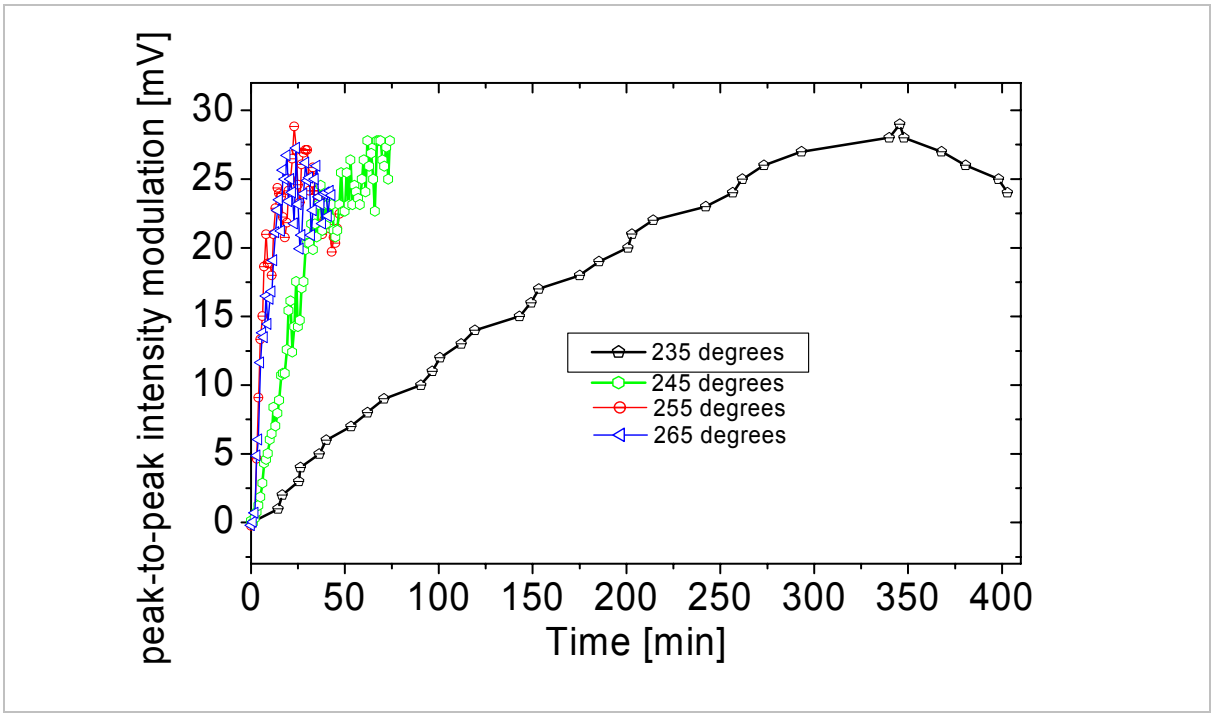

Figure 7.4. Measurement of the evolution of the electro-optic coefficient at different poling temperatures. By increasing the temperature the evolution becomes much faster, but the shape is more or less preserved with *a peak after a certain time followed by a slow decay.*

7.4 Optical response

The characterization of the poled devices at room temperature was carried out as before with the active fiber as one arm of the Mach-Zehnder interferometer. A tunable laser was

exploited, since by adjusting the wavelength one can chose the operation point of the interferometer (for example, in quadrature, or at maximum extinction). The active fiber was characterized both before and after poling by applying a 0 - +3 kV linear voltage ramp to the anode electrode and detecting the optical intensity in one of the two output fiber ports. The voltage ramp was sufficiently fast (10 ms) to eliminate the thermal fluctuations of the MZI, which slowly changed the operation point over times of several seconds.

The phase change is related to the refractive index change through: $\Delta\phi = (2\pi L\Delta n) / \lambda$, where L is the length of the region where the index change is induced. By using the expression for Δn from eq. 2.5.6 describing the refractive index change with an applied electric field and assuming that the power in both arms are equal to give total extinction, the optical output of the interferometer is described by (modified from [77]):

$$I_1 = I_o\left\{ 1 + \cos\left[\Delta\phi - \Delta\phi_o\right] \right\} = I_o\left\{1 + \cos\left[\frac{3\pi L}{\lambda n_o}\chi^{(3)}\left(E_{ext}^2 + 2E_{ext}E_{rec} + E_{rec}^2\right) - \Delta\phi_o \right]\right\} \quad \textit{(eq. 7.1)}$$

where I_o is the modulation amplitude, L is the length of the active region, λ is the operating wavelength of the interferometer (1.55 μm), n_o is the unperturbed refractive index, $\chi^{(3)}$ is the third-order nonlinear coefficient and E_{ext} and E_{rec} the externally applied- and recorded field, respectively. $\Delta\phi_o$ is the residual phase change due to the difference in arm lengths and thermal/mechanical instabilities. Note that in this description, if the arms are not equal in length then $\Delta\phi_o$ is a function of λ. Before poling, $E_{rec} = 0$ and $\Delta\phi \propto E_{ext}^2$ while after poling $\Delta\phi \propto (E_{ext}+E_{rec})^2$. An externally applied voltage is assumed to give an electric field inside the fiber, $E_{ext} = V_{ext} / d$, where d is the distance between the holes. Likewise, it is assumed that $E_{rec} = V_{rec} / d$. These hypotheses are not as simple as they may seem at first and have an implicit assumption that the change in resistivity of the glass during poling does not affect the way in which the voltage is divided at room temperature. This is a violation of Ohm's law, since the depletion region is (nearly) free from cations and has a resistivity orders of magnitude larger than that of unpoled glass. The justification for this assumption – which seems to work in general – is that a poled fiber at room temperature behaves more as a charge capacitor than as a resistor. The charges are frozen and the resistivity is so large - even where some impurity remains - that the drift current at room temperature can be considered zero. At high temperature the glass behaves more like resistor.

As mentioned above, the phase change after poling is $\Delta\phi \propto (E_{ext}+E_{rec})^2$, while before it was $\Delta\phi \propto E_{ext}^2$. Since the recorded field E_{rec} is a constant, the phase has the same quadratic dependence of the externally applied field, E_{ext}, as before poling under the assumption that the field distribution between electrodes does not change because of poling ($E_{ext} = V_{ext} / d$), and that $\chi^{(3)}$ does not change. A change in $\chi^{(3)}$ has been reported by several groups [8], but as discussed below in our work with thermal poling of optical fibers we have not found evidence that this happens. Within the error bar of our measurements, $\chi^{(3)}$ remains constant.

Before poling, the parabola has minimum at $E_{ext} = 0$, while after poling the parabola is translated by the recorded field E_{rec}, so that with $E_{ext} = 0$ the phase change $\Delta\phi$ is no longer near its minimum, as illustrated in Figure 7.5. The fact that the quadratic term disappears in poled samples and that the linear electro-optic effect does not is because for small

modulation around $E_{ext} = 0$ the phase excursion is approximately linear as illustrated by the dotted line in Figure 7.5. This was recently pointed out in the literature [78].

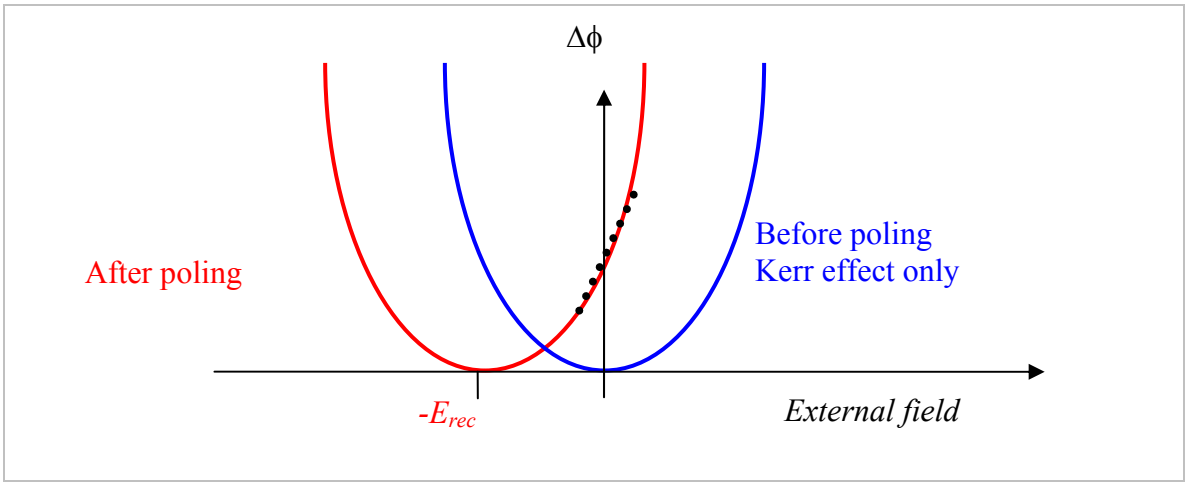

Figure 7.5. Phase shift vs. applied field before and after poling. The drawing assumes that the creation of a depletion region does not alter the relation $V_{ext} = E_{ext}\, d$, where d is the distance between electrodes and that $\chi^{(3)}$ remains constant. The parabola that relates the phase shift to the externally applied field due to the Kerr effects is displaced by E_{rec} but maintains its shape after poling, i.e. same opening. The linear electro-optic effect is experienced for small applied fields (dotted line).

Figure 7.6 below illustrates the first characterization results obtained for the MZI driven with a voltage ramp where it is seen that for the unpoled fiber $\Delta\phi \approx 1.5\ \pi$ for 3 kV applied, while for the same applied voltage, $\Delta\phi \approx 2.5\ \pi$ for the poled fiber. For this 20 cm long fiber, $V_\pi \approx 1.37$ kV at 1550 nm. The inset of Figure 7.6 shows the quadratic relation between the phase and V_{ext} derived to give the best fit of equation (eq. 7.1) to the two experimental curves shown. The parabolas give a value to $\chi^{(3)}$ and E_{rec}, which determine the opening and the position of the minimum of the curves, respectively. A good fit for a value of $\chi^{(3)}$ in the range $(2.1\pm0.3)\text{x}10^{-22}$ m^2/V^2 before and after poling was obtained, in relatively good agreement with the value of $\chi^{(3)}$ expected for Ge-doped silica.

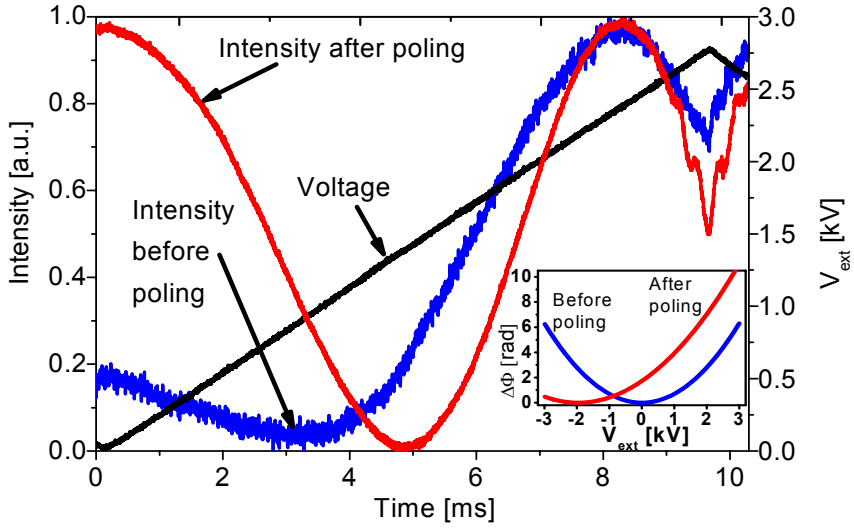

Figure 7.6. Intensity response of a Mach-Zehnder interferometer with the fiber component as the active arm. V_π 1.37 kV at 1550 nm after poling. The intensity response is given by Eq. 7.1. The inset shows the parabolic relation between $\Delta\phi$ and the applied voltage, V_{ext}, obtained by fitting Eq. 7.1 to the measured intensity. The signal is noisier before poling because the fiber was not as firmly mounted as after poling.

When closely examining the results in Figure 7.6 it was found that a fit to such a limited phase excursion is very imprecise when determining $\chi^{(3)}$ and E_{rec}. Figure 7.7 illustrates the small difference in fitting curves obtained when V_{rec} is varied widely from 1200 V to 1950 V, leading to a $\chi^{(3)}$ value that varies from 1.86 to 2.36×10^{-22} m^2/V^2. The conclusion is that such a fit is too inaccurate for the determination of the equivalent recorded voltage V_{rec}, and an alternative measurement is desired.

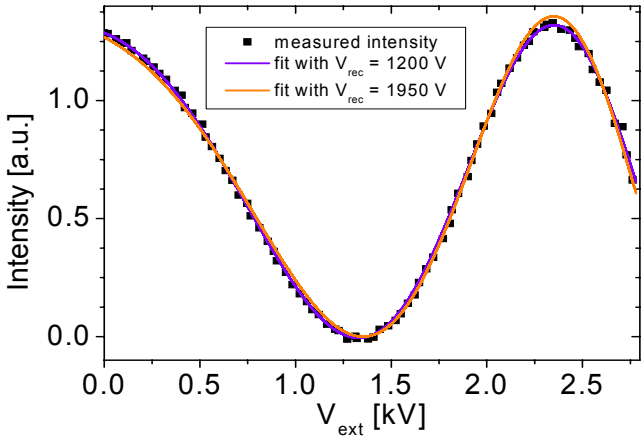

Figure 7.7. Optical intensity versus applied voltage for the data points shown in Figure 7.6(red) after poling. Two relatively good fittings are shown using Eq. 7.1, where very different values of V_{rec} are used (1200 V and 1950 V). This shows that the fit using such a limited phase excursion is very imprecise when determining the recorded field. Likewise, the value of $\chi^{(3)}$ inferred varies from 1.86x10^{-22} m^2/V^2 (violet curve) to 2.36x10^{-22} m^2/V^2 (orange curve). Both fittings are well within the error margin of the experiment.

7.5 Recorded electric field

To directly measure the field recorded after poling, the fiber was kept in the same MZI as described in chapter 3.1, and probed with a 400 V AC peak-to-peak voltage at 1 kHz added to a DC bias. The optical intensity showed a modulation resulting from the AC voltage, and the peak-to-peak excursion was recorded for different applied DC voltages. By slightly adjusting the wavelength of the laser, the interferometer was placed in quadrature before each measurement. Minimum modulation of the optical signal, i.e., minimum excursion of the 1 kHz signal, is achieved when the external DC bias cancels the recorded field. In this case, the red parabola is brought back to the position of the blue parabola in Figure 7.5. The result of the measurement is shown in Figure 7.8 (left). The external voltage was measured to be –1.1 kV, and thus the equivalent recorded voltage is V_{rec} = + 1.1 kV. This is significantly lower than the voltage used during poling of the device (4.3 kV). In another measurement carried out at a later stage with another piece of fiber (with improved oven uniformity), we were able to record a field more than twice as high, 2.5 kV, as shown in Figure 7.8 (right). With this method it is possible to get a much more accurate measurement of the recorded electric field. Notice that the peak-to-peak modulation becomes constant for DC biases higher than 2.5 kV in the right figure. This is because the phase shift, $\Delta\phi$, introduced by the AC signal is larger than π, thus saturating the optical response since the maximum modulation depth is obtained for $\Delta\phi \geq \pi$.

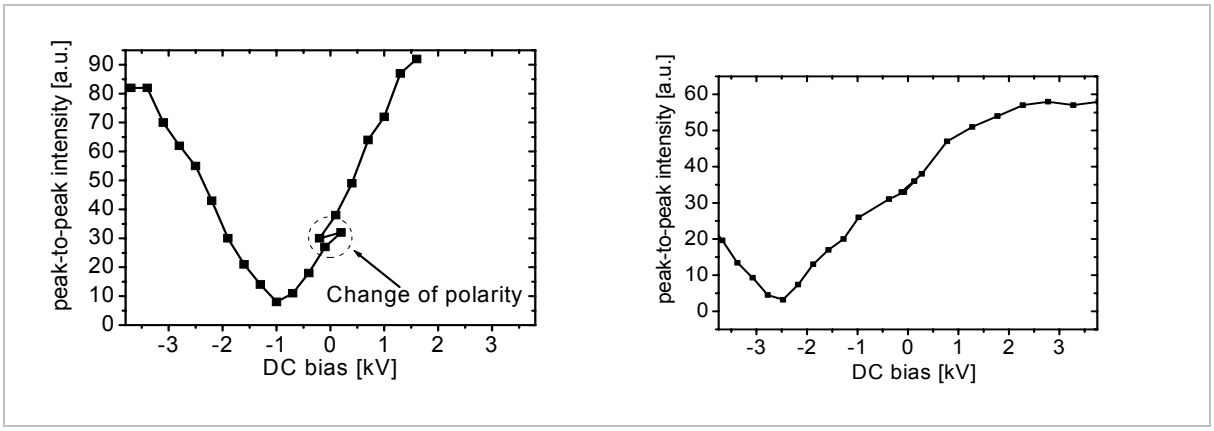

Figure 7.8. Peak-to-peak optical signal excursion when the MZI is driven by a 400 V sine voltage added to a DC bias. The minimum corresponds to the external voltage that cancels the effect of the recorded field. The left figure shows a fiber with ~1 kV recorded and the right figure shows a fiber with ~2.5 kV recorded.

7.6 Etching of poled fused silica

Fused silica is very resistant to most substances. The only chemical that efficiently etches silica is hydrofluoric acid (HF). A solution with 40 % concentration of HF etches silica at ~1 μm/minute [79]. The etching rate in a direction parallel to the recorded electric field is reported to be depending on the electric field in the glass [79] and has been used to determine the electric field recorded in poled samples. The etching rate is easily monitored in a set-up with a HeNe laser reflected of the surface being etched and a reference surface (the top surface of the sample), a scheme similar to a Michelson interferometer. The poled sample is etched parallel to the anodic surface and the optical path length in that arm therefore changes which is detected in the interference fringes of the interferometer. Etching of poled samples in 40 % HF showed that the electric field is almost constant in the entire nonlinear layer (Figure 6.1) except for fluctuations near the anode surface [73]. Upon etching through the entire nonlinear layer in bulk samples the etching rate abruptly changes to a value close to that of an unpoled sample. In chapter 6.2 it was described that an electric field is present also outside of the depletion region, however, for bulk samples it is very weak.

The spatial distribution of the recorded effective nonlinearity is very important since it determines the amount of nonlinearity experienced in the core of the fiber. By only measuring the electro-optic effect it is not possible to obtain information about the distribution of the nonlinearity in the glass. By completing the characterizations with etching experiments, a more complete picture can be obtained. Figure 7.9 shows an example of a poled, cleaved and etched bulk sample, visualized with a phase contrast microscope. In this experiment the etch direction is orthogonal to the recorded electric field. The technique to etch cleaved samples to study the depletion region was originally demonstrated by Alley and Brueck [80] using an atomic force microscope, AFM. The etch rate of silica glass depends on the electric field in the direction of etching. When etching fibers the recorded field is orthogonal to the etch direction and therefore the etching does not reveal the magnitude of the field. Nevertheless, the pattern that is generated can be used to determine the location of the depletion region since the etching rate depends on the fringing field and/or differences in charge carrier concentration.

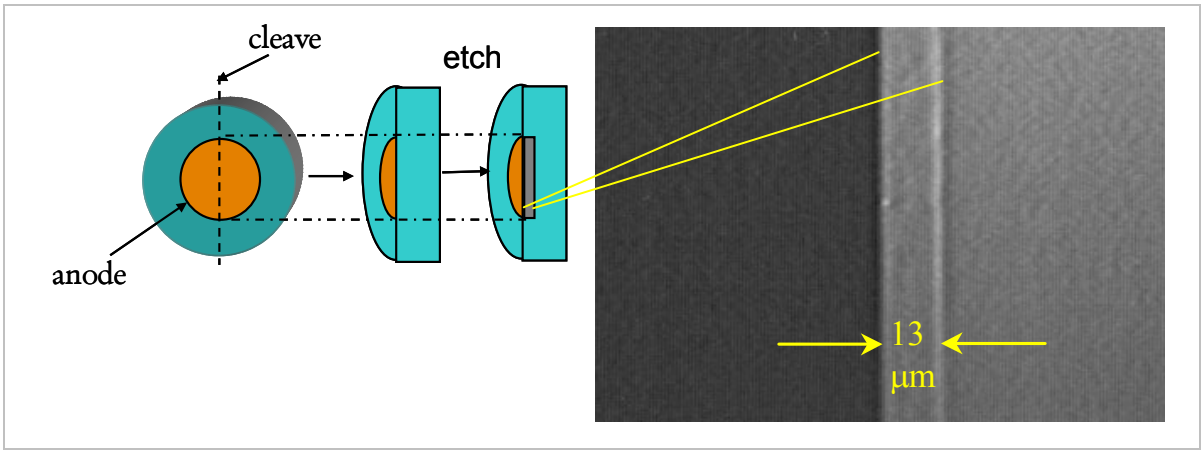

Figure 7.9. Depletion in thermally poled bulk fused silica. The sample was cleaved and etched for 30 seconds. The picture was taken with a phase contrast microscope [paper II]. The etch direction is orthogonal to the electric field.

The fibers to be characterized were first poled and cooled down to room temperature. After poling, the acrylate coating was removed and the fiber cleaved several times in the poled region. In order to reveal the recorded electric field the cleaved ends of the fiber pieces were etched in 40 % hydrofluoric acid (HF) for 45 seconds [7]. After etching, the fibers were cleaned with distilled water and dried by first using compressed air followed by heat treatment at 150 °C. This procedure has been previously used to image the depletion region in poled fibers, since the etching rate is affected by the presence of an electric field as described above. The difference in etching rate results in topographical differences, which can be visualized by scanning electron microscopy (SEM) [81], atomic force microscopy (AFM) [80,82] and by phase contrast microscopy (PCM).

The main drawback of using AFM is that it is very difficult to obtain accurate information when scanning the cleaved end of a twin-hole fiber. First of all, the fiber is very thin and easily moves with the touch of the probe tip. Secondly, the depletion region is located close to the anode electrode and when the fiber is cleaved and etched the electrode sometimes protrude from the hole and sometimes it is hidden in the hole. In either case, the AFM probe is easily destroyed when hitting the electrode/edge of the hole. Because of these two reasons it was very time consuming to obtain a usable image. Nevertheless, it is possible to obtain very detailed images as seen in the right picture of Figure 7.10.

When hitting the fiber with the electron beam of the SEM the surface of the fibers was charged, which completely distorted the image. By carefully mounting the fibers and grounding everything but the cleaved end with conductive paint, this problem could be avoided to some extent. Using low acceleration voltage for the electron beam also made this problem less severe. Even with all these precautions, it was difficult to obtain sharp pictures and the resolution was usually far from optimum. An example of a SEM image is shown in the middle picture in Figure 7.10.

The PCM is a very fast way to characterize the cleaved and etched fibers and height differences of only a few 100 nm is easily seen. A set of samples can be scanned quickly to

determine if the poling process was successful. For the above mention reasons PCM was found to be by far the quickest and most efficient method to visualize the etched region.

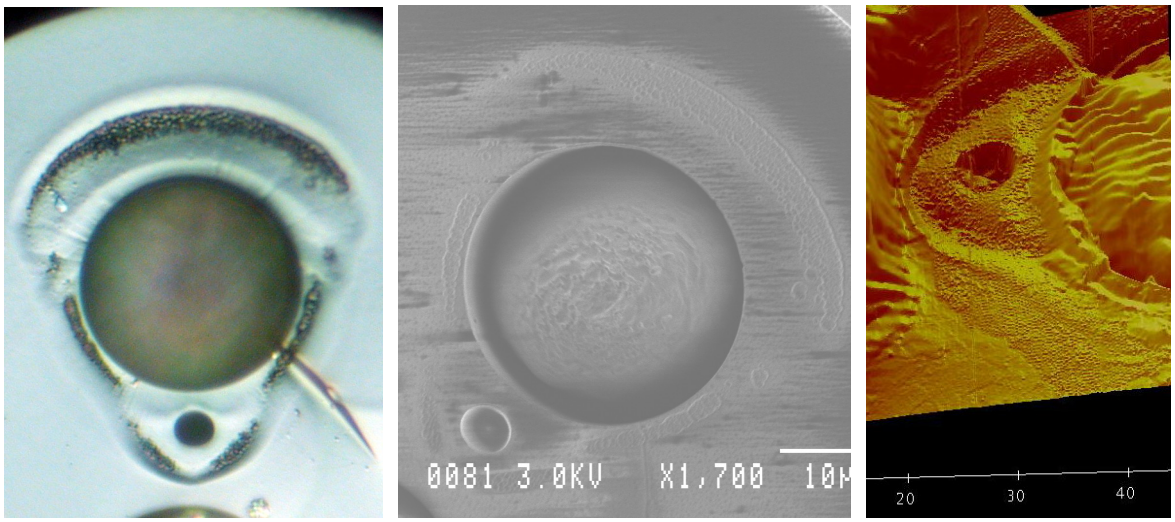

Figure 7.10. Depletion region in fiber etched in HF during 45 seconds and visualized with different techniques. The left image was obtained with a phase contrast microscope, notice the crack on the right side of the hole introduced when cleaving the fiber. The middle picture shows a SEM image with excellent spatial resolution in the plane but poor resolution in the longitudinal direction. The right image was obtained with AFM, giving very high resolution, but the measurement is difficult to perform because of the geometry of the fiber.

Etching revealed that under the present poling conditions the depletion region in the present fiber the depletion region is wedge-shaped and points towards the cathode, see Figure 7.11 (left), in contrast to the round shape previously reported by the research group at the university of Sydney [82]. The depletion layer extends furthest between the electrodes, 13 µm, which to the best of our knowledge is by far the widest depletion region recorded in a fiber. It is obvious from Figure 7.11 (left) that here the poling time was excessive, and that the depletion region is unnecessarily wide, since it extends past the core. The recorded field in the core can be increased with shorter poling times. At the side of the anode opposing the core the depletion layer is also quite wide (10.2 µm). This indicates that the electric field during poling must have been almost as strong between the anode and the outer surface of the fiber as between the two electrodes. This implies that the outer surface of the glass fiber behaves as if it was electrically grounded during poling, which is expected since the fiber was placed on a grounded metal hotplate. It is therefore likely that it can gather a large density of charge of the appropriate sign from the surrounding heated air, in spite of the electrically isolating primary coating. From work carried out by Faccio et. al. [67] it is known that the thickness of the depletion region developed during a certain poling time interval depends on the electric field applied. The field distribution in the fiber during poling was simulated (Figure 7.11, right) to determine if the pointed shape could be explained by the electric field during poling. Good agreement with the observed etched pattern was observed when the outer surface potential was simulated to be equal to the cathode potential (electrically grounded).

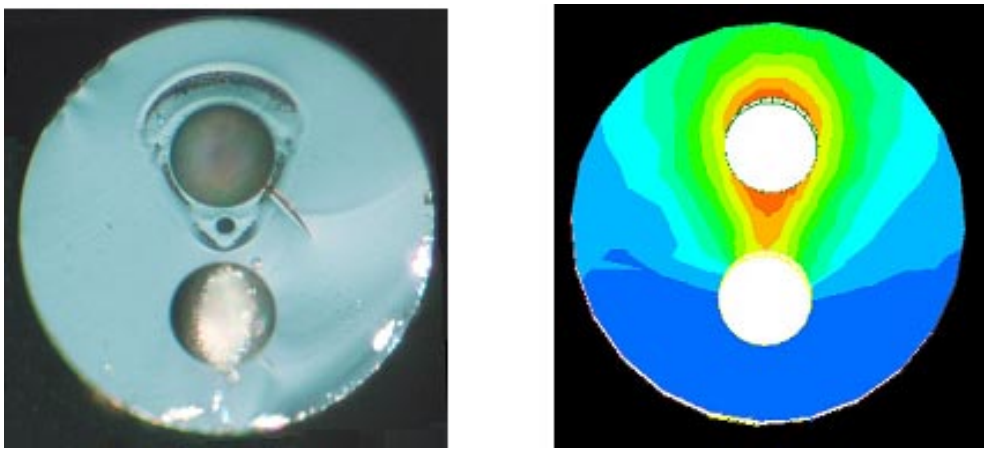

Figure 7.11 Left: Poled 125 μm fiber etched for 45 seconds and imaged using a phase contrast microscope. Right: simulation of the electric field applied during poling, assuming that the outer surface of the fiber is grounded. The agreement is good and explains the pointed shape of the depletion region [paper IV].

7.7 Spatial evolution of the nonlinear region

In Figure 7.4 it is shown that the effective electro-optic coefficient grows and decreases in time. This growth is associated with the creation of a space charge region. The growth of the electro-optic coefficient is to some extent associated with the increasing overlap between the recorded field and the optical mode. In order to study this evolution it is very useful to etch fibers poled during different time intervals. In order not to have to pole a new fiber for each poling time, one fiber was placed in a temperature gradient and poled. Since the evolution speed of the electro-optic coefficient is dependent on the poling temperature as seen in Figure 7.4, it is assumed that poling at a slightly lower temperature is equivalent to shortening the poling time. This is a good assumption if the process is diffusive and dominated by a single time constant – not the case in poling. Nevertheless, the experiment is then simplified and still gives useful information about the evolution of the depletion layer. The evolution of the depletion region is shown in Figure 7.12, where the picture (i) is the same as in Figure 7.11 showing the final state of the depletion region, with a complete overlap with the core. From pictures (a-c) of Figure 7.12 it is clear that the nonlinear region does not reach the core of the fiber. In picture (h-i) it is seen that the core affects the evolution of the poling process. Perhaps the high Ge concentration acts as a barrier to the mobile sodium ions, thereby changing the recorded field in the neighborhood of the core. The field distribution schematically shown Figure 6.2 then raises the following question: if the core is located outside of the depletion region when poling is interrupted, is the recorded field experienced by the core reversed, i.e., points from the cathode side to the anode side? Also, if the negative charge distribution is located in the middle of the core, is the recorded field experienced by the light zero? A sign reversal of the electric field as a function of poling time in optical fibers has not been reported in the literature, and this can be an indication that the understanding of the process of poling was incomplete or incorrect. A new experiment was then designed, where the recorded field magnitude and direction is recorded for different poling times.

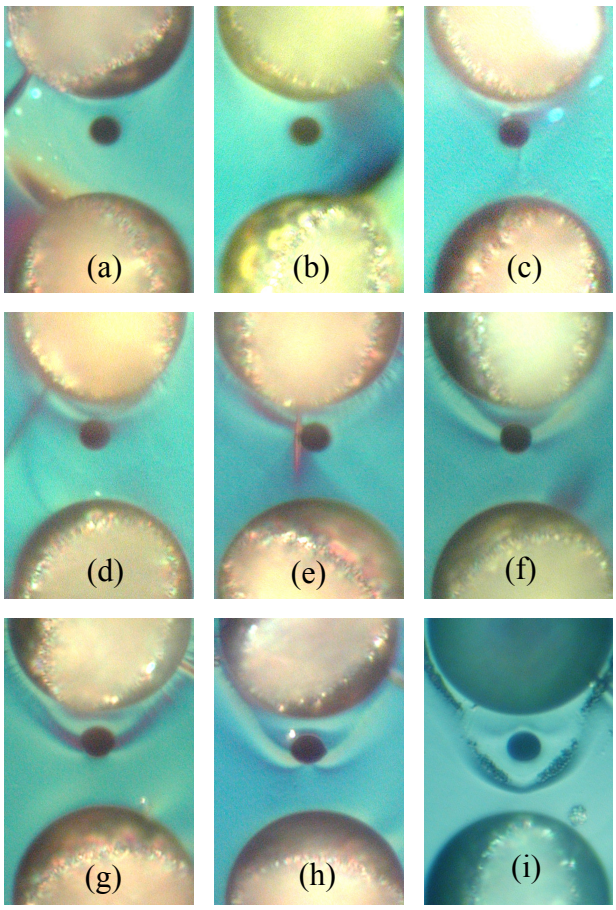

Figure 7.12. Spatial evolution of the depletion region measured by etching. Sample (a) was subjected to the lowest temperature and (i) to the highest. The overlap between the depletion region and the core improves until the region encompasses the entire core. Note the substructure in (i) just above the core, it cannot be ruled out that the high Ge-concentration in the core acts as a barrier to the mobile ions [paper V].

Unfortunately, the fiber used in the measurement shown in Figure 7.12 was consumed in various experiments and a new fiber, F040407-1b2 was drawn with core-anode separation 7 µm (rather than 5.5 µm in the previous one). The slightly larger distance meant that the poling time interval necessary for a good overlap with the core was expected to be slightly longer than for the previous fiber. When etching a poled fiber it was found that the distinct wedge shaped depletion region created by poling in the previous fiber (F031023-1c) was not reproduced in this fiber. The recorded field in this fiber was also lower than in the previous fiber, and in none of the ~20 poled samples the recorded voltage exceeded 3 kV.

To get a better understanding of how the nonlinear layer evolves, a new experiment was designed, similar to the one previously described in Figure 7.12. This time the poling time rather than the poling temperature was varied. Since the hotplate previously used has a high thermal capacity and therefore cools slowly, a different oven was utilized which was 2.5 cm long and had an opening so that the fiber could be inserted from the side, as can be seen in Figure 7.13. The oven was previously developed at Acreo for processing of fiber Bragg gratings at high temperature [83].

A piece of fiber was provided with long electrodes, and inserted from the side of the oven with the high voltage applied. In this way, 2.5 cm long sections of the fiber were poled for times ranging from 1 minute to several hours. Since the thermal mass of an optical fiber is very small, side-insertion makes it possible to pole a fiber during as little as one second, but this was not necessary here. Every poled fiber section was separated by 5 cm from the previous one and the experiment was carried out at a poling temperature of 255 °C and poling voltage 4.3 kV.

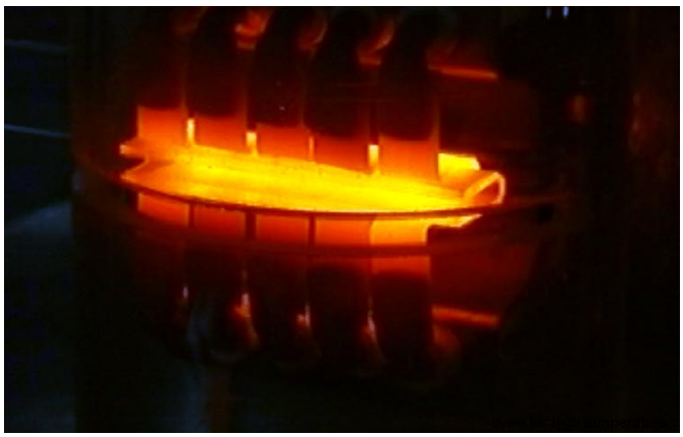

Figure 7.13. Oven used to pole the fiber for different time intervals. The oven is open at one side so that fibers can be quickly inserted and removed, and has a low temperature gradient in the hot zone.

As expected, it was possible to observe a gradual increase in the width of the depletion region with poling time as is shown in Figure 7.14. The shape of the region revealed by etching was initially round and evolved towards a guitar-like shape. The region is somewhat pointed, but far less than what was measured with the previous fiber, which is peculiar, since during fabrication attempts was made to reproduce the same manufacturing conditions. Note also that the side of the depletion region facing the outside of the fiber is narrower compared to in the previous fiber. This could be explained by the fact that the fiber was suspended in air during poling and not placed on a grounded hotplate as was the case for the previous experiment. After a poling time t = 64 minutes the region extends past the centre of the core, implying that it should be possible to see a sign reversal in such experiments. The two rings shown on the bottom right photograph are a preliminary attempt to explain the guitar shape, and mark the transition between two perform tubes of fused silica glass. By etching an unpoled fiber, this transition was clearly seen and it is possible that this interface acts as a barrier to the mobile ions during poling. This needs further investigation.

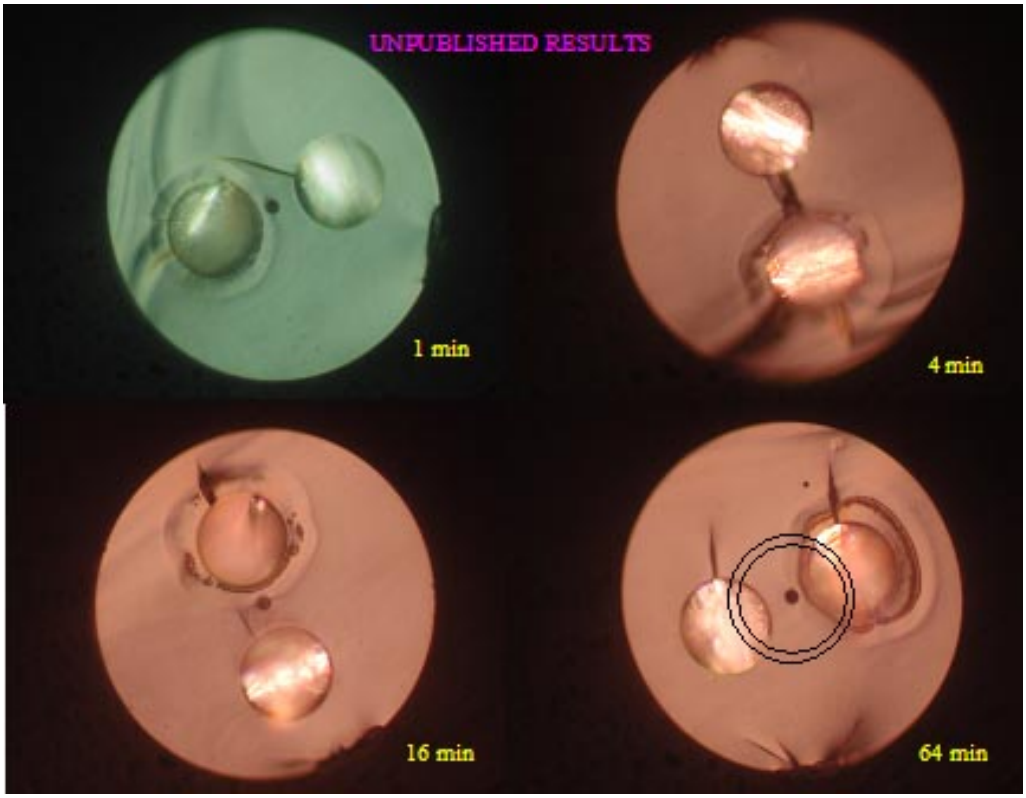

Figure 7.14. Spatial evolution of the depletion region in new fiber, F040407-1b2, poled at 255 °C for various time intervals. The two rings drawn in the lower right picture indicate a transition between two perform tubes, which could explain the strange shape of the depletion region.

After poling and etching, a new piece of fiber was prepared with 1.2 m long electrodes and poled at 5 kV and 255 °C for various time intervals in succession. The equivalent recorded voltage was measured for each poling time by applying an external DC bias to one electrode, as in Figure 7.8, and applying a small AC voltage to the other electrode. When the recorded and external voltages cancel, the interferometer temporarily loses its linear electro-optic response, and the optical modulation has a minimum. Figure 7.15 (left) shows an alternative approach of measuring the recorded voltage which is fast to perform. By applying a linear voltage ramp, which cancels the recorded voltage, it is possible to reach the minimum of the phase-shift-parabola as shown in Figure 7.5. The parabola was obtained by fitting a curve to the measured optical response to recover the phase shift. Since the phase shift is equal on both sides of the minimum in the parabola, this produces a symmetry point in the optical response. Figure 7.15 (right) shows the recorded field vs. time displayed on a log scale (horizontal axis) to expand the shorter time intervals. It is clear that until the fiber has been poled for approximately 20 minutes, the recorded field has negative sign, i.e., points from the cathode to the anode, since the depletion region does not yet cover the core. It is also apparent that when the edge of the depletion region crosses the core position, the sign of the field changes. In this and another similar measurement the maximum field recorded after long poling times, many hours, is similar to the largest obtained with opposite sign for short poling times i.e., at t = 9 and at t = 1000 minutes the field is comparable. This is expected from the geometry of the fiber since for short poling

times i.e. 9 minutes the depletion region reaches all the way to the core, while for long poling times i.e. the depletion region completely overlaps with the core. The corresponding electric fields are found as in section 6.3. The conclusion from the measurements is that indeed the recorded field can point in either direction depending on the position of the core and the extent of the depletion region.

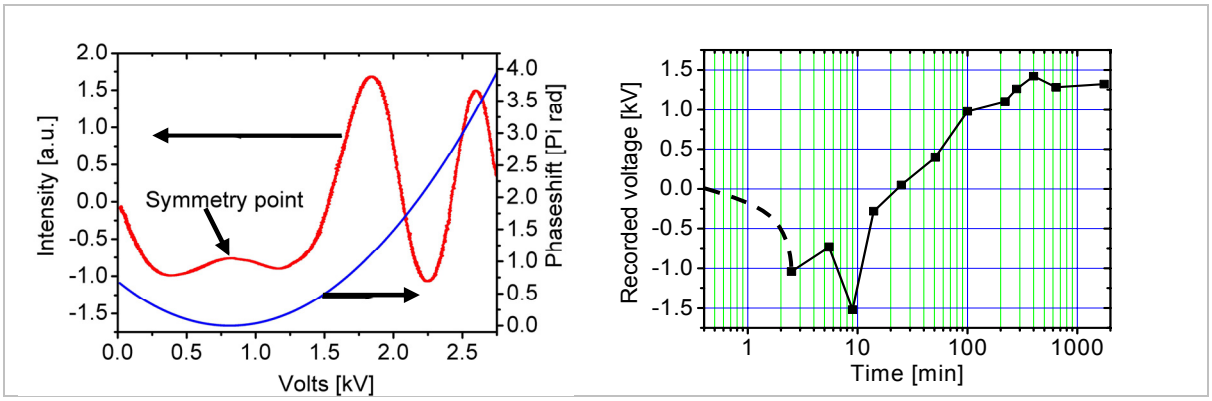

Figure 7.15. The left figure (red) shows the intensity response to a linear voltage ramp. When the phase-shift-parabola (blue), has a minimum a symmetry point is produced in the intensity response. The right figure shows the recorded voltage vs. time. The sign reverses after ~20 minutes, and it can also be seen that the recorded voltage for short times is of equal magnitude, but opposite in sign compared to the voltage recorded for long poling times.

Further evidence of the sign reversal is shown in Figure 7.16, where the phase shift (in π radians) is plotted as a function of applied voltage for another poled fiber. The minimum of the parabola for a poling time 60 minutes is positive, i.e., the recorded field is negative. After a longer poling time, the minimum of the parabola shown in Figure 7.16 (right), becomes negative, indicating that the recorded field is now positive. This is further evidence that there is a recorded electric field present outside of the depletion region in poled fibers.

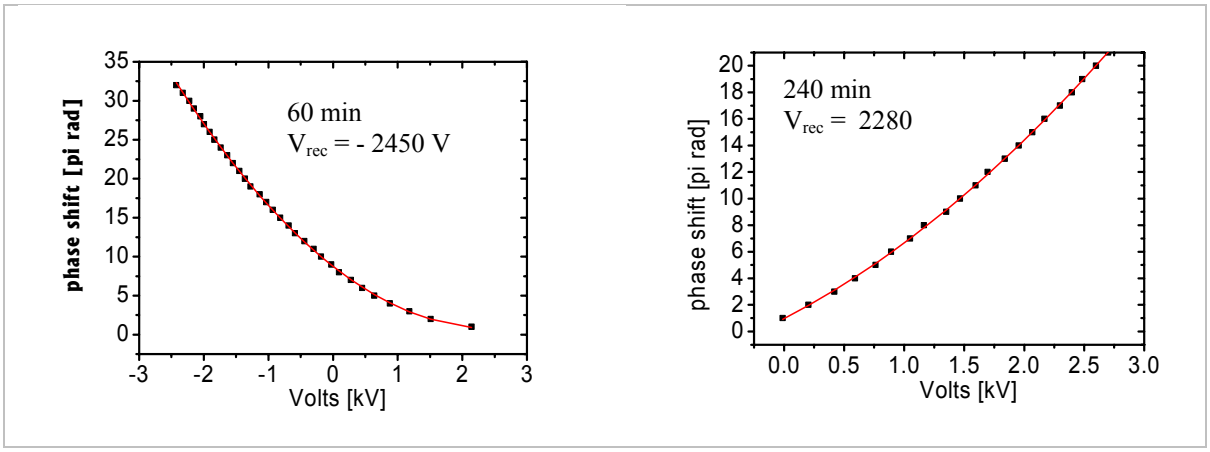

Figure 7.16. Measurements of the phase shift induced as a function of the external voltage applied for two poling times, 60 minutes left, and 240 minutes right. The minimum of the parabola goes from positive (left curve) to negative (right curve), showing that the recorded field has reversed direction during poling. The solid line is the best quadratic fit.

7.8 New poling technique

It is fair to say that the Glamorous project led to a much better understanding of the mechanisms behind poling. Making use of the information contained in the previous sections, a new poling technique was developed, which allowed substantially higher electric fields to be recorded in the poled fibers, and thereby significantly reducing the switching voltage. The main performance parameters are expected to be the same as in conventional thermal poling, such as the stability. A patent application has been submitted, and at present, we are waiting for a judgment from the patent office, while we further investigate the characteristics of poling in this new way. Unfortunately, this information cannot be revealed until the patent is issued. Much of the new understanding comes from discussions/papers from Yves Quiquempois who is gratefully acknowledged.

8 Packaging of poled fibers

Most characterizations can be done by splicing a poled fiber into a Mach-Zehnder interferometer and keeping the loose fibers on the optical table. Even so, external influences such as temperature changes and mechanical vibrations introduce a phase shifts in the interferometer that becomes very noisy. In order to improve the tolerance to thermal and mechanical fluctuations a few interferometers with poled fibers were placed in special packages. Many different packages were tried but they operated more or less the same way, mainly differing in design. The packages contained a rigid base that the fibers were glued to, which eliminated most external influences. The base was in some packages insulated with e.g. Styrofoam, to further improve the stability performance. An example of one of the first packaged interferometers is shown in Figure 8.1.

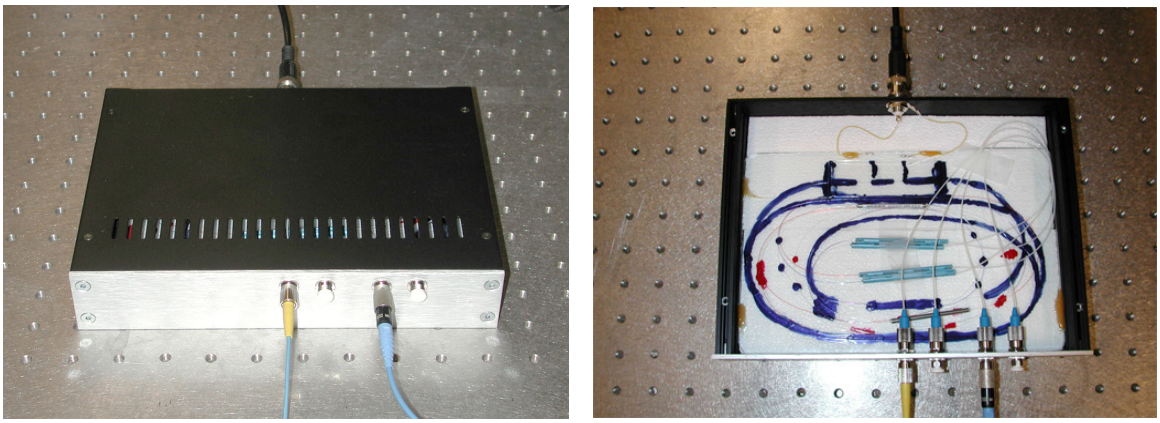

Figure 8.1. Packaged 2x2 Mach-Zehnder interferometer. Left figure shows assembled device with four optical contacts on the front side and a BNC connector for the electrical control signal on the backside. The right picture shows the inside with the two fibers in the interferometer were mounted on top of each other and attached to a glass base with blue nail varnish. Four splice protectors are seen in the middle of the picture and two thin wires are attached between the fiber electrodes and the BNC connector.

One of the goals of the Glamorous project was to develop a commercially viable technology. The package shown in Figure 8.1 worked very well, but did not have the appearance of a product ready to hit the market. A new fiber was poled and spliced between two couplers. The interferometer was then mounted in a slim package as shown in Figure 8.2 to give it a nice appearance and demonstrated at ECOC 2004 in Stockholm were it received much attention.

Figure 8.2. Optical modulator in new package as demonstrated at ECOC in September 2004 in Stockholm. A CW laser was coupled into the modulator, which was driven with the signal from a DVD player (~5 MHz). The modulated optical signal was detected with a photo diode and displayed on a TV screen to show the overall performance of the device. The two optical pigtails and the SMA connector for electrical drive signal can be seen.

At the end of a project a final demonstrator was prepared as shown in Figure 8.3. It was a 2x2 switch and the packaged used was designed by Avanex, one of the partners in the project. The device had four fibers for the optical inputs/outputs and two pins for applying the drive signal. This modulator was used when mode-locking since it did not have any connectors and therefore could be spliced to minimize reflections. More information on packaging related issues is given in a Glamorous report [84].

Figure 8.3. Final demonstrator of the Glamorous project. The package was designed by Avanex, one of the partners in the consortium. The interferometer was produced and tested by the author. This device has an optical bandwidth of 7 nm and V_π = 230 V [paper VI].

9 Performance of poled devices

9.1 Switching voltage

The same fiber as previously described, (F031023-1c, Figure 7.2), was used in the first attempt to measure V_π. The fiber was filled with an AuSn alloy and contacted. The fiber had a fused silica cladding with 1 ppm sodium and an active region that was ~25 cm long. Since the primary coating of the fiber becomes black when the fiber is heated to 300 ^oC it was impossible to tell exactly where the electrodes started and ended and the accuracy of the 25 cm is to within ± 1 cm. The fiber was poled at 260 ^oC with the voltage ramped to 2.3 kV during the first 5 minutes (in order to minimize the risk of dielectric breakdown) and then kept at 2.3 kV for another 10 minutes for a total poling time of 15 minutes. The poled fiber was placed in one arm of a MZI built with two 50/50 fiber couplers. A tunable 1.5 μm laser was connected to the input coupler of the Mach-Zehnder setup. The two arms of the coupler at the output side of the interferometer were coupled into a differential detector/amplifier (New Focus 2017 Nirvana). One arm of the Mach-Zehnder interferometer was ~15 cm longer than the other so the bandwidth of the Mach-Zehnder was very limited, meaning that even a small change of the wavelength led to a modulation of the output intensity of the interferometer. Therefore, by tuning the wavelength of the input laser the interferometer could be placed in quadrature to give maximum modulation for a given applied voltage. The optical response to an applied linear voltage ramp is shown in Figure 9.1 from which V_π can be found by inspecting the voltage needed to change the output of the interferometer from maximum to minimum intensity (taking into account the small DC bias present at the minimum), which gives V_π = 1.59 kV. Since then the switching voltage has been much improved.

The fiber shown in Figure 9.1 was the first one proved to be thermally poled in our lab. By carefully checking the poling procedure, many improvements were made. The temperature of the oven that was used for poling had a spatial gradient, which meant that different sections of the fiber were subjected to different temperatures. As shown in Figure 7.12 the evolution of the nonlinear layer is very temperature dependent. A fiber poled on this hotplate thus had had regions where the depletion region completely overlapped with the core and regions where the depletion region did not yet develop to reach the core. The directions of the electric field in these regions are opposite and when applying an external field, the refractive index changes in these sections cancel. As an example, if half the length of the poled region has one sign of the recorded electric field and the other half has opposite sign, then the refractive index change is given by: $\Delta n \propto (L / 2) (E_{ext} + E_{rec})^2 + (L / 2) (E_{ext} - E_{rec})^2 = L ((E_{ext})^2 + (E_{rec})^2)$, where L is the total length of the poled region. The cross terms, $E_{ext} E_{rec}$, cancels because of the different sign for the refractive index change in the two sections of the fiber and since $E_{rec} >> E_{ext}$ it follows that $E_{ext} E_{rec} >> (E_{ext})^2$. The conclusion is that the fiber is not very sensitive to externally applied fields, in fact. In this fiber the recorded field does not enhance the modulation and the fiber would behave like an unpoled fiber, only exhibiting Kerr effect [paper I].

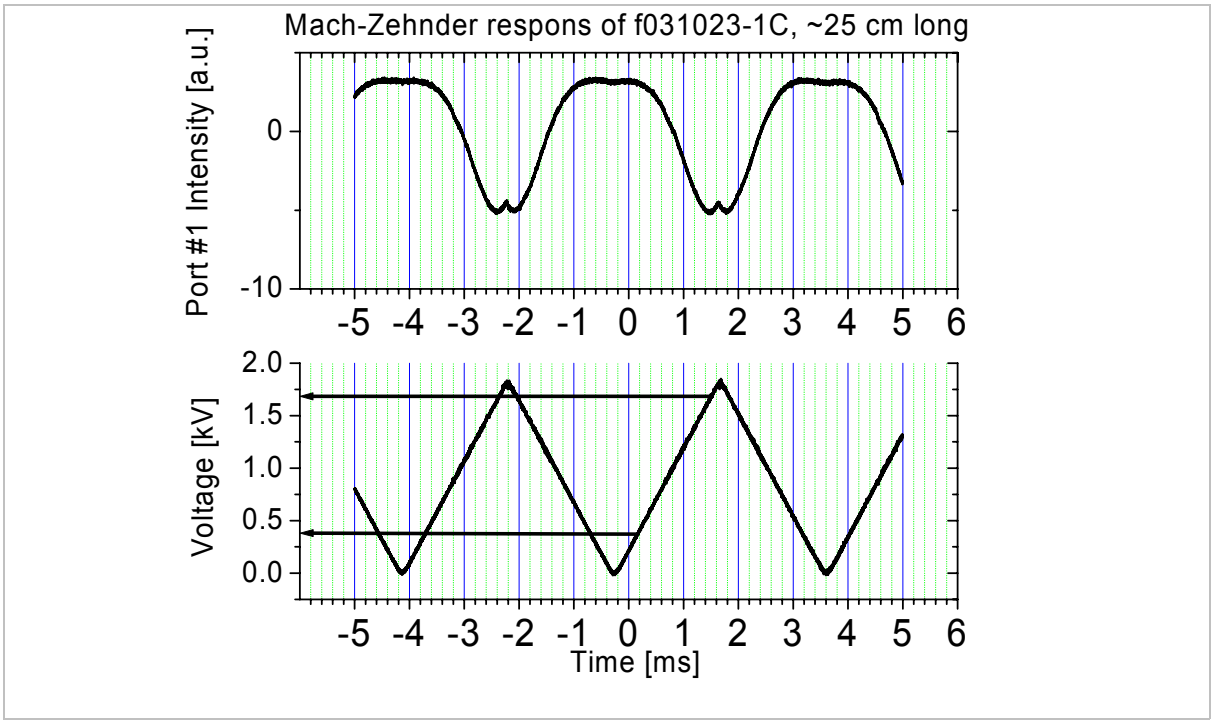

Figure 9.1. The optical response of a Mach-Zehnder interferometer with a poled fiber in one of the arms. The applied triangular voltage modulates the phase of the light in the fiber to switch the output from one arm to the other. The switching voltage V_π is determined as the voltage needed to go from a maximum to a minimum in intensity, in this case $V_\pi = 1.59$ kV.

A number of actions were taken to optimize the response of the fiber. By carefully monitoring the evolution of the electro-optic effect during poling, it is possible to stop the poling process when the effect is at its maximum and thus ensure the lowest possible switching voltage. To further enhance the response the length of the active region was increased compared to the previous fiber, to 37 cm since the phase shift scales linearly with the length as seen in (eq. 7.1). The length can be further increased at the expense of increasing the loss. The new poling technique was also utilized which unfortunately cannot be described since a patent is being processed as this thesis is written. A new fiber was poled at 265 °C with 4.4 kV applied during 43 minutes, with the above-mentioned improvements to the poling procedure. The result is shown in Figure 9.2 and it can be seen, by counting the periods in the figure, that for 2.75 kV applied a ~13 π phase shift was obtained. The linear voltage ramp was applied to the cathode while grounding the anode electrode. Since the recorded electric field is pointing from the anode towards the cathode, the external field to some part canceled the recorded field. Since the recorded field is cancelled the voltage needed to go from a maximum to a minimum increases with increasing external voltage. In Figure 9.2 this is seen as an increase in the period of the optical modulation. For $V_{ext} = 0$, $V_\pi = 210$ V while for $V_{ext} = 2.75$ kV, $V_\pi = 270$ V (the voltage to add a phase shift of π). It is desirable to further decrease the switching voltage since it makes it much easier to find a suitable driver for the device and this is one of the main challenges for future devices.

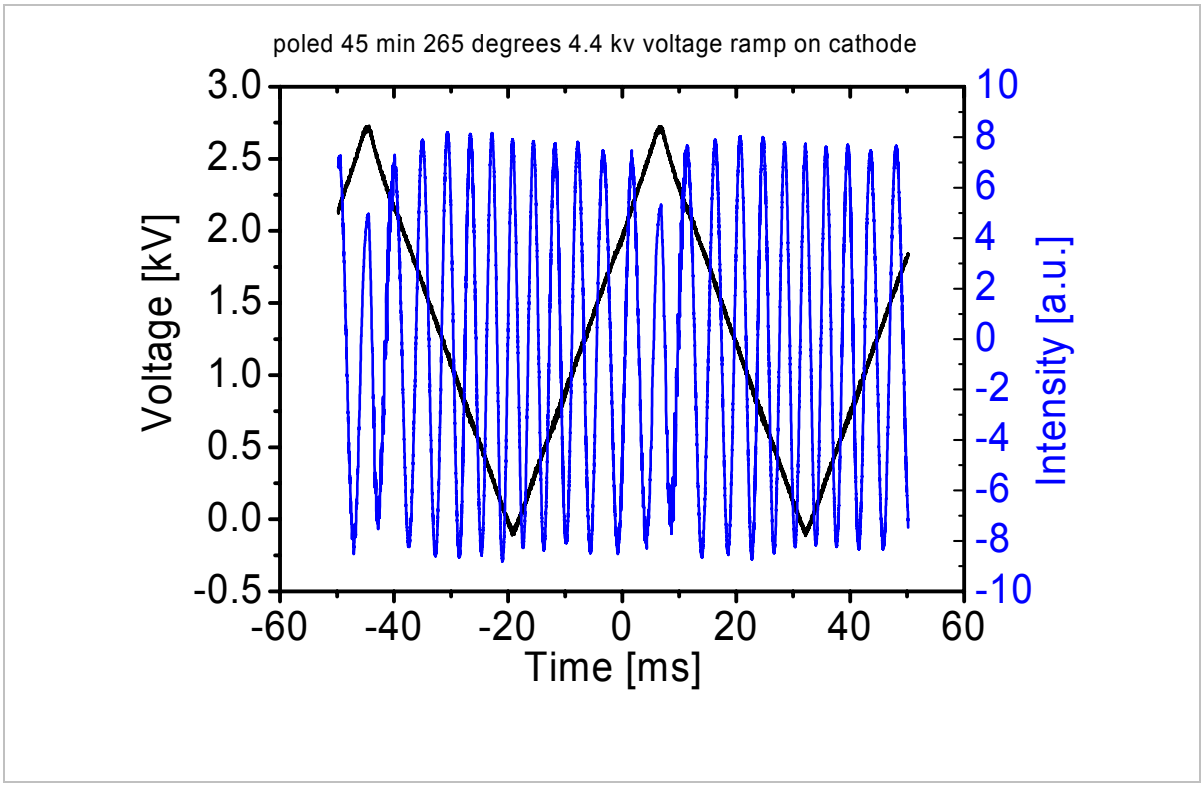

Figure 9.2. Linear voltage ramp applied to the cathode of a poled fiber. Note that the applied field cancels the recorded field so that the period of the optical modulation is chirped with the longest period for the highest applied voltage. V_π = 210 V to the best of our knowledge this is the lowest switching voltage for any poled fiber/waveguide at 1550 nm ever reported.

Most reports on thermally poled fiber modulators found in the literature describe experiments were HeNe lasers, at 633 nm, are used to probe the nonlinearity [26-28,62,72]. At this short wavelength, compared to 1.55 μm, the optical mode is more confined to the core and the loss is greatly reduced. A fiber suitable for telecom applications usually has a cutoff wavelength of 1200 nm, and at 633 nm these fibers can support more than one propagating mode. When modulating a fiber supporting many modes it is difficult to distinguish between phase modulation and mode modulation. Since the Glamorous project aims at telecom applications, most of the poled fibers were characterized at 1550 nm, however, some fibers had too high loss at 1550 nm and shorter wavelengths had to be used to get a detectable optical transmission. A fiber modulator with a switching voltage V_π = 200 V at 1550 nm would in principle have V_π = 80 V at 632 nm.

9.2 Modulation speed

There are many limits to the electro-optical response time of a device based on poled fibers. These can be divided into fundamental material properties of the poled glass, and limitations caused by the structure used to apply the electric field to the fiber. The fundamental response time of silica glass is given by the time for the electrons to respond to an external field. It has been argued from theoretical models that the response is in the

order of 1 fs [85], but it is very difficult to measure directly since this time is shorter than the shortest optical pulses available (~10 fs). In any way, the intrinsic response time of the glass is much faster than what is required from our devices and the limitation lie elsewhere.

The electrodes inside the fiber are very similar to the electrodes in an RF waveguide were the silica glass works as a dielectric substrate. When designing the different fibers used throughout this work no care was taken to match the propagation speed of the electrical control pulses to the optical pulses. Furthermore, no effort was made to improve the RF wave guiding properties of the fiber since the project was initially aiming at low frequencies (<10 kHz). Without a proper traveling wave design, the performance deteriorates when the dimensions of the device approach the RF wavelength. If the length of the electrodes in the fiber is 0.3 m, this produces a cut-off somewhere above 100 MHz. Another way to estimate the cut-off frequency is to consider the fiber as a charging capacitor with a characteristic capacitance- and resistance per unit length. The rise time of this equivalent circuit determines another limitation to the maximum modulation frequency. The capacitance per unit length of a two-wire transmission line is given by [86]:

$$C = \frac{\pi\varepsilon}{a\cosh(D/(2h))} \qquad \textit{(eq. 9.1)}$$

where $\varepsilon = \varepsilon_o\ \varepsilon_r$ is the electric permittivity, with ε_r= 3.78 for silica. h = 15 μm is the radius of the electrodes and D = 50 μm is the distance between the electrodes. These values give a capacitance of roughly 100 pF/m or C = 30 pF for a 30 cm long device. This formula assumes that the electrodes are embedded in an infinite dielectric medium, not the case in a fiber where the RF field is present also outside of the glass. Nevertheless, it was later confirmed experimentally that the 30 pF is in good agreement with that of a real fiber. The resistance of the electrodes was measured to be ~1000 Ω/m or R = 300 Ω for a 30 cm long fiber. The time to charge this capacitor is given by the well-known formula t = 2.2 RC = 20 ns, equivalent to roughly 50 MHz.

Of all the limitations described, the single one with the lowest cut-off determines the highest possible modulation frequency of the device, which is thus 50 MHz, corresponding to 20 ns. This is very fast within the scope of the Glamorous project since one of the aims was to reach a response time faster than 100 μs, which is the speed required if the switch is to be used as a protection switch in a telecom network. Protection switches are usually employed between two nodes in a network connected by more than one fiber. In the case of a failure in one of the fibers the traffic can quickly be switched to a new link without severe interruptions in the traffic.

A set-up was built for testing the rise time of a fiber component with cross section shown in Figure 5.3. The fiber was poled at 260 ^{o}C and the voltage was ramped to 2.6 kV during 5 minutes and kept at 2.6 kV for 10 minutes for a total poling time of 15 minutes. In this early study, the electrodes were gold-coated tungsten wires, manually inserted into the fiber through polished holes on the side of the fiber, and produced an active length of 11 cm. The light source was a 1550 nm linearly polarized laser diode which was coupled through an erbium doped fiber amplifier (EDFA) and then into the poled fiber component using a bare fiber holder. The output of the fiber component was coupled to a standard telecom fiber

using another bare fiber holder and then fed into a fiber coupled polarization splitter with one of the output arms connected to a 2.5 GHz detector. Square voltage pulses of 20 ns duration with amplitude 400 V and sub ns rise time were applied to the electrodes in the fiber and the optical response measured. Since the refractive index change in the two optical axis of the fiber is slightly different for the same applied voltage, the polarization was slightly rotated which changed the amplitude of the detected signal. When the voltage pulses were launched, the system picked up electrical noise that made it impossible to detect the true optical response. To overcome this problem, a 5 km delay fiber was spliced between the polarization splitter and the detector, which gave a delay of ~26 μs between the switching of the voltage pulse and the arrival of the modulated optical signal. This time was long enough for all electrical noise to decay and made it possible to measure the optical response of the component, as shown in Figure 9.3. The rise time of the component is ~6 ns which is approximately what was expected from the theory. The oscillations in the signal mainly arise from the electrical reflections at the impedance step between the coax cable transporting the voltage pulse and the poled fiber.

The response time measured in Figure 9.3, ~6 ns is shorter than the value calculated above, ~20 ns. This is attributed to the fact that the electrodes are shorter, 11cm as compared to 30 cm used in the calculations. In order to test the modulation performance of a device the small signal response was tested for two poled and packaged fibers. Continuous radiation at 1.5 μm was fed into one of the input ports of the 2x2 switches and the amplitude of the resulting optical modulation was measured. Before each measurement point, the interferometer was positioned at the quadrature point by slightly adjusting the wavelength of the laser.

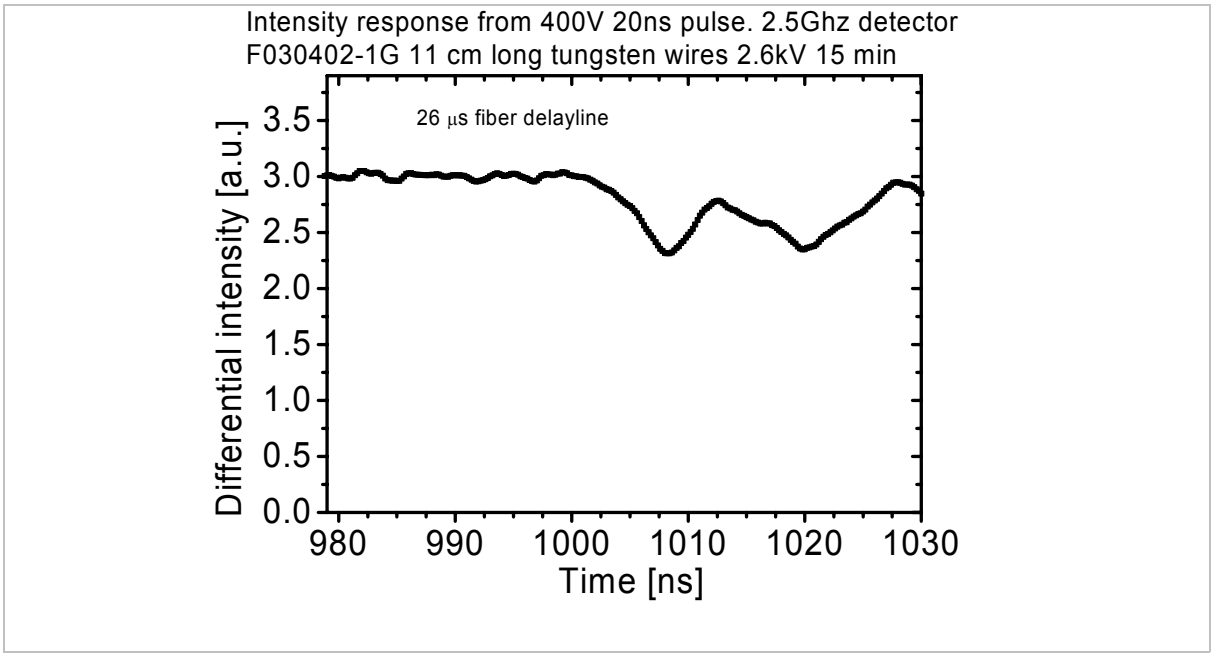

Figure 9.3. The optical response from a 20 ns, 400 V square voltage pulse applied to the electrodes in a fused silica fiber. The oscillations in the optical signal are due to multiple reflections of the voltage pulse since the electrical connections were not properly impedance matched.

The two figures in Figure 9.4 show two devices with different device length, the upper one having 120 cm and the lower having 37 cm long electrodes, respectively. It is apparent

from the figure that the device with the longer electrodes has a lower cut-off at around 16 MHz as compared to the device with shorter electrodes, 30 MHz. It might well be that the higher capacitance of the long electrodes limit the rise time of the electric field. Notice the sharp increase in the optical modulation amplitude in the lower figure at around 20 MHz. This might be caused by an acousto-optic change of the refractive index induced by small transversal vibrations of the electrodes [87-89]. The fundamental transverse resonance frequency can be found by calculating the roundtrip time for a sound wave to propagate back and forth through the cross-section of the fiber, that is $f_r = v / 2h = 23.8$ MHz where $v = 5950$ m/s is the speed of sound in silica glass and $h = 125$ μm is the diameter of the fiber. The electrostrictive contribution near resonance is expected to be $r_{33} = 28$ pm/V [90], and thus the effect is about two orders of magnitude greater than that of the electro-optic contribution. This effect could be utilized in applications operating at a single frequency near the resonance of the fiber, but for most applications it is desirable to have a linear frequency response and stay out of frequency ranges with acoustic resonances.

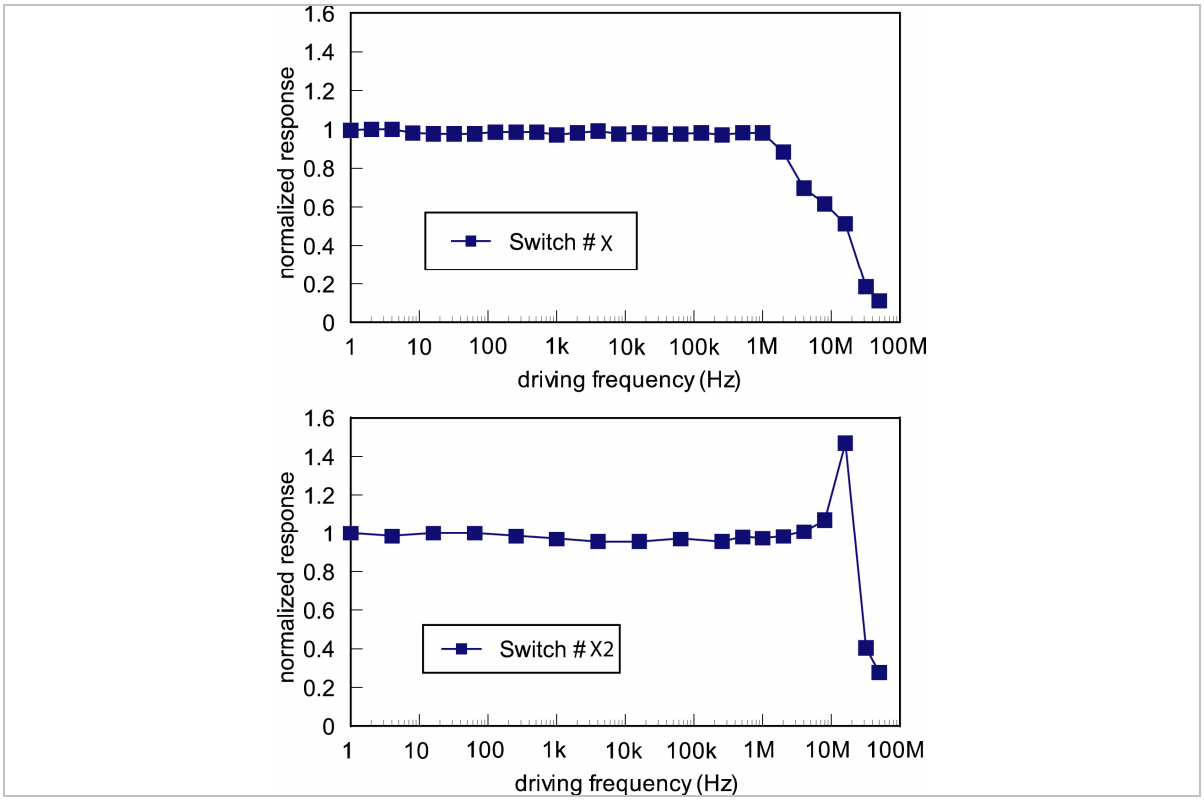

Figure 9.4. The small signal response of two poled and packaged fiber devices. The upper figure shows the response of a device with 120 cm long electrodes and the lower figure shows a device with 37 cm long electrodes. In the lower figure a resonance is seen at ~24 MHz, most likely a transversal acoustic resonance of the fiber. Notice that the fiber with longer electrodes has a lower cut-off, and does not have a clear resonance frequency.

Compared to the rise time measured, 6 ns, and the theoretical cut-off at ~50 MHz the tested devices seems to have slightly worse performance than predicted. At present experiments are performed to determine if the electrical connections, such as the coax cables between the RF driver and the device, affect the measurement.

Preliminary studies also showed that when the frequency is increase to 30 MHz or more the fiber is heated due to absorption of the RF signal in the electrodes. This changes the refractive index of the fiber and thereby the operation point of the interferometer, which might prove to be a serious limitation when trying to increase the cut-off frequency.

9.3 Lifetime of the switching voltage

One of the main concerns with thermal poling is the expected lifetime of the device. If the technology cannot be proven to be stable over a long period of time, it cannot compete with existing solutions. The second-order nonlinearity is reported to be extremely stable at room temperature in bulk fused silica [7] and about 150 minutes at 200 °C [91] and according to [92] the stability can be further enhanced by co-doping the glass with Al and B. There are a few reports on the stability of the nonlinearity in poled fibers. The group in Sydney reported a decay time of only 45 days [93]. Intuitively the stability of poled fibers should be approximately as good as the stability of bulk samples. The stability of the switching voltage, which is directly related to $\chi^{(2)}$, was measured during a 12 months period during which no change was detected to within the accuracy of the measurement, Figure 9.5. One should always be careful when extrapolating this type of information, but it indicates that the second-order nonlinearity in our type of fibers is stable over at least several years.

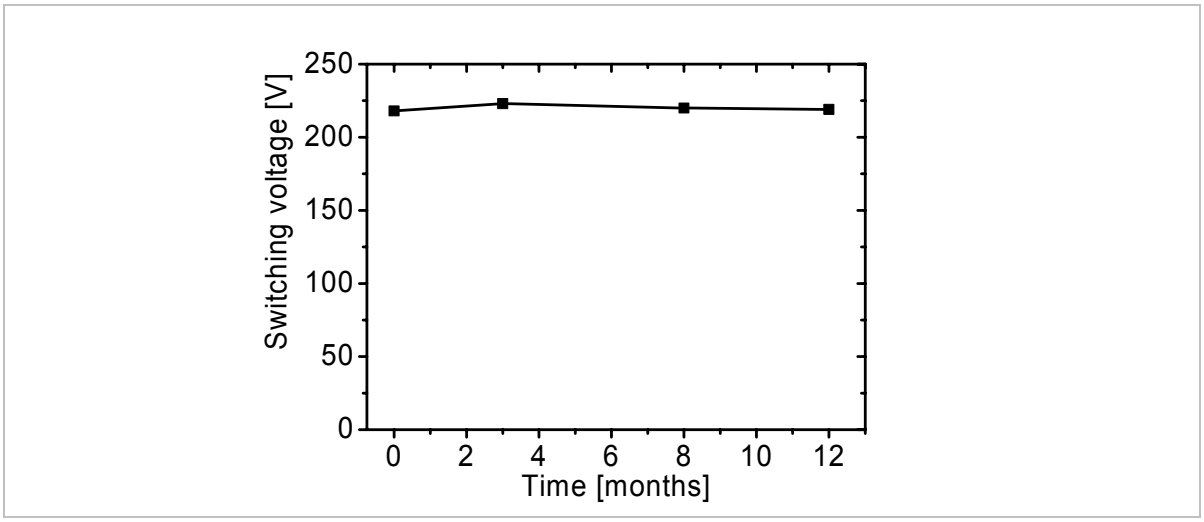

Figure 9.5. Switching voltage vs. time. To within the measurement error, no change in the switching voltage was detected over a 12 months period.

9.4 Testbed performance

A broadband testbed has been deployed at Acreo. It is used to evaluate new services and products before deploying them in commercial systems. A poled and packaged device was characterized in a 40 Gb/s transmission test. The switch slightly reshaped the optical pulses but no degradation of the bit error rate (BER) was observed [paper VII]. This looks very promising for telecom applications. By applying a voltage, V_π, to the switch the data stream could be switched from one output port to the other, much like a protection switch.

9.5 Performance summary of packaged devices

An overview of the performance of some packaged devices is presented in Table 9-1. The fiber F031023-1d always produced a higher recorded field than F040407-1b2 and thus the switching voltage was lower for the same fiber length. Since the core was placed further from the anode electrode in F040407-1b2, 7 μm, compared to 5.5 μm for F031023-1d, the loss per unit length was lower. This made is possible to use a longer active region, and explains why V_π voltage is about equal for the devices #1 - 4. The ER is given by the power balance in the two arms and the optical bandwidth is determined by the accuracy when matching the arm lengths. As can be seen there is a considerable improvement from the first device, 0.08 nm, to the last device, 20 nm.

Name	Switch #1 Ms. Pockel's	#2 ECOC modulator	#3 El poco	#4 Avanex demonstrator	#5 Push-Pull Switch
Date Built	2004-04-28	2004-05-17	2004-09-28	2004-11-17	2004-12-27
Fiber	F031023-1d	F031023-1d	F040407-1b2	F040407-1b2	F040407-1b2
Poling	4.4 kV, 255 °C, 45 min	4.4kV, 265 °C, 40 min	4.3kV, 255 °C, 30 min	4.3 kV, 255 °C, 40 min	4.3 kV, 255 °C, 40 min
V_π	220 V	210 V	190 V	230 V	350 V
ER	7.3 dB		30 dB	20 dB	
Bandwidth	0.08 nm	0.2 nm	4 nm	7 nm	20 nm
Cut off	16 MHz	30 MHz	4 MHz		
Electrode	AuSn	AuSn	AuSn	AuSn	AuSn
Active Length	42 cm	37 cm	120 cm	70 cm	70 cm
Wavelength	1550 nm	1550 nm	1550 nm	1550 nm	1550 nm
Package	Elfa Box	Ericsson EDFA	Elfa Box	Avanex Package	Glass Plate
Insertion Loss	5 dB				
Other	Stability check				

Table 9-1 Summary of the performance of poled and packaged devices.

10 Applications of an all-fiber modulator

10.1 Introduction

At the end of the Glamorous project, the poling technology had been developed to a point that required a serious market consideration. The original idea was to develop devices for various telecom applications, but with the downsizing of this market potential applications and customers in other areas were sought. In order to probe the market and disseminate the results of our project a poled fiber device was demonstrated at the ECOC conference in Stockholm 2004. The electrical signal from a DVD player was used to modulate a CW laser at 1550 nm coupled into the device. The modulated optical signal was transmitted over a fiber link, detected and displayed on a TV screen as shown in Figure 10.1. From the interest and feedback given from various companies, it was understood that there is a large and expanding market for fiber lasers and that the technology developed in this thesis could prove useful for mode-locking and Q-switching of such lasers. The existing solutions based on optical fibers usually involve some type of acousto-optic scheme and thus operate in a narrow frequency range around the resonance of the system [94], which means that the cavity length has to be carefully matched to the resonance of the modulator. Since devices based on poling operate with the electro-optic effect, they have a large frequency span, up to at least 10 MHz over which the response is linear and therefore this technology has clear advantage compared to other fiber based solutions.

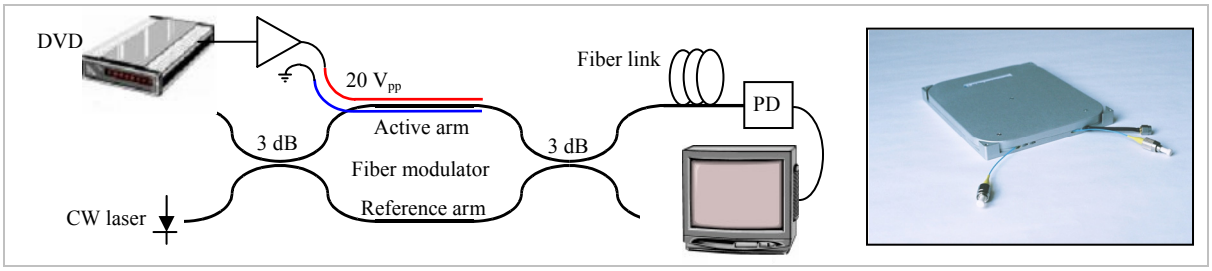

Figure 10.1 Set-up used to demonstrate electrical-to-optical conversion of a ~10 MHz signal from a DVD player. The modulated optical signal was detected with a photodiode and displayed on a TV screen.

10.2 Mode-locking

The set-up shown in Figure 10.1 worked well for video transmission, and when everything was optimized it was difficult to distinguish the picture fed directly from the DVD to the TV set from one transmitted optically with the fiber modulator. This encouraging result suggested that a poled fiber modulator should provide for mode-locking. To this end, a ring laser with a 3 meter long erbium-doped fiber with small signal gain of ~10 dB was constructed [paper VI]. By pumping the Er fiber at 980 nm and coupling a photodiode, see Figure 10.2, to an electrical spectrum analyzer, it was possible to measure the fundamental frequency of the cavity, determined by the roundtrip time. In the present cavity, a strong peak was detected at 12.66 MHz indicating that the laser cavity length was ~16 m. As explained in section 3.2 of this thesis, a modulator with different arm lengths have transmission that is wavelength dependent and periodic. Therefore, a tunable band pass filter was used so that a single transmission peak of the modulator could be chosen. When

the laser was pumped above threshold, it lased at the wavelength determined by the tunable filter.

A second peak appeared in the electrical spectrum analyzer when the RF driver was switched on, corresponding to the modulation of the optical carrier. When this frequency peak was tuned to coincide with the fundamental frequency peak of the cavity, the laser became mode-locked. By analyzing the mode-locked signal in the ESA it was revealed that it consisted of discrete frequency components spaced by 12.66 MHz and ranging all the way up the limit of the ESA, 2.9 GHz. In this regime, the laser delivered pulses spaced by 80 ns as determined by the cavity roundtrip time. The pulses had duration of less than 1 ns and by examining the pulses in a fast sampling oscilloscope it was noticed that the pulses contained several short pulses of duration as little as 50 ps, possible due to multiple reflections of the tunable filter. Some optical spectral broadening was also measured, e.g, from 0.01 nm to 0.03 nm.

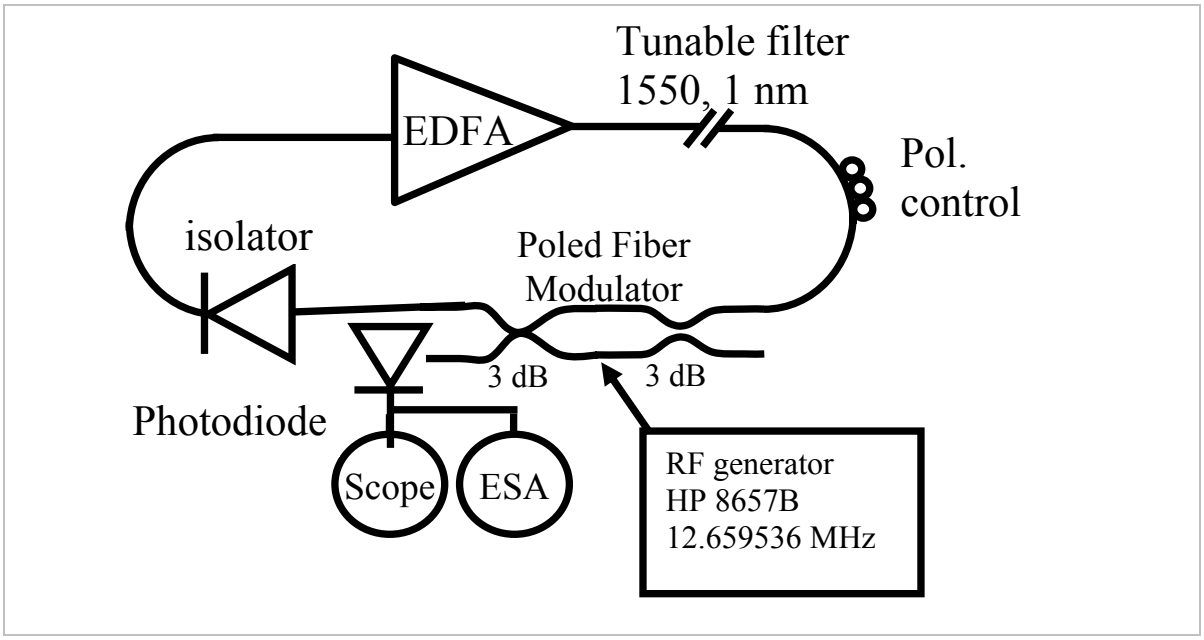

Figure 10.2. Set-up used to mode-lock a fiber ring laser. The laser was mode-locked by tuning the frequency of the RF signal to closely match the fundamental frequency of the cavity.

10.3 Electro-optic tuning

The transmission of the fiber modulator depends on the wavelength and also on the applied voltage. It was realized that the modulator could be used to tune the wavelength of the laser. To this end, the tunable filter shown in Figure 10.2 was removed and instead a sampled reflection grating, spliced to a circulator, was inserted, Figure 10.3 left. The grating was designed for WDM applications and had 16 reflection peaks separated by 50 GHz (0.4 nm) and side lobe suppression of ~20 dB as shown in Figure 10.3, right. This is also discussed in [paper VI].

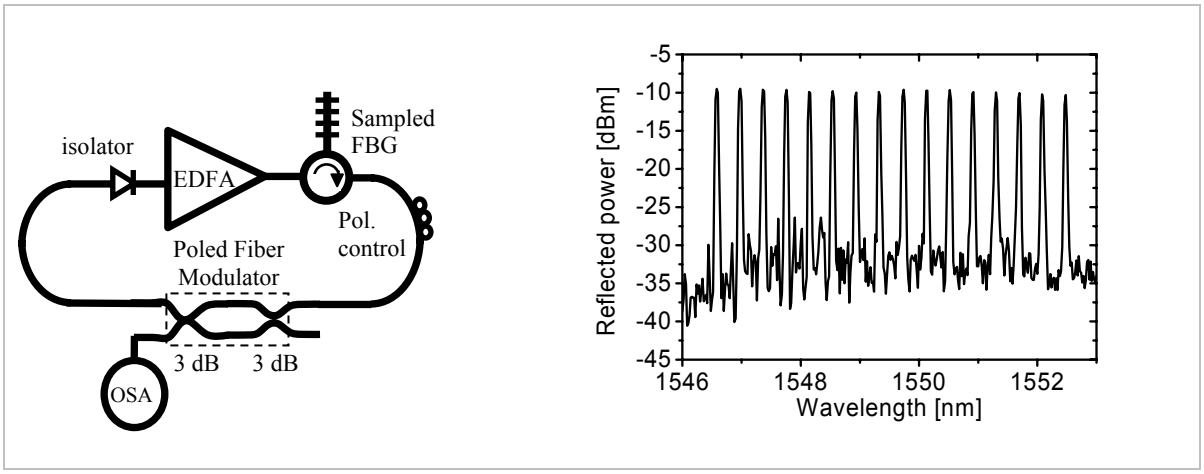

Figure 10.3. Left picture: set-up used to tune the laser. Right: Grating used to discretely tune the fiber laser. The grating has reflection strength of ~20 dB and 16 channels separated by 50 GHz (0.4 nm).

The optical bandwidth, $\Delta\lambda$, determined by the mismatch in length in the two fibers, was measured to be 7 nm and thus the modulator had transmission peaks at $\lambda_o \pm m\Delta\lambda$, where λ_o is the center wavelength, m is a positive integer and $\Delta\lambda$ is the spacing of two adjacent transmission peaks, 7 nm in this case. The switching voltage, V_π, of the device was 230 V and by applying V_π to the modulator a phase shift of π is introduced, corresponding to a tuning of $\Delta\lambda$ / 2, see Figure 10.4, right. With 200 V applied the transmission peak was tuned ~3.5 nm. When the sampled FBG was inserted into the cavity, the output wavelength of the laser locked to one or two of the peaks of the grating. The center wavelength λ_o of the modulator could be changed by applying voltage as demonstrated in Figure 10.4 left. In this case, the laser could be tuned to a desired peak of the sampled grating. If the transmission maximum of the modulator was positioned between two peaks of the grating, the laser operated at two different wavelengths. It was easy to force the laser to operate at a single wavelength by tuning the modulator to within 0.1 nm of a grating peak. All tuning was done solely by changing the voltage applied to the modulator. In this way, 11 of the 16 peaks of the grating could be selected. In order to select the remaining five, the polarization had to be slightly adjusted or else the laser could not be forced to operate on a single peak. Since the optical bandwidth of the modulator, (~7 nm), is approximately equal to the distance between the two outermost peaks of the grating, (~6 nm) is was difficult to chose a single lasing peak when two transmission peaks of the modulator were located on each side of the wavelength span of the sampled FBG. By choosing a modulator with wider optical bandwidth it should be possible to circumvent this problem.

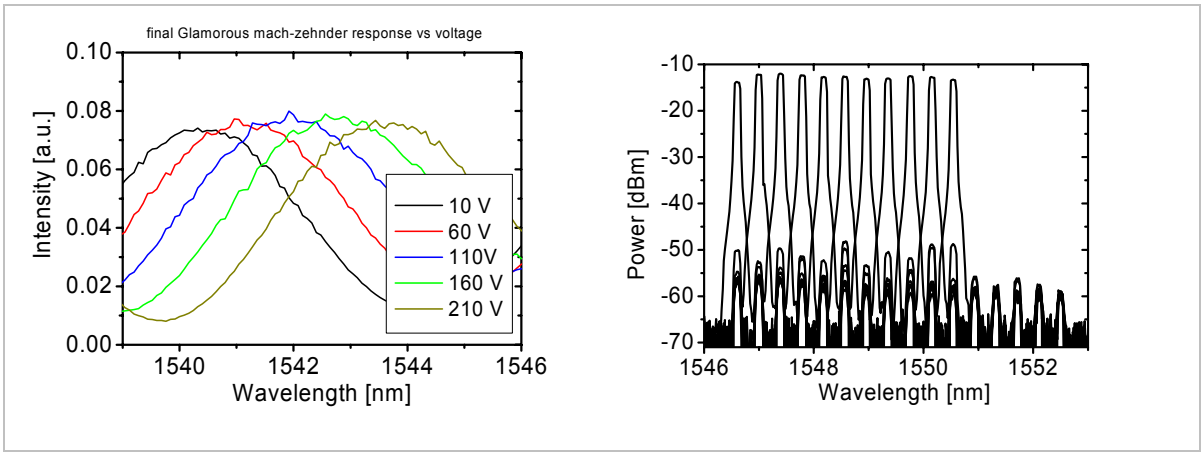

Figure 10.4. The left figure shows tuning of the transmission peak, λ_o, of the Mach-Zehnder modulator with voltage. The wavelength is tuned almost 4 nm when 200 V is applied to the device. The right figure shows how 11 of the 16 peaks are selected by applying a voltage from 10 V (rightmost peak) to 207.5 V (leftmost peak).

The 3dB-width of a single reflection peak of the grating was measured to be 0.058 nm and the laser linewidth was narrower than the limit of our wave meter, 0.01 nm. Attempts were made to measure the time it takes to switch the laser from one wavelength to another. However, this was found to be difficult since the laser had a tendency to Q-switch. The response time of the modulator is ~20 ns and by optimizing the laser design is should be possible to perform rapid tuning.

11 Ablation of silver electrodes

11.1 Electric field induced second harmonic generation

When applying an electric field to silica glass at room temperature the symmetry is broken and the material can frequency double. This process is called electric field induced second harmonic generation (EFISH) and resembles the phenomena observed during poling, the main difference being that the electric field is not permanently recorded. EFISH is an efficient way of determining how a fiber responds to applied electric fields [5], given that it is not easily poled optically.

An experiment was done with a standard germanium core fiber. The fundamental of a Nd:YAG laser (1.064 μm) was coupled into the core using a 10x microscope objective as shown in Figure 11.1. The laser was Q-switched and mode-locked with a repetition rate of 3.4 kHz and typically each Q-switched pulse contained 20 mode-locked pulses of 120 ps duration. After a few minutes of laser exposure the fiber was poled optically, which made the EFISH signal hard to resolve since the signal arising from optical poling was much stronger than the EFISH signal. To overcome this problem a new fiber with a pure silica core was designed, supposedly much more resistant to optical poling. The index step of this fiber was created by doping the cladding with fluorine, thus lowering the refractive index. Square voltage pulses were applied to the electrodes inside the holes of the fiber, separated by 45 μm, and the second harmonic was measured with a photo multiplier (PM).

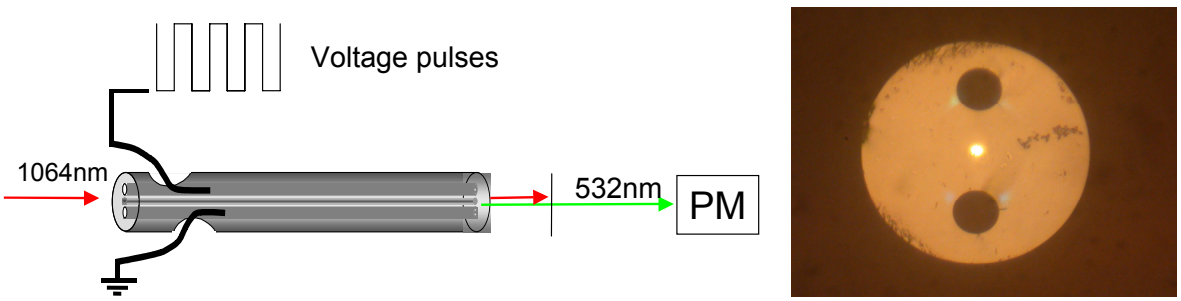

Figure 11.1. The experimental set-up used when probing a fiber with EFISH. A voltage is applied to the electrodes in a twin-hole fiber so that the applied field generates weak (<nW) SH signal. A picture of the cross section of the fiber taken with an optical microscope is shown on the right picture. The core was illuminated from the backside of the fiber to make it visible.

11.2 Ablation of silver electrodes

The nonlinear coefficient obtained in thermally poled optical fibers is usually less than 0.5 pm/V but since it is possible to use long lengths of fiber this value is more than enough for making all-fiber electro-optic switches. When designing a wavelength converter, not only the nonlinear coefficient, but also the phase matching properties determine the efficiency of the device. Since different wavelengths experience different refractive indices, the spatial length over which the process is constructive is often limited to tens of micrometers. To

make an efficient device the process must be phase matched, which can be achieved in different ways, e.g. by quasi phase matching (QPM) (see chapter 2.4). This has been shown in d-fibers with periodic electrodes created with photolithography [13]. A new method to create QPM in fibers was invented. A thin film electrode is deposited in the holes of a fiber and periodically ablated so that when a voltage is applied to the electrodes a periodic electric field is generated.

The electrodes are deposited by mixing two solutions, one containing dextrose solved in H_2O and the other containing $AgNO_3$ and NH_3 solved in H_2O. When the two solutions are mixed, the silver ions are reduced to atomic silver and deposited on any suitable nearby surface. Different waste products also form and these particles quickly grow larger than the diameter of the holes in the fiber (30 μm), and therefore clog them. To overcome this problem a Y-junction was built where the two solutions are mixed in a 1 mm^3 chamber just before entering the fiber, which limited the size of the particles so that the solution could flow for several hours without clogging the holes. This time was sufficient to form a ~1 μm thick conducting silver film with a length >2 m.

Setting up the Y-junction cell was rather time consuming and a different approach was tried where the two solutions were cooled down in a fridge (8 $^{\circ}$C), mixed and kept at this temperature during the whole filling process. The low temperature of the solution slowed down the reaction speed so that the size of the waste particles was kept small. It took only ~30 seconds for the solution to travel through the fiber, which was shorter than the time it takes to form particles larger than the hole diameter. One end of the fiber was kept in the fridge, but the main part of it was kept at room temperature where the reaction speed was faster which created a sharp gradient in the thickness of the silver film in the region where the fiber left the fridge. With this filling technique it was possible to create conducting electrodes up to 3 m long.

Typically, the deposited film has a resistance of 1000 Ω/m. Because the electrodes are thin (~1 μm) it is possible to splice the fiber to a standard telecom fiber without removing the metal. Once the electrodes are created they are structured by periodically ablating them from the side using a frequency doubled mode-locked Q-switched Nd:YAG laser giving 0.532 μm radiation. The average power needed for ablation varies with the thickness of the silver film, but typically 17 mW, focused with a 30x microscope objective, was sufficient. Every pulse train carried 1/3 of the total power and 2/3 was carried in the prelase. Typically the repetition rate of the Q-swithced pulses was set to 1 kHz, which gave ~20 pulses, 120 ps long in each Q-switched pulse. An attenuator was used to lower the power so that the system could be aligned without ablating the electrode. The laser beam was then scanned along the fiber and the periods written by periodically exposing the electrode to the beam during less than 1 s. After ablation, the electrodes were still continuous and conducting since only the part of the electrode closest to the core was ablated as shown in Figure 11.2. A picture of the ablated electrode is shown in Figure 11.3.

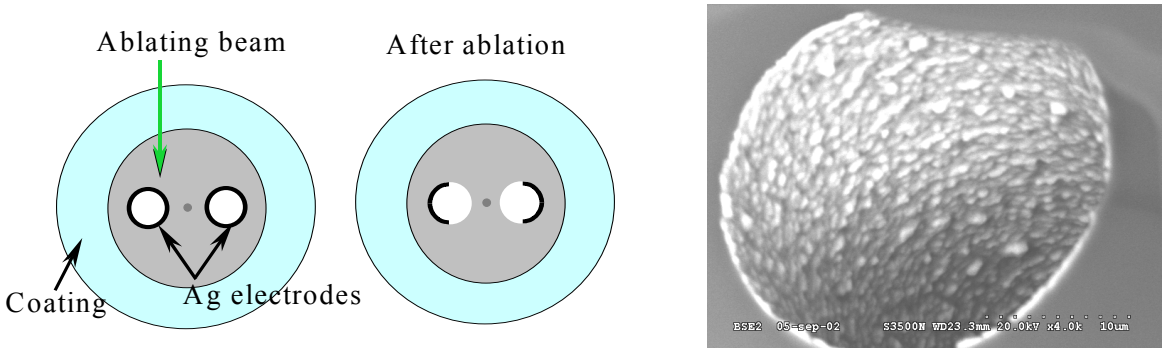

Figure 11.2. The left pictures show how the ablating laser beam removes a part of the electrode. After ablation, the electrode is conducting since the part of the electrode farthest from the core is untouched. The right picture shows the silver film inside one of the holes prior to ablation.

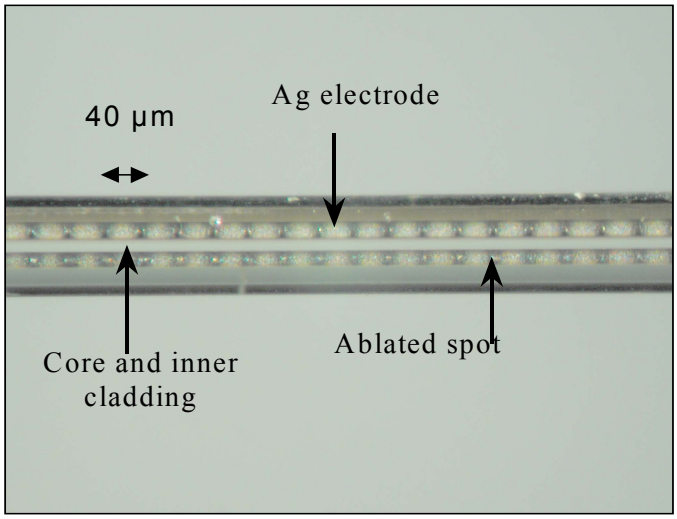

Figure 11.3. A fiber silver film electrodes showing some 18 ablated spots. The period here is 40 µm, but it can easily be changed simply by translating the beam farther between each ablated spot.

In order for the spatial resolution of the electric field to be good, the resistance in the ablated spots must be very high and in order to measure this, an experiment was designed. A silver stripe, 20 mm long and 1.5 mm wide was deposited on a 1.5 mm thick fused silica glass disk, Figure 11.4. The silver film was contacted with thin gold plated tungsten wires, attached to the film with conducting silver epoxy and connected in series with a current meter and a 19.7 MΩ resistor. A voltage was applied to the circuit and the current monitored. The focused beam of a frequency doubled Nd:YAG (the same used when ablating the fiber electrodes) was scanned across the film to cut it off. In the first attempt the 19.7 MΩ resistor was shortcut, and the beam scanned in steps of 100 µm across the film while the resistance through the film was monitored. During the first 16 steps the resistance

was 47 Ω, ablating another 100 µm increased the resistance to 48 Ω while during the last 100 µm the resistance increased to more than 2 MΩ. In a second experiment, four ablations were made across the entire film while the current was monitored. The resistance of the silver film was found using Ohm's law. Each new ablated stripe, on average, introduced an extra 4.55 MΩ of resistance to the circuit. Using an optical microscope, the ablated stripes were estimated to be 45 µm wide. The small current measured after the film was ablated mainly flows through the glass sample on which the film is deposited. Since the resistance increases dramatically when the electrode is ablated this indicates that the technique can be used to define periodic electric field in a fiber, as is shown in [paper III] of this thesis.

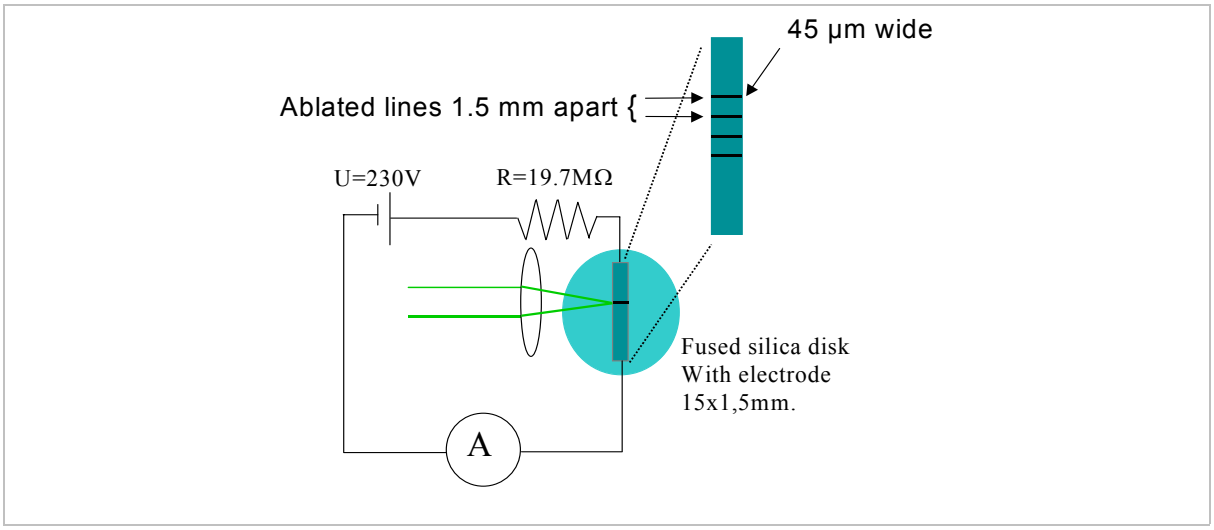

Figure 11.4. Set-up for measuring the resistance introduced when ablating stripes across a thin silver film deposited on a fused silica substrate. The current is monitored while the silver strip is ablated. For each ablation the resistance of the circuit increases by 4.55 MΩ.

12 Description of original work and author contribution

Paper I

A Fibre-Based Kerr Switch and Modulator
M. Fokine, L. Kjellberg, P. Helander, N. Myrén, L. Norin, H. Olsson, N. Sjödin and W. Margulis

The authors report for the first time on an all-fiber Kerr switch based on a twin-hole fiber. The device has very low insertion loss of ~1dB and a switching voltage of 100 V. By biasing the fiber with several kV from a small power supply and feeding the switch/modulator with a signal from a DVD player, video transmission is demonstrated. Since the device operates with the Kerr effect there is no concern with the lifetime, as can be the case for thermally poled fibers.

Contributions of the author: Participated in designing the fiber, in discussions and in writing the paper. The author presented the work at ECOC, 2004.

Paper II

Measurement of Depletion Region Width in Poled Silica
C. S. Franco, G. A. Quintero, N. Myrén, A. Kudlinski, H. Zeghlache,H. R. Carvalho, A. L. C. Triques, D. M. González, P. M. P. Gouvêa, G. Martinelli, Y. Quiquempois, B. Lesche, I. C. S. Carvalho, W. Margulis

The width of the depletion region in thermally poled fused silica samples is investigated experimentally with four previously reported characterization techniques, in an attempt to unify their findings. The authors explain how an assumed electrical field distribution in the nonlinear layer affects the maximum $\chi^{(2)}$ and it was found that the maximum nonlinearity varies by as much as ~45% depending on which profile is assumed. It is also reported that a phase contrast microscope can be used to obtain detailed information about the depletion layer.

Contributions of the author: Did the etching and characterization with phase contrast microscope and performed the simulations used to compare the methods. Participated in discussions and in writing the paper.

Paper III

In-fiber electrode lithography
N. Myrén, M. Fokine, O. Tarasenko, L-E Nilsson, H. Olsson, W. Margulis

The paper describes a new method to produce periodic structures in thin film electrodes deposited in the holes of a fiber. By choosing a period that matches the beat-length of the fiber it is possible to enhance the conversion efficiency by quasi phase matching. The authors describe how 1 μm thick silver film electrodes are deposited in the fiber. By

exposing the electrode to the 532 nm radiation from a Q-switched and mode-locked frequency doubled Nd:YAG laser it was possible to ablate parts of the electrode. A proof-of-concept experiment is performed were it is verified that the conversion efficiency is enhanced as the number periods is increased.

Contributions of the author: The author did the experimental work and participated in preparing the manuscript.

Paper IV

Wide wedge-shaped depletion region in thermally poled fiber with alloy electrodes
N. Myrén, H. Olsson, L. Norin, N. Sjödin, P. Helander, J. Svennebrink and W. Margulis

The authors describe thermal poling of a fused silica fiber. For the first time the depletion region is reported to be wedge-shaped. A simulation was performed to explain the shape of the nonlinear layer. The width of the depletion region is reported to be 13 μm, far wider than in existing papers, and has complete overlap with the core. For the first time a poled fiber is characterized at 1550 nm, which is usually difficult because of the high loss caused by the electrodes.

Contributions of the author: The author did the experimental work, took part in discussions and participated in preparing the manuscript.

Paper V

Time evolution of frozen-in field during poling of fiber with alloy electrodes
N. Myrén and W. Margulis

The evolution of the depletion region in a thermally poled fiber is described. A fiber was poled in a temperature gradient, cleaved and etched, which revealed how the depletion layer grows from the anode electrode. It is suggested that an electric field is present also outside of the depletion region, and that the direction is opposite to that of the field inside the depletion region. A new fiber is poled for different time intervals, and the recorded electric field measured. The authors prove that for short poling times, when the depletion region does not yet overlap with the core, the recorded field is pointing in the opposite direction as the applied poling field. After poling the fiber for a longer time the depletion region overlap the core and the recorded field switches sign. So far, all reports on poled fiber use fibers with the core placed close to the anode electrode to ensure good overlap the created nonlinearity. The present paper shows that this is not necessary, which opens the door to new fiber designs.

Contributions of the author: The author did the experimental work, took part in discussions and participated in preparing the manuscript.

Paper VI

All-fiber electrooptical mode-locking and tuning
N. Myrén and W. Margulis

The paper describes a ring laser based on an Er doped fiber pumped at 980 nm. The laser has a roundtrip time corresponding to 12.65 MHz. A modulator based on a poled fiber is inserted into the cavity so that the transmission can be modulated by applying a voltage to the device. By supplying an RF signal precisely tuned to the fundamental frequency of the cavity, the laser is mode-locked. This is the first time a poled fiber has been used to mode-lock a laser and in this regime the laser produced sub ns pulses. It is also showed that the poled fiber modulator has transmission peaks that can be tuned by 4 nm by applying 200 V. This could be useful in a reconfigurable add/drop multiplexer.

Contributions of the author: The author did most of the experimental work and improved the laser. The author built the fiber modulator and took part in discussions and in preparing the manuscript.

Paper VII

Systems measurements of 2x2 poled fiber switch
J. Li, N. Myrén, W. Margulis, B. Ortega,G. Puerto, D. Pastor, J. Capmany, M. Belmonte and V. Pruneri

The authors describe for the first time system tests of a poled fiber switch. A digital transmission test showed that there was no detectable degradation of the bit error rate for a 40 Gb/s data stream transmitted through the interferometer. In another set-up it was demonstrated that the device can be used as a protection switch at 10 Gb/s. Since the device is all-fiber it inherits the attractive characteristics of a standard silica fiber, such as low loss, small size, ease of splicing and low cost.

Contributions of the author: The author took part in discussions and assisted in some experiments. The author built the switches/modulator that were characterized and took part in writing the paper.

A note regarding all the above papers: The author took part in designing the special fibers used in these papers, but the manufacturing was done by colleagues in Hudiksvall. A special thanks to Håkan Olsson, Lars Norin, Niclas Sjödin and Per Helander.

13 Conclusions

Optical fibers have great potential to take over some of the functions performed by nonlinear crystals in today's optical networks. The main advantages of devices based on optical fibers are the potentially low manufacturing cost and ease of integration with other fiber based components. The two functions that are dealt with specifically in this thesis are wavelength conversion and optical switching.

Wavelength conversion was demonstrated in a fiber with thin silver electrodes. The electrodes were periodically ablated so that when a voltage was applied a periodic electric field was created. This quasi phase matching enhanced the conversion efficiency of the 1.06 radiation of a Nd:YAG laser to 532 nm. The effectiveness of the device was determined in part by the number of periods and the precision of the grating ablated in the electrode. This process can be automated and scaled for industrial production.

Fibers that were poled and etched showed that the depletion region was 13 μm wide and wedge-shaped, which is in good agreement with the simulated electric field during poling. In all previous reports the depletion region in poled fibers has been round.

An optical switch was constructed with V_π = 190 V and it is possible to further lower this value by using longer active regions. By actively tuning the lengths of the arms in the switch it was possible to create optical bandwidth in excess of 20 nm. The modulation cut-off frequency was measured to be higher than 30 MHz and the best extinction ratio obtained was 30 dB. The insertion loss of the best device was less than 5 dB and can be optimized further by improving the splices between the twin-hole fibers and standard telecom fibers.

A time resolved poling experiment showed that for short poling time, when the depletion region did not yet overlap with the core, the field in the core had opposite direction to that of the applied poling field. This led to the conclusion that there is an electric field present also outside of the depletion region. This new insight opens the door to new fiber designs where the core is placed far from the light absorbing electrodes.

A ring laser was constructed with an erbium doped fiber. When a fiber modulator was inserted into the cavity and modulated with a sine voltage having the same period as the roundtrip time of the cavity, the laser was mode-locked. The pulses had duration of less than 1 ns and the laser showed excellent stability. Furthermore, the laser could be tuned by inserting a sampled grating into the cavity and applying ~200 V to the modulator. This changed the transmission peak of the device and made it possible to choose a single peak of the sampled grating to lase at. The tuning range was up to 6 nm, limited by the optical bandwidth of the modulator and the design of the grating.

Future efforts will be on decreasing the switching voltage, mainly by increasing $\chi^{(3)}$ since the recorded field is already close to the breakdown limit of silica. The loss will be further reduced by optimizing the fiber design to take advantage of the fact that an electric field is present also outside of the depletion region. A non-technical task will be to raise money to complete the development of this technology into a commercial product.

14 References

1. P.N.Butcher, D.Cotter: "The Elements of Nonlinear Optics," Cambridge University Press, (1990)

2. M.V.Klein and T.E.Furtak,. "Optics". John Wiley & Sons, (1986)

3. G.P.Agrawal: "Nonlinear Fiber Optics," Academic Press, (1995)

4. R.W.Terhune, D.A.Weinberger; "Second-harmonic generation in fibers," J.Opt.Soc.Am.B., **4**, 661 (1987)

5. R.Kashyap; "Phase-matched periodic electric-field-induced-second-harmonic generation in optical fibers," J.Opt.Soc.Am.B., **6**, 313 (1989)

6. I.C.S.Carvalho, W.Margulis, and B.Lesche,. "Second-Order Nonlinear Effects in Optical Fibers". (2003)

7. R.A.Myers, N.Mukherjee, and S.R.J.Brueck; "Large second-order nonlinearity in poled fused silica," Optics Letters, **16**, 1732 (1991)

8. D.Wong, W.Xu, S.Fleming, M.Janos, and K.-M.Lo; "Frozen-in Electrical Field in Thermally Poled Fibers," Opt.Fib.Tech., **5**, 235 (1999)

9. David N.Nikogosyan: "Principles of Optical and Laser-Related Materials - A Handbook," John Wiley & Sons Ltd, (1997)

10. W.Margulis, F.Laurell, and B.Lesche; "Imaging the nonlinear grating in frequency-doubling fibres," Nature, **378**, 699 (1995)

11. D.T.Reid; "Engineered quasi-phase-matching for second-harmonic generation," J.Opt.A: Pure Appl.Opt., **5**, 97-102. (2003)

12. P.G.Kazansky, V.Pruneri; "Electric-field poling of quasi-phase-matched optical fibers," Optical Society of America, **14**, 3170-3179. (1997)

13. V.Pruneri, G.rate, P.G.Kazansky, D.J.Richardson, N.G.Broderick, J.P.de Sandro, C.Simonneau, P.Vidakovic, and J.A.Levenson; "Greater than 20%-efficient frequency doubling of 1532-nm nanosecond pulses in quasi-phase-matched germanosilicate optical fibers," Optics Letters, **24**, 208-210. (1999)

14. C.Corbari, A.Canagasabey, M.Ibsen, F.Mezzapesa, C.Codemard, J.Nilsson, and P.G.Kazansky; "All-fibre frequency conversion in long periodically poled silica fibers," OFC, **OFb3**, (2005)

15. R.Kashyap: "Fiber Bragg Gratings," Academic Press, (1999)

16. D.Statman, J.A.George III; "Charge dynamics and poling in glass waveguide," J.Appl.Phys., **80**, 654-661. (1996)

17. J.Arentoft, M.Kristensen, K.Pedersen, S.I.Bozhevolnyi, and P.Shi; "Large second-harmonic generation in thermally poled silica waveguides," OFC, **1**, MC6-1-MC6-3. (2001)

18. D.Pureur, A.C.Liu, M.J.F.Digonnet, and G.S.Kino; "Absolute measurement of the second-order nonliearity profile in poled silica," Opt.Lett., **23**, 588-590. (1998)

19. M.Qiu, T.Mizunami, R.Vilaseca, F.Pi, and G.Orriols; "Bulk and near-surface second-order nonlinearities generated in a BK7 soft glass by thermal poling," J.Opt.Soc.Am.B., **19**, 37-42. (2002)

20. W.Margulis, U.Ostberg; "Dye laser pumped by Nd YAG laser pulses frequency doubled in a glass optical fiber," Optics Letters, **11**, 516 (1986)

21. P.G.Kazansky, P.S.J.Russell, and H.Takebe; "Glass poling and applications," Phot.Tech.Lett., **15**, 1484-1493. (1997)

22. R.H.Stolen, H.W.K.Tom; "Self-organized harmonic generation in optical fibers," Opt.Lett., **12**, 585-587. (1987)

23. M.C.Farries, P.St.J.Russel, M.E.Ferman, and D.Pureur; "Second harmonic generation in an optical fiber by self-written chi2 grating," Electron.Lett., **23**, 324 (1987)

24. E.M.Dianov, P.G.Kazansky, and D.Yu.Stepanov; "Problem of the photoinduced second harmonic generation," Sov.J.Quantum Electron., **19**, 575-576. (1989)

25. V.Dominic, J.Feinberg; "Growth rate of second-harmonic generation in glass," Opt.Lett., **17**, 1761-1763. (1992)

26. X.C.Long, R.A.Myers, and S.R.J.Brueck; "A Poled Electrooptic Fiber," IEEE Photonics Technology Letters, **8**, 227-229. (1996)

27. T.Fujiwara, D.Wong, and S.Fleming; "Large Electrooptic Modulation in a Thermally-Poled Germanosilicate Fiber," IEEE Photonics Technology Letters, **7**, 1177 (1995)

28. P.G.Kazansky, P.St.J.Russell, and C.N.Pannell; "Optical fibre elecrets: observation of electro-acousto-optic transduction," Electronics letters, **30**, 1436 (1994)

29. K.Geary, S-K.Kim, B-J.Seo, and H.R.Fetterman; "Mach-Zehnder modulator arm length mismatch measurement and analyses," CLEO, **1**, (2004)

30. A.J.Ikushima, T.Fujiwara, and K.Saito; "Silica glass: A material for photonics," Applied Physics, **88**, 1201-1213. (2000)

31. C.Chang-Hasnain,. "Optical fiber ". EECS 233. (2002)

32. G.Cocito, L.Cognolato, E.Modone, and G.Parisi; "Flourine in MCVD fibers," Journal of Non-Crystalin Solids, **93**, 296-302. (1987)

33. B.Wu, P.L.Chu; "Fabrication of High Concentration Rare-Earth-Doped Silica-Based Waveguide by MCVD Method," Phot.Tech.Lett., **7**, 655-657. (1995)

34. J.B.MacChesney, K.L.Walker; "High rate MCVD," Journal of Non-Crystalin Solids, **38-39**, 831-836. (1980)

35. S.R.Nagel, J.B.MacChesney, K.L.Walker: "Optical fiber communications," (1985)

36. A.J.Morrow, A.Sarker, P.C.Schultz: "Optical fiber communications," (1985)

37. N.Niizeki, N.Inagaki, T.Edahiro: "Optical fiber communications," (1985)

38. B.Srinivasan, R.K.Jain; "First demonstration of thermally poled electrooptically tunable fiber Bragg grating," Phot.Tech.Lett., **12**, 170-172. (2000)

39. F.Haberl, J.Hochreiter, J.Zehetner, and A.J.Smith; "Electrical breakdown in ge-doped silica glass fibers," International Journal of Optoelectronics, **4**, (1990)

40. M.Fokine, L.E.Nilsson, A.Claesson, D.Berlemont, L.Kjellberg, L.Krummenacher, and W.Margulis; "Integrated fiber Mach Zehnder interferometer for electro-optic switching," Optics Letters, **27**, 1643 (2002)

41. P.G.Kazansky, L.Dong, and P.St.J.Russell; "High second-order nonliearities in poled silicate fibers," Optics Letters, **19**, 701 (1994)

42. R.A.Myers, S.R.J.Brueck, and R.P.Tumminelli; "Stable second-order nonlinearity in SiO2-based waveguides on Si using temperature/electric-field poling". Proc.SPIE - Doped Fiber Devices and Systems **2289**, 158 (1994)

43. T.G.Alley, S.R.J.Brueck, and M.Wiederbeck; "Secondary ion mass spectroscopy study of space-charge formation in thermally poled fused silica," Journal of Applied Physics, **86**, 6634 (1999)

44. Y.Quiquempois; "Model of chargemigration during thermal poling in silica glasses: Evidence of a voltage threshold for the onset of a second-order nonlinearity," Physical Review Letters, **65**, 043816-1-043816-14. (2002)

45. P.G.Kazansky, A.R.Smith, and P.St.J.Russell; OSA Technical Digest Series, **22**, 175 (1995)

46. N.Mukherjee, R.A.Myers, and S.R.J.Brueck; "Dynamics of second-harmonic generation in fused silica," J.Opt.Soc.Am.B., **11**, 701-703. (1994)

47. P.G.Kazansky, P.St.J.Russell; "Thermally poled glass: Frozen-in electric field or oriented dipoles," Opt.Commun., **101**, 614 (1994)

48. A.Okada, K.Ishii, K.Mito, and K.Sasak; "Second-harmonic generation in novel corona poled waveguides," Applied Physics Letters, **60**, 2853-2855. (1992)

49. P.G.Kazansky, A.Kamal, and P.St.J.Russell; "High second-order nonlinearities induced in lead silicate glass by electro-beam irradiation," Opt.Lett., **18**, 695 (1993)

50. T.Fujiwara, D.Wong, Y.Zhao, S.Fleming, S.Poole, and M.Sceats; "Electro-optic modulation in germanosilicate fiber with UV-exited poling," Electron.Lett., **31**, 575 (1995)

51. T.Fujiwara, A.J.Ikushima; "Recent progress on second-order optical nonlinearity in UV-poled glass," BGPP OSA trends in Optics and Photonics, **33**, 391-392. (2000)

52. T.Fujiwara, D.Wong, Y.Zhao, S.Fleming, S.Poole, and M.Sceats; "Comparison of linear electro-optic coefficient induced by UV-excited and thermal poling in a germanosilicate fibre," CLEO, Pacific Rim conference, 177 (1995)

53. J.Khaled, T.Fujiwara, and A.J.Ikushima; "Optimization of second-order nonlinearity in UV-poled silica glass," Optical Materials, **17**, 275-278. (2001)

54. L.Canioni, M.O.Martin, B.Bousquet, and L.Sarger; "Precise measurements and analyses of linear and nonlinear optical properties of glass materials near 1.5 um," Optics Communication, **151**, 241-246. (1998)

55. C.J.Marckmann, G.Genty, Y.Ren, J.Arentoft, and M.Kristensen; "Bragg gratings as probes to determine nonlinearities induced by thermal poling," BGPP, BFC3-1. (2001)

56. A.Liu, M.Digonnet, and G.Kino; "DC Kerr coefficient in silica: theory and experiment," Proc.SPIE, **3542**, 102-107. (1998)

57. C.J.Marckmann, J.Arentoft, and M.Kristensen; "Measuring poling-induced nonlinearities in Ge:SiON waveguides using a Bragg grating," OFC (in press), (2001)

58. A.Boskovic, S.V.Chernikov, and J.R.Taylor; "Direct continuous-wave measurement of n2 in various types of telecommunication fiber at 1.55 mm ," Opt.Lett., **21**, 1966-1968. (1996)

59. A.von Hippel; "Electric breakdown of glasses and crystals as a function of temperature," Pysical review, **59**, 820-823. (1941)

60. W.T.Lynch; "Calculation of electric field breakdown in quartz as determined by dielectric dispersion analysis," J.Appl.Phys., **43**, 3274-3278. (1972)

61. K.Lee, P.Hu, and J.L.Blows; "A 200 m long fiber with internal electrode and poling demonstration," ECOC, Stockholm, (2004)

62. W.Xu, J.Arentoft, D.Wong, and S.Fleming; "Evidence of Space-charge Effects in Thermal Poling," Phot.Tech.Lett., **11**, 1265 (1999)

63. Y.Quiquempois, G.Martinelli, P.Bernage, M.Douay, P.Niay, E.Delevaque, H.Poignant, B.Loisel, and J.F.Bayon; "Study of organized $c^{(2)}$ susceptibility in germanosilicate optical fibers," Optical Materials, **9**, 361-367. (1998)

64. A.Kudlinski, G.Martinelli, Y.Quiquempois, and H.Zeghlache; "Microscopic model for the second-order nonlinearity creation in thermally poled bulk silica glasses," BGPP, TuC3 (2003)

65. T.G.Alley, S.R.J.Brueck, and R.A.Myers; "Space charge dynamics in thermally poled fused silica," Journal of Non-Crystalin Solids, **242**, 165 (1998)

66. D.W.Shin, M.Tomozawa; "Effects of fictive temperature and water content on electrical conductivity of silica glasses," Journal of Non-Crystalin Solids, **203**, 262-267. (1995)

67. D.Faccio, V.Pruneri, and P.G.Kazansky; "Dynamics of the second-order nonlinearity in thermally poled silica glass," Applied Physics Letters, **79**, 2687 (2001)

68. D.E.Carlson; "Anodic proton injection in glasses," Journal of the american ceramics society, **57**, 461-466. (1974)

69. A.L.C.Triques, I.C.S.Carvalho, M.F.Moreira, H.R.Carvalho, R.Fischer, B.Leche, and W.Margulis; "Time evolution of depletion region in poled silica," Applied Physics Letters, **82**, 2948-2950. (2003)

70. Y.Quiquempois, M.Lelek, A.Kudlinski, H.Zeghlache, and G.Martinelli; "Nonlinear distribution reconstruction in poled silica glasses with sub-micron resolution," BGPP, (2003)

71. Y.Quiquempois, A.Kudlinski, and G.Martinelli; "Zero potential condition in thermally poled silica samples: Evidence of a negative electric field outside the depletion layer," J.Opt.Soc.Am.B., **22**, 598 (2005)

72. X.C.Long, R.A.Myers, and S.R.J.Brueck; "Measurement of linear electro-optic effect in temperature/electric-field poled optical fibres," Electron.Lett., **30**, 2162 (1994)

73. A.L.C.Triques, C.M.B.Cordeiro, V.Balestrieri, B.Lesche, W.Margulis, and I.C.S.Carvalho; "Depletion region in thermally poled fused silica," Applied Physics Letters, **76**, 2496 (2000)

74. D.E.Carlson; "Ion depletion of glass at a blocking anode: I. Theory and experimental results for alkali silicate glasses," Journal of the american ceramics society, **57**, 291-294. (1974)

75. M.Abe, T.Kitagawa, K.Hattori, A.Himeno, and Y.Ohmori; "Electro-optic switch constructed with a poled silica-based waveguide on a Si substrate," Electron.Lett., **32**, 893-894. (1996)

76. H.L.An, X.Z.Lin, E.Y.B.Pun, and H.D.Liu; "Multi-wavelength erbium-doped fiber ring laser with a novel dual-pass Mach-Zehnder comb filter," APCC/OECC Fifth Asia-Pacific Conference, **2**, 1495-1498. (1999)

77. R.Kashyap, F.C.Garcia, and L.Vogelaar; "Nonlinearity of the electro-optic effect in poled waveguides," BGPP, TuC2 (2003)

78. F.C.Garcia, L.Vogelaar, and R.Kashyap; "Poling of a channel waveguide," Optics Express, **11**, 3041 (2003)

79. B.Lesche, F.C.Garcia, E.N.Hering, W.Margulis, I.C.S.Carvalho, and F.Laurell; "Etching of Silica Glass under Electric fields," Physical Review Letters, **78**, 2172 (1997)

80. T.G.Alley, S.R.J.Brueck; "Visualization of the nonlinear optical space-charge region of bulk thermally poled fused-silca glass," Optics Letters, **23**, 1170 (1998)

81. H-Y.Chen, J-S.Sue, Y-H.Lin, C-S.Tsai, P-T.Wu, and S.Chao; "Thermal poling and ultraviolet erasure characteristics of type-III ultraviolet grade fused silica and application to periodic poling on planar substrates," Applied Physics, **94**, 1531-1538. (2003)

82. P.Blazkiewicz, W.Xu, D.Wong, and S.Fleming; "Mechanism for the thermal poling in twin-hole silicate fibers," J.Opt.Soc.Am.B., **19**, 870 (2004)

83. M.Fokine; "High temperature miniature oven with low thermal gradient for processing fiber Bragg gratings," Rev.Sci.Intrum., **72**, 3458 (2001)

84. http://www.glamorous-eu.com/ . (2005)

85. S.Smolorz, F, and .Wise; "Femtosecond two-beam coupling energy transfer from Raman and electronic nonlinearities," J.Opt.Soc.Am.B., **17**, 1636 (2000)

86. "http://www.mathworks.com/access/helpdesk/help/toolbox/rfblks/twowiretransmissionline.html". mathworks. (2005)

87. I.Abdulhalim, C.N.Pannell; "Photoelastic In-Fiber Birefringence Modulator Operating at the Fundamental Transverse Acoustic Resonance," IEEE Photonics Technology Letters, **5**, 1197 (1993)

88. N.Godbout, S.Lacroix, Y.Quiquempois, G.Martinelli, and P.Bernage; "Measurement and calculation of electrostrictive effects in a twin-hole silica glass fiber," J.Opt.Soc.Am.B., **17**, 1-5. (2000)

89. P.G.Kazansky, P.St.J.Russell, and C.N.Pannell; "Optical fibre elecrets: observation of electro-acousto-optic transduction, " Electron.Lett., **30**, 1436-1437. (1994)

90. A.C.Liu, M.J.F.Digonnet, and G.S.Kino; "Measurement of the dc Kerr and electrostrictive phase modulation in silica," J.Opt.Soc.Am.B., **18**, 187 (2001)

91. O.Deparis, C.Corbari, P.G.Kazansky, and K.Sakaguchi; "Stability of the second-order optical nonlinearity in poled glasses, " Proceedings BGPP, 216 (2003)

92. O.Deparis, C.Corbari, P.G.Kazansky, and K.Sakaguchi; "Enhanced stability of the second-order optical nonlinearity in poled glasses," Applied Physics Letters, **84**, 4857-4859. (2005)

93. M.Janos, W.Xu, D.Wong, H.Ingles, and S.Fleming; "Growth and decay of the electrooptic effect in thermally poled B/Ge Codoped fiber," Journal of lightwave technology, **17**, 1037-1041. (1999)

94. N.H.Ky, H.G.Limberger, R.P.Salathé, and G.R.Fox; "Optical performance of miniature all-fiber phase modulators with ZnO coating," Journal of lightwave technology, **14**, 23-26. (1996)